

Some Influences of Tribology in Resistance

Spot Welding of Aluminum Alloys

by

Muhammad Rashid

A thesis
presented to the University of Waterloo
in fulfillment of the
thesis requirement for the degree of
Doctor of Philosophy
in
Mechanical Engineering

Waterloo, Ontario, Canada, 2007

© Muhammad Rashid 2007

AUTHOR'S DECLARATION

I hereby declare that I am the sole author of this thesis. This is a true copy of the thesis, including any required final revisions, as accepted by my examiners.

I understand that my thesis may be made electronically available to the public.

Muhammad Rashid

Abstract

The influence of the tribology during resistance spot welding (RSW) of aluminum alloy 5182 with spherical-tip electrode has been investigated at both the electrode-worksheet (E/W) and faying surface (FS) interfaces. In RSW, electrode life is limited by poor current transport to the FS interface caused by extensive pitting of the electrode tip surface. The primary focus of the present research was to extend electrode life by using the knowledge gained from studying the contact mechanics at both of these interfaces. Series of experiments were conducted and finite element analysis was employed to investigate the contact mechanics at the interfaces. Based on these findings, a practical way to extend the electrode life was developed.

In a series of initial experiments, it was found that attempts to alter the worksheet surface roughness caused damage to the surface oxide layer which resulted in decrease of electrical contact resistance at the E/W interface. The oxide layer on the worksheet surface contained aluminum and magnesium oxide regions and abrasion of the worksheet surface reduced the oxide layer thickness and made it more uniform in composition because when the magnesium oxide regions were abraded, a thin layer of aluminum oxide re-formed immediately while it take specific conditions to re-form magnesium oxide. These factors decreased the electrical contact resistance of the E/W interface compared with the as-received surface, thus reducing heat generation and the associated pitting of the electrode surface during RSW.

Further experimental investigations and finite element analysis showed that the contact mechanics that occurred during the loaded “squeezing” phase of the welding sequence, but before current was applied to cause RSW, had a significant effect on the electrode pitting behaviour and nugget formation. At the E/W interface, squeezing caused high shear stress and slip at the periphery of the contact region. This slip disrupted the oxide layer and reduced the electrical resistance. At the beginning of the current phase of the weld sequence, the reduced electrical resistance caused current to concentrate near the periphery but constriction resistance still produced enough heat generation to cause alloying, pickup and eventually pitting of electrode in a ring around the contact centre.

At the FS interface, experiments and finite element analysis showed that sheet separation and thus bending occurred during the squeezing phase and this had a profound influence on nugget formation. Experimental observations showed that the bending caused enlarged and aligned cracks in the surface oxide layers which promoted good metal-to-metal contact near the periphery of the FS. As at the E/W interface, high current densities occurred at the beginning of the current phase and the constriction resistance caused significant heat generation in this zone due to an increasing constriction resistance. Consequently, the melting at the FS started near the periphery and moved in towards the central zone of the contact region melted to produce a “doughnut-shaped” nugget with a filled-in but thin central region.

Low electrical contact resistance at the E/W interface led to longer electrode tip life because less pitting occurred. In addition, higher current densities could then develop at the FS to affect RSW and achieve good nugget formation despite the rather uneven peripheral heat generation. In attempts to reduce the electrical resistance at the E/W interface, several boundary lubricants were placed on the worksheet surface a short time before starting RSW and they altered the tribology. Both increased and decreased electrode degradation rate were found in electrode life tests. One lubricant was found to be particularly effective in lowering the electrode pitting rate. It extended the electrode life to almost double that occurring with as-received (unlubricated) surfaces. Detailed analysis revealed that the effective boundary lubricant had a beneficial chemical influence on the surface of the AA5182 worksheet. The lubricant chemically attacked the oxide layer thus reducing its thickness and reducing electrical contact resistance of the E/W interface at the critical peripheral region. The result was a lower electrode pitting rate and an extended electrode life.

The improved understanding of the current flow during the critical initial period and its dependence on the contact mechanics of the E/W and FS interfaces was considered important in developing ways of improving weld strength and increasing electrode life. The finding of a boundary lubricant that acted to reduce oxide layer thickness was considered an important starting point for industrial development of RSW with longer electrode life. It could be employed without interrupting the RSW process and its efficacy was well-supported by the present contact mechanics studies in which the key role of the oxide layer was demonstrated.

Acknowledgements

In the name of Allah, Most Gracious, Most Merciful. All praise to Allah (Subhanahu-wa-Ta'ala), the Almighty, Who Gave me this opportunity, courage, and patience to carryout this work. I feel privileged to glorify His name in the sincerest way through this small accomplishment.

Without the support of my family, the completion of this thesis, certainly, would not have been possible. My deepest appreciation is extended to my parents for taking the pains to fulfill my academic pursuits and shaping my personality. I would like to express my deepest gratitude to my wife Ambreen and my children for willingly relinquishing the time which should have been theirs so that I may achieve my goals. I Acknowledge with sincerity, the affection and encouragement of my parents-in-law, my brothers, my sisters, my brothers-in-law, and my sisters-in-law for their moral support during this hard work.

I wish to express my sincere appreciation to my supervisors Dr. N. Y. Zhou and Dr. J. B. Medley for their encouragement, criticism, and perseverance throughout the course of this study. Their insight advice, invaluable guidance, immense patience, and friendly personality had a positive influence on my work. The time and efforts thy devoted to my PhD work are truly appreciated.

I am grateful to Dr. S. Lawson for his valuable thoughts and enlightening discussion during several stages of this work. I would also like to thanks my examining committee Dr. M. Worswick, Dr. M. A. Polak, and Dr. R. Rogers for their valuable comments.

I would also like to acknowledge the Natural Science and Engineering Research Council Canada (NSERC), Ontario Ministry of Education, Auto21, and University of Waterloo for their financial support and ALCAN Inc and Centerline Ltd for materials and equipment used in this study. I am grateful to Centre for Advanced Materials Joining (CAMJ) and Department of Mechanical and Mechatronics Engineering at the University of Waterloo.

I am also grateful to my friends and fellow graduate students at the University of Waterloo for providing me a wonderful company during my PhD work.

Dedicated to

My Parents

My Wife

and

My Children

Table of Contents

1	INTRODUCTION	1
1.1	Resistance Spot Welding	1
1.1.1	Process Description.....	2
1.1.2	Parameters Influencing RSW.....	5
1.2	Aluminum Alloys	6
1.2.1	RSW of Aluminum Alloys	7
1.3	Objective.....	9
1.4	Approach	9
1.5	Thesis Outline.....	10
2	LITERATURE REVIEW	11
2.1	Electrical Contact Resistance	11
2.2	Some Tribological Features of the E/W and FS Interfaces	13
2.2.1	Surface Oxide Layer	13
2.2.2	Removal or Cracking of the Surface Oxide Layer.....	18
2.2.3	Surface Roughness.....	21
2.2.4	Lubrication of the E/W Interface	23
2.3	Electrode Degradation Mechanisms	24
2.4	Sheet Separation	29
2.5	Variability of the Experimental Data.....	29
2.6	Various Research Approaches.....	31
2.6.1	Surface Treatment.....	31
2.6.2	Welding Parameter Selection.....	31
2.6.3	Electrode Material	32
2.6.4	Electrode Surface Coatings.....	33
2.6.5	Electrode Geometry	34

2.6.6	Re-dressing the Electrode Tips	34
2.6.7	Simulation with Finite Element Analysis	35
2.7	Concluding Remarks	37
3	MATERIALS AND METHODS	39
3.1	Materials	40
3.2	Equipment.....	43
3.3	Welding Parameters.....	46
3.4	Surface Preparation.....	48
3.4.1	Mechanical Procedures	48
3.4.2	Chemical Procedures	49
3.4.3	Omission of Oxide Layer Geometry.....	49
3.4.4	Overall Comments on Surface Preparation.....	50
3.5	Experimental Procedures.....	51
3.5.1	Electrode Life Test.....	51
3.5.2	Electrode Life Criteria	52
3.5.3	Carbon Imprint.....	52
3.5.4	Weld Shear Strength	53
3.5.5	Metallography	53
3.5.6	Electrical Contact Resistance.....	54
3.5.7	Contact and Weld Diameters	55
3.5.8	Statistical Analysis.....	56
3.5.9	Peltier Effect	56
3.6	Finite Element Analysis.....	57
3.7	Concluding Remarks	63
4	THE ELECTRODE-WORKSHEET INTERFACE.....	64
4.1	Introduction	64
4.2	Results	65
4.2.1	Experiments	65
4.2.2	Electrical Contact Resistance of E/W Interface.....	67
4.2.3	Effect of Surface Abrasion on Electrode Degradation.....	70
4.3	Discussion.....	74
4.3.1	Effect of Surface Roughness.....	75
4.3.2	AA5182 Oxide Layer Composition	77
4.3.3	Effect of Grinding/Abrading on the Surface Oxide Layer.....	82

4.3.4	Effect of Oxide Geometry and Composition on Electrical Contact Resistance, Pitting of the Electrode and Weld Strength	85
4.4	Concluding Remarks	87
5	CONTACT MECHANICS AT THE E/W INTERFACE	88
5.1	Introduction	88
5.2	Experimental Investigations	89
5.2.1	Electrode Pitting	89
5.2.2	Contact Diameter	93
5.2.3	Effect of Squeezing on the Worksheet Surface	96
5.3	Finite Element Analysis (FEA)	101
5.3.1	Formulation.....	101
5.3.2	Shear Stress Distribution	101
5.3.3	Pressure Distribution	104
5.3.4	Slip along the E/W Interface.....	104
5.3.5	Contact Mechanics at the E/W Interface	110
5.4	Concluding Remarks	111
6	CONTACT MECHANICS AT THE FAYING SURFACE	113
6.1	Introduction	113
6.2	Experimental Investigation.....	113
6.2.1	Nugget Formation, Growth and Shape	114
6.2.2	Start and Progress of Melting at the FS	119
6.3	Finite Element Analysis (FEA) with Additional Experiments.....	122
6.3.1	Formulation.....	123
6.3.2	Contact Pressure and Contact Diameter	123
6.3.3	Sheet Separation	124
6.3.4	Effect of Sheet Separation	126
6.3.5	Location of Sheet Separation.....	128
6.3.6	Plastic Deformation Zone	130
6.4	Concluding Remarks	130
7	EFFECT OF BOUNDARY LUBRICANTS.....	132
7.1	Introduction	132
7.2	Electrode Life Experiments.....	133
7.2.1	Screening of Different Lubricants	133
7.2.2	Electrode Life	137

7.2.3	Rate of Electrode Pitting.....	141
7.3	Features of Boundary Lubricated RSW.....	145
7.3.1	Initial Joint Shear Force.....	146
7.3.2	Nugget Diameter.....	147
7.3.3	Electrode Indentation into the Worksheet.....	148
7.3.4	Heat Generation at E/W Interface.....	149
7.3.5	Surface Oxide Layer.....	151
7.3.6	Alloys on the Electrode Surface.....	156
7.3.7	Electrical Contact Resistance.....	159
7.4	Concluding Remarks.....	161
8	CONCLUSIONS.....	162
8.1	Electrode Worksheet Interface (Chapter 4).....	163
8.2	Contact Mechanics at the E/W Interface (Chapter 5).....	164
8.3	Contact Mechanics at the FS (Chapter 6).....	165
8.4	Effect of Boundary Lubricants (Chapter 7).....	166
8.5	Recommendations.....	167
	REFERENCES.....	169
	APPENDIX A.....	181
	APPENDIX B.....	185
	APPENDIX C.....	190

List of Figures

Figure 1.1: Typical configuration for RSW.....	3
Figure 1.2: The process sequence for RSW.	4
Figure 1.3: Use of aluminum alloys in autobody structure [19].....	7
Figure 2.1: Electrical resistances in the current path during RSW.....	12
Figure 2.2: Schematic illustration of oxide growth of aluminum alloys (AA5182 in particular) from Kucza et al [37].....	14
Figure 2.3: The differences in material transfer mechanisms for thick and thin oxide layers according to Patrick et al [33]. The oxide layer thickness was exaggerated to permit a view of the mechanisms.	17
Figure 2.4: Schematic illustration of metal-to-metal contact formation at the FS interface from Mohamed et al [50]......	20
Figure 2.5: Schematic of different contact regions between two surfaces from Studer [52]. Region A was the actual metallic contact without any oxide film. Region B was the area where a mixed metallic contact and an oxide film were present. Region C showed an air gap between the two surfaces and thus a lack of contact of any kind. Finally, Region D and E showed contacts with oxide layers between them.....	22
Figure 2.6: Material transfer morphology by Dilthey et al [56]. Case A represents a situation where the intermetallic Cu-Al phase remained stick to the electrode and is known as ‘pick-up’. Case B represents a situation where the intermetallic Cu-Al phase breaks from the electrode and remains with the worksheet and is known as ‘pitting’. Case C is a situation where both pick-up and pitting happened partially and simultaneously. In all cases, subsequent welding with the same electrode would cause further current concentration and enhance the material transfer and thus electrode degradation.	25
Figure 2.7: Shear force versus weld number for RSW of aluminum sheet [59].	26
Figure 2.8: Schematic illustration of the four-stages of electrode life; correlating the joint strength with contact area between electrode and worksheet and pitting of electrode....	27
Figure 2.9: Four steps of electrode degradation in RSW of aluminum alloys according to Lum et al [59]......	28
Figure 2.10: Plastic strain distribution (after squeezing only) defining the contact area at the interfaces [60]. Min (1) 2.20×10^{-3} , Max (8): 27×10^{-2} , Inc: 3.54×10^{-3}	37

Figure 3.1: Dimension and orientation of sheared strips used for sample preparation	41
Figure 3.2: Geometry of weld specimens and orientations for welding (a) 10-weld standard coupon and (b) conditioning coupon.....	42
Figure 3.3: Geometry and orientation of overlapped specimen for joint shear force measurement.....	42
Figure 3.4: Electrode geometry (all dimensions in mm).....	43
Figure 3.5: MFDC Resistance spot welder used in the present study.....	44
Figure 3.6: Typical current wave-form of the MFDC spot welder.....	45
Figure 3.7: Schematic of RSW setup showing the interfaces and application of lubricant. ...	49
Figure 3.8: Schematic of joint shear force measurement.....	53
Figure 3.9: Schematic illustration of four-point method for measuring the electrical resistance across the E/W interface.....	54
Figure 3.10: Schematic illustration of contact diameter at the E/W interface.....	55
Figure 3.11: The load application during squeezing.....	58
Figure 3.12: Decomposition of total strain into elastic (ϵ^{el}) and plastic (ϵ^{pl}) components [93].	60
Figure 3.13: FEA mesh and boundary conditions for the axisymmetric representation of RSW during squeezing.....	62
Figure 4.1: Electrical contact resistance variation during successive measurements with the same electrode pair.....	67
Figure 4.2: Electrical contact resistance at the E/W interface for rough and smooth surfaces.	68
Figure 4.3: Electrical contact resistance at the E/W interface for as-received and ground surfaces.....	69
Figure 4.4: Electrode tip pitting as measured by carbon imprints.....	72
Figure 4.5: Joint shear force comparisons for as-received and abraded surfaces.....	74
Figure 4.6: Surface morphology of AA5182 showing non-uniform bright spots.....	78
Figure 4.7: Line scan chemical analysis (EDS) analysis of non-uniform spots showing intensities of Aluminum (Al), Magnesium (Mg), and Oxygen (O).....	80
Figure 4.8: Line scan chemical analysis (EDS) analysis of non-uniform spots showing intensities of Aluminum, Magnesium, and Oxygen.....	81
Figure 4.9: Effect of grinding and abrading on the surface oxide layer of AA5182.....	83
Figure 4.10: Chemical analysis of as-received, ground, and abraded surfaces of AA5182....	84
Figure 5.1: As-received worksheet surface with alloying regions indicating electrode pitting.	90
Figure 5.2: Chemical analysis (EDS) of the alloyed spots on worksheet (from Figure 5.1)...	91

Figure 5.3: Carbon imprints of electrodes, ring-pitting pattern during the early stages of electrodes life for as-received and abraded surface; the dotted circle had a diameter of 5.0 mm and linked the local pitted regions together.....	92
Figure 5.4: Contact diameter between electrode and worksheet for different weld times in ms (note that 1 ms = 0.06 cycles).....	95
Figure 5.5: Tip surface of a typical as-received electrode showing machining marks ($R_a = 1.48 \pm 0.04 \mu\text{m}$).	97
Figure 5.6: Tip surface of a typical polished electrode ($R_a = 0.25 \pm 0.01 \mu\text{m}$) showing faint evidence of the original machining marks.....	98
Figure 5.7: A series of SEM micrographs of the worksheet contact area (when using as-received electrodes) from the periphery into the centre after only the squeezing period of the RSW procedure.....	99
Figure 5.8: A series of SEM micrographs of the worksheet contact area (when using the smooth electrode tips) from the periphery into the centre after only the squeezing period of the RSW procedure.	100
Figure 5.9: Shear Stress (MPa) distribution due to squeezing of electrode into the worksheet; contours showing the shear stress distribution in the entire model.	102
Figure 5.10: Shear Stress distribution along the E/W interface.	103
Figure 5.11: Frictional Shear Stress distribution between electrode and worksheet surfaces.	103
Figure 5.12: Pressure distribution along the E/W interface.....	104
Figure 5.13: Shear Stress as a fraction of Pressure at the E/W interface.	105
Figure 5.14: The amount of slip between electrode and worksheet at the E/W interface.	107
Figure 5.15: Shear stress as fraction of Pressure at the E/W interface ($\mu = 0.3$).....	108
Figure 5.16: Shear stress as fraction of Pressure at the E/W interface ($\mu = 0.3$).....	108
Figure 5.17: Relative tangential motion (slip) along the E/W interface ($\mu = 0.3$).	109
Figure 5.18: Relative tangential motion (slip) along the E/W interface ($\mu = 0.3$).	109
Figure 6.1 Nugget cross-sections showing the shape and nugget growth for different current time (1 – 5 cycles).	116
Figure 6.2: Average joint shear strength of RSW when welded for different current time. .	117
Figure 6.3: Shape of the nugget after RSW of AA5182 with 20kA for 1 current cycle.	118
Figure 6.4: SEM micrographs showing heat generation and start of melting at the faying surface spot welded at low currents (10 – 20 kA) for short current time (1 cycle).	121
Figure 6.5: Start and progress of heat generation (melting) at the faying surface spot welded at low current of 10 kA for different weld time (1 – 3 cycles).....	122
Figure 6.6: Distribution of contact pressure at the faying surface after squeezing.	123

Figure 6.7: Contact diameters of the FS and E/W interface obtained experimentally and through FEA.	124
Figure 6.8: Axial position of the two worksheets at the FS showing sheet separation at the end of the contact.	125
Figure 6.9: Schematic illustration of experimental measurement of sheet separation due to squeezing; the average value of A is $91 \pm 13 \mu\text{m}$	126
Figure 6.10: Effect of bending on surface layer; enlarged and aligned cracks are visible on bent surfaces.	127
Figure 6.11: SEM micrographs showing the effect of sheet separation on the surface layer of AA5182; visible cracks at the periphery of the contact at the FS	128
Figure 6.12: Location and movement of sheet separation at different stages of squeezing. .	129
Figure 6.13: Equivalent plastic strain distribution in the sheet. Min (1) – 8.0×10^{-3} ; Max (8) – 3.6×10^{-2} ; Inc – 4.0×10^{-3}	130
Figure 7.1: Surface conditions of lubricated and as-received samples (a) A-surface, all surfaces are in as-received condition and (b) L-surface, E/W interfaces were lubricated and FS was as-received.	135
Figure 7.2: Optical stereomicroscope images of the positive electrodes after performing 100 spot welds on different surfaces.	137
Figure 7.3: Electrode life results for L2-surfaces with horizontal dashed line representing the failure strength.	139
Figure 7.4: Electrode life results for A-surfaces with horizontal dashed line representing the failure strength.	140
Figure 7.5: Electrode life results for L6-surfaces with horizontal dashed line representing the failure strength.	140
Figure 7.6: Carbon imprints of upper (positive) electrodes at different stages of electrode life used for L2-surface.	142
Figure 7.7: Carbon imprints of upper (positive) electrodes at different stages of electrode life used for A-surface.	143
Figure 7.8: Carbon imprints of upper (positive) electrodes at different stages of electrode life used for L6-surface.	144
Figure 7.9: Average joint shear force of A-surface and L2-surface; each set welded with the same pair of electrodes.	147
Figure 7.10: Average nugget diameter of A-surface and L2-surface; each set welded with the same pair of electrodes.	148
Figure 7.11: Electrode indentation into the worksheet for A-surface and L2-surface; each set welded with the same pair of electrodes.	149
Figure 7.12: Typical nugget cross section of spot weld of A-surface and L2-surface.	150

Figure 7.13: Optical microscopy showing the effect of good lubricant (L2) on an unpolished worksheet surface.	152
Figure 7.14: SEM micrographs showing the effect of good lubricant (L2) on unpolished worksheet surfaces (equivalent spots and may not be exactly the same position).	153
Figure 7.15: Optical microscopy showing the effect of good lubricant (L2) on a polished worksheet surface.	154
Figure 7.16: Thickness of the oxide layers on A- and L2-surfaces from ESCA; intensity of Oxygen in oxides of the worksheet of AA5182 surface.....	155
Figure 7.17: Schematic illustration of the influence of the boundary lubricant L2 on the surface (oxide) layer of AA5182.....	156
Figure 7.18: Typical XRD intensity spectra showing different Cu-Al intermetallic phases found on the electrode surfaces after 100 spot welds on A-surface and L2-surface; small window is showing the standard XRD pattern for CuAl ₂ phase.	157

List of Tables

Table 1.1: General Properties of Aluminum and Steel [15, 23].	8
Table 3.1: Chemical composition of AA5182.	40
Table 3.2: Welding parameters for RSW of AA5182.	47
Table 3.3: Mechanical properties of worksheet and electrode materials [94].	60
Table 3.4: True stress and plastic strain values for worksheet and electrode.	61
Table 4.1: Centerline average roughness (Ra) of the contacting surface of the worksheet.	66
Table 4.2: Ra values and electrical contact resistance of as-received and abraded surfaces.	71
Table 4.3: Chemical analysis (EDS) of as-received surface of AA5182.	78
Table 4.4: General properties of oxide layer (Al ₂ O ₃ and MgO) and bulk of AA5182 [23,40]	86
Table 5.1: Randomized sequence of RSW tests involving different current times (note that 1 cycle = 16.67 ms).	94
Table 6.1: RSW test sequence involving different current magnitude and current times (note that 1 cycle = 16.67 ms).	120
Table 7.1: General description of the lubricants used for the screening tests.	134
Table 7.2: Significant events of electrode life during life tests for each surface condition.	141
Table 7.3: Intermetallic reaction for different Cu-Al phases [104].	158
Table 7.4: Electrical contact resistance at the E/W interface and centerline average roughness (Ra) of the worksheet.	160

Chapter – 1

1 Introduction

1.1 Resistance Spot Welding

In resistance welding, electrical current is passed through the interface between two work pieces to produce enough heat to cause welding by fusion or, in some cases, by brazing or solid state diffusion [1-5]. The bonded zone consists only of the materials from the work pieces in contrast to the filler rods that are used in other welding processes. Resistance spot welding (RSW) is resistance welding over a small region or spot at the work piece interface. It is widely used for applications where parts to be joined do not need to be gas-tight or liquid-tight [6]. The process is generally used for sheet metal applications and this application is examined in the present thesis. However, there are other applications, such as “cross-wire” joining of thin wires and very small scale resistance spot welding for medical devices and electronic components [7].

For most sheet metal applications, RSW is one of the main joining methods. Sheet metals up to 3.2 mm (1/8 inch) thick can be successfully joined by this process [8]. There are several advantages of RSW process; one of the main advantages is its readiness for automation. In most cases, the welding parameters are fixed and can be programmed with no subsequent adjustment needed and this clearly simplifies the automation of the process. Also, RSW is fast, does not require skilled labour and can be very inexpensive compared with other methods of welding [9].

1.1.1 Process Description

Although the interactions among the process variables are very complex, from the manufacturing viewpoint, RSW of sheet metals is simple to implement. A typical configuration for RSW of sheet metals (Figure 1.1) includes two metal worksheets with both upper and lower electrodes. The worksheets are clamped between electrodes by a “weld” force and current is applied for enough time to produce the heat needed for welding. Cooling water runs through electrodes and absorbs heat from the system for quick solidification and to keep the temperature of the electrodes low enough for continuous operation.

The contacts involved in RSW are between the upper electrode-worksheet, the faying surfaces of the two work sheets and the lower electrode-worksheet as shown in Figure 1.1. Often to simplify descriptions, the interface between the two faying surfaces is identified as *the* faying surface and so in the subsequent text of the present thesis the term faying surface (FS) is used to designate this interface. Electrode degradation occurs more readily at the upper (positive) electrode-worksheet interface contact and so it is studied in the present thesis and referred to as the electrode-worksheet interface (E/W interface). Problems with nugget size and strength involve the FS contact and so study is also focused on this contact.

The engineering area concerned with the study of interacting (including contacting) surfaces in relative motion is known as tribology. Usually, the relative motion is tangential to the load acting through the contact but the relative motion can be in the direction of the load (and this is the case in RSW).

Either alternating or direct current can be employed in RSW. Coordinated actions must be made including force application, electrical current flow and both heating and then cooling of the molten pool to produce the weld. The current is applied for a small part of the total process time (Figure 1.2) that requires the completion of four steps [10, 11] as described subsequently.

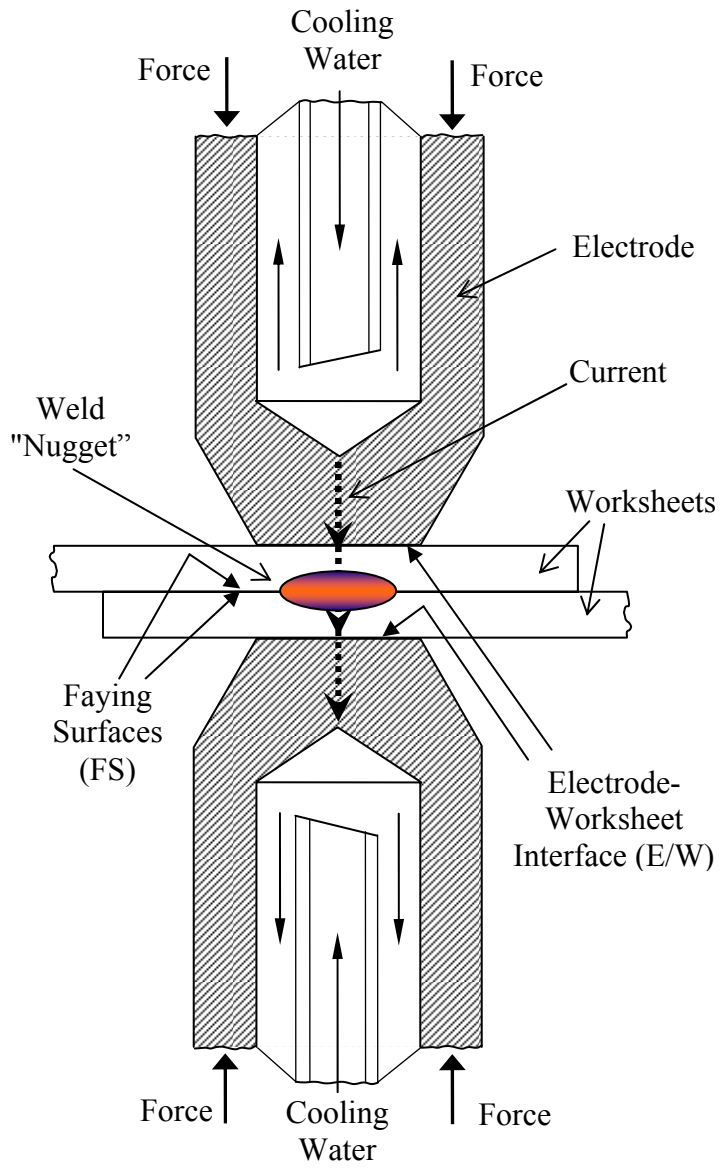


Figure 1.1: Typical configuration for RSW.

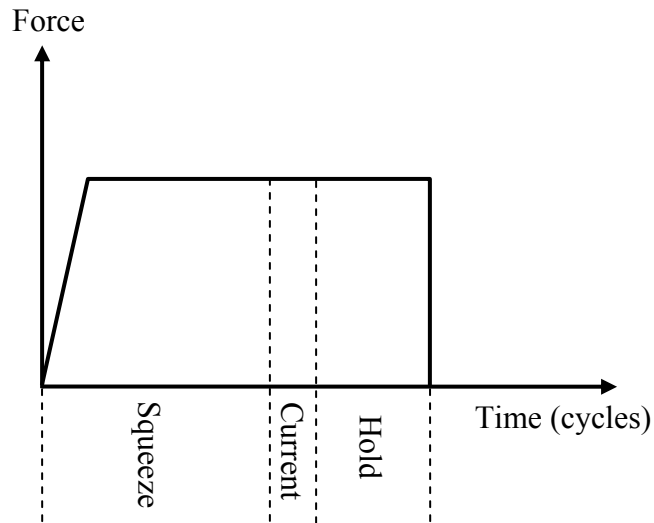


Figure 1.2: The process sequence for RSW.

(i) Squeeze

A force is applied to squeeze the surface together and close any initial gap between them that may arise from small misalignments, component deformity and surface roughness. This stage is important to achieve a uniform distribution of current and thus an even heat distribution for RSW.

(ii) Current

A large current is passed for a relatively small part of the process time. Heat is generated at the contact zones, because of their high electrical resistance, and local melting occurs.

(iii) Hold

Current is stopped but the force is held for additional time to allow solidification of the weld nugget.

(iv) Off

The release of force completes the weld cycle.

1.1.2 Parameters Influencing RSW

In RWS, most of the heat that causes the weld to form is generated at the faying surface (FS) where the two worksheets are in contact. The heat generation can be expressed by the following equation [6].

$$Q = I^2 R t \qquad \text{Equation 1.1}$$

where

Q = heat generated (J)

I = current (A)

R = electrical resistance (Ω)

t = time (s)

The specific terms in Equation 1 are themselves influenced by a cascading series of terms that can be considered variables, parameters or constants depending on how readily they change in experimental investigations. For the purposes of the present discussion, all influencing terms are described as parameters and later on in the experimental investigations of the present thesis a more precise differentiation is made into variables, parameters and constants.

The manufacturing process parameters are force, current and time (Figure 1.1 and Figure 1.2) along with the weld process cycle rate and choice of alternating or direct current for the heat source. As indicated in Equation 1, electrical resistance (R) is an important parameter and depends mainly on cascading series of parameters related to the properties of the workpiece

materials to be joined. This series of parameters represent bulk mechanical, electrical and thermal properties as well as the tribological characteristics of the contacts (E/W interface and FS) that include the oxide layer, the surface roughness and the presence of boundary lubricants. The use of the term "boundary lubricants" requires some explanation. A lubricant is usually a liquid (but can be a gas or a solid) that is interposed between the contacting surfaces to reduce friction. However, for the purposes of the present thesis, this definition is broadened to include any added substance that influences the interaction of the surfaces. In the context of RSW, a lubricant (solid or liquid or liquid that becomes dry with time) can be added to the upper worksheet surface and upon subsequent RSW acts to modify the tribology of the contact at the E/W interface.

Also, following Ikeda et al [13], there are parameters related to the electrodes that play important roles during the weld process. The electrodes should have a geometry and yield stress that allow the stresses caused by the force imposed during squeezing to act without causing plastic deformation. These electrodes should have electrical properties that permit an efficient current path for heat generation at the FS. At the same time, the electrodes should have thermal properties that transfer heat quickly from the molten nugget to the cooling water and thermal-mechanical properties that allow them to withstand high temperature deformation. Therefore, a careful selection of electrode materials and geometry is very important for successful RSW.

1.2 Aluminum Alloys

There are several types and grades of aluminum alloys that are designed for specific uses [14]. Aluminum alloys possess several special properties that make them one of the most popular engineering materials. For example, they have a high strength-to-weight ratio [15] and excellent corrosion resistance, both of which make them ideal in the automotive and aerospace industries for better fuel economy and reduced environmental damage.

For the automotive body, up to 46% weight can be reduced by using aluminum alloys instead of steel [16-18]. Several automotive manufacturers (Figure 1.3) are already using aluminum alloys in their bodies [19, 20]. In sheet metal applications, the 5xxx series aluminum alloys are generally used because they have good formability and strength [13].

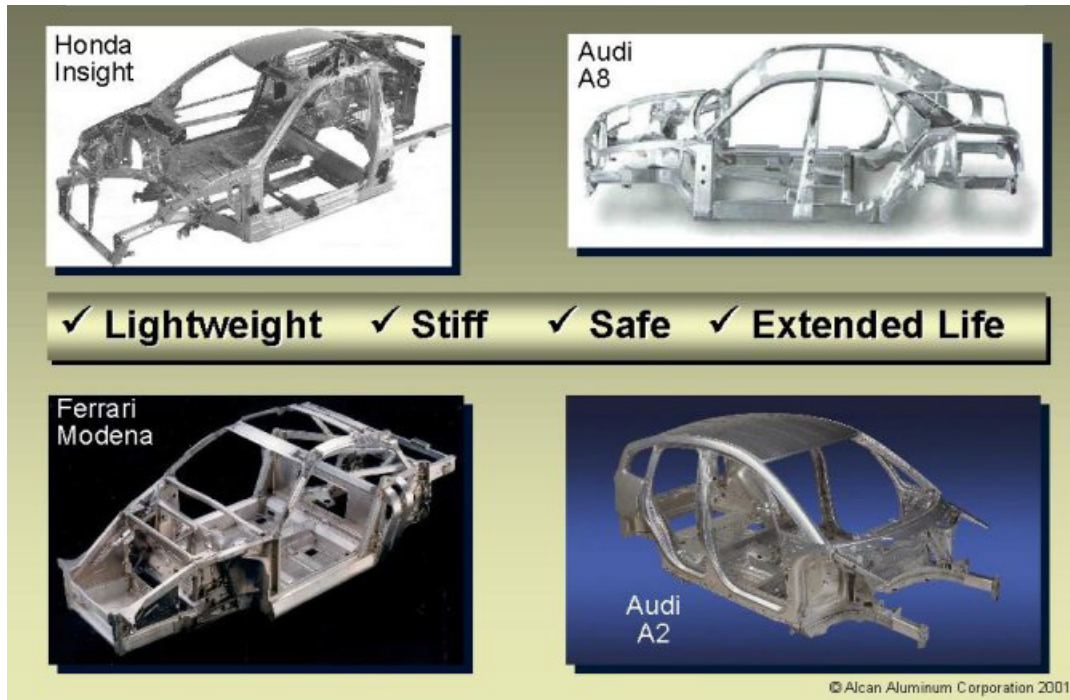


Figure 1.3: Use of aluminum alloys in autobody structure [19].

1.2.1 RSW of Aluminum Alloys

RSW of aluminum alloys compared with steel has two major problems; short electrode tip life and inconsistent weld quality or joint quality (joint strength, nugget size and shape, and microstructure of the weld pool) [21, 22]. The physical properties of aluminum are quite different from steel (Table 1.1) [15, 23]. Aluminum has three times the thermal and electrical conductivity of steel and a higher coefficient of thermal expansion. Thus, about three times more current is required to generate sufficient heat to perform resistance welding of aluminum alloys compare with similar gauges of steel [24]. At the same time, aluminum alloys form an oxide layer which has a high resistance to electrical current flow and thus

causes high contact resistance and generates high amounts of heat at the interfaces. This heat generation is essential at the FS for proper nugget formation but it is not welcome at the E/W interface. Furthermore, aluminum has a relatively low melting temperature (660 °C) which causes local melting of the sheet at the E/W interface. This local melting leads to early failure of the electrode and is discussed in next chapter.

Table 1.1: General Properties of Aluminum and Steel [15, 23].

Properties	Aluminum	Steel
Density (kg/m ³)	2700	7800
Melting Temperature (°C)	660	1510
Electrical Resistivity (μ Ω-cm)	2.82	18-45
Electrical Conductivity (%IACS)	65	10
Thermal Conductivity (W/m-K)	237	80
Coefficient of Thermal Expansion (10 ⁻⁶ /°C)	23	12
Heat Capacity (J/kg-K)	902	450

Due to these different characteristics of aluminum alloys compared with steel, the knowledge developed for RSW of steel cannot simply be applied to RSW of aluminum alloys. Therefore, a complete understanding of the RSW of aluminum alloys is necessary for successful mass production in auto industry.

1.3 Objective

For RSW of aluminum alloys, the early failure of the electrode to produce welds of adequate strength is a significant problem. It is necessary to understand the tribology of the E/W interface and FS contacts to address this problem. Thus, the main objective of this research is to relate electrode degradation and poor nugget formation during RSW of aluminum alloys to the tribology. The influence of the oxide layer, surface roughness and boundary lubrication at the E/W contact is to be examined in detail along with the macro-geometry of the E/W and FS contacts. The long term objective is to use the developed understanding to design ways to extend the effective life of the electrodes.

1.4 Approach

It is recognized that the entire RSW process involving materials, heat transfer, electrical current flow and solid mechanics, influences electrode degradation and nugget formation. Considerable research has been performed on the influence of the major process parameters (current, time and force), the design of the electrode itself and the influence of sheet thickness. However, the tribological features of the E/W and FS contacts have not been as rigorously examined. Thus, in the present thesis, the investigative focus is on the tribology with a particular emphasis on the E/W interface with both experimental and theoretical (FEA) approaches.

For the purposes of the present thesis, the major constants are force, current and time and they are held at typical values. In addition, all investigations were performed with a specific aluminum alloy (AA5182) and its bulk mechanical, electrical and thermal properties are also constants. However, various features of the oxide layer, surface roughness and boundary lubrication treated as independent variables while the dependent variables are the weld shear strength, electrical resistance, and contact area at the interfaces. In some cases, magnitude of

the current and current time were changed from typical values and used as independent variables.

Finally, based on the findings, a practical solution was presented to improve the electrode tip life during the RSW of aluminum alloys.

1.5 Thesis Outline

This thesis consists of eight chapters. Chapter 1 provides a background of RSW process, use of aluminum alloys and identifies a major problem associated with the RSW of aluminum alloys. This chapter gives some background, states the objectives and outlines the approaches of the present thesis. Chapter 2 presents a literature review on electrode degradation mechanism, contact resistance at the interfaces, effect of tribological characteristics (oxide layer, surface roughness, and boundary lubrication). Chapter 3 provides details of the experimental protocols, process constants, material constants, equipment and the application of finite element analysis (FEA). Chapter 4 presents the effects of certain features of the oxide layer and surface roughness on the electrical contact resistance at the E/W interface and the resulting pitting behaviour of electrode during the RSW process. Chapter 5 deals with the contact mechanics at the E/W while Chapter 6 deals with the contact mechanics of the FS interfaces. The results of FEA are also presented in these chapters. Chapter 7 presents a practical solution to improve the electrode tip life for RSW of aluminum alloys that consists of using a boundary lubricant at the E/W interface to increase the electrode tip life during RSW of aluminum alloys. Chapter 8 gives the conclusions of the present thesis and proposes future work.

Chapter-2

2 Literature Review

It was mentioned in the previous chapter that the RSW of aluminum alloys differ from that of steel although the basic principle is same. The RSW of steel is well established and presented in literature. Unfortunately, the knowledge available for steel cannot be readily transferred to the RSW of aluminum alloys. The selection criterion of welding parameters and welding schedule are not similar than that of steel and require a complete understanding of surface tribology as well as other electrical, thermal, and mechanical properties for a successful RSW of aluminum alloys. Considerable research has been done to understand RSW of aluminum alloys for developing optimal welding conditions and to improve the weld quality, including joint strength and the structural consistency of the weld (that can influence its long term fatigue life). However, more research is required before it can be successful in mass production. In particular, the present review of RSW considers the tribology of the electrode/worksheet (E/W) interface and faying surface (FS).

2.1 Electrical Contact Resistance

The essence of RSW is the use of electrical current flow with electrical resistance across the FS to focus the heat that is needed to cause a spot weld. However, this FS resistance is not the only electrical resistance in the system. In a typically RSW procedure (see Figure 1.1 in Chapter 1), there are seven electrical resistances (Figure 2.1) in series along the current path [8, 25-28]. These resistances sum to give the total resistance. The bulk resistances of

aluminum ($R_{worksheet}$) and the copper of the electrode ($R_{electrode}$) are minimal compare with the contact resistances ($R_{E/W}$ and R_{FS}) at the interfaces [26, 29]. Thus, unlike steel, the main heat generation is a consequence of the contact resistance at the interfaces rather than the bulk resistance of the worksheet [24-26].

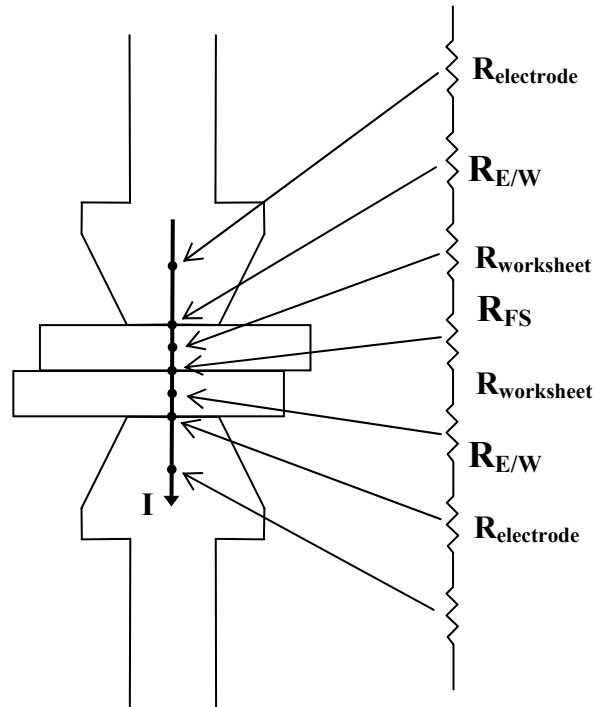


Figure 2.1: Electrical resistances in the current path during RSW.

The electrical contact resistance across the FS interface provides the main source of heating required for the formation of the weld nugget (Equation 1.1) while the electrical contact resistance across the E/W interface is generally unwanted because it reduces electrode tip life and has an indirect, often harmful, influence on weld quality [22, 26, 29-32]. A large electrical contact resistance at the FS is advantageous for the formation of a spot weld since it causes the heating that forms the weld. However, because the aluminum alloys have low bulk resistance, the resistance across the FS interface should not be too high because some of the current may then be diverted in the lateral direction to previously-formed neighboring

spot welds which could cause low heat generation and insufficient melting for a good joint. In addition, very high contact resistance can make nugget formation difficult to control in the early part of the welding process sequence (or "welding cycle") [31]. Overall, for a better weld quality, it is desirable to have a low contact resistance across the E/W interface along with a moderately high and uniform contact resistance across the FS interface [33].

The electrical contact resistances at these interfaces can be related to various tribological features of the contacting aluminum sheets. These features include the microstructure, consistency and thickness of the oxide layer; the height distribution of the surface roughness and the presence of a boundary lubricant at the worksheet surface [22, 26, 31-34]. The electrical contact resistance also depends very much on the extent of plastic deformation at the asperity contacts [29, 35-36]. In the subsequent sections of the present chapter, the term "contact resistance" refers to *electrical* not thermal contact resistance.

2.2 Some Tribological Features of the E/W and FS Interfaces

The short electrode tip life (compared with RSW of steel worksheets) is the consequence of the rapid development of pitting of the electrode surface due to high electrical contact resistance across the E/W interface [33]. The tribological characteristics of the aluminum alloy were considered to be the main reason for the high contact resistance. The present thesis has a focus on the E/W interface and considers the worksheet surface oxide layer, roughness and the presence of a boundary lubricant. Thus, these topics are considered in the following sections of the present literature review.

2.2.1 Surface Oxide Layer

Due to the reactivity of aluminum, an oxide surface layer is always present and quickly reforms if mechanically or chemically disrupted. According to Patrick et al [33], the rate of

oxide growth is a function of both time and temperature. The oxide layer is also influenced by alloy composition and the humidity of the storage conditions [37-39]. The oxide layer on an aluminum surface is often considered to be a uniform ceramic layer of aluminum oxide known as alumina. While this may be close to reality for high purity aluminum, the oxide layer on the aluminum alloy sheets for automotive bodies is very complex and with the addition of high temperature processes can result in formation of other oxide species such as magnesium oxide known as magnesia [33, 37].

Kucza et al [37] studied the effect of oxide characteristics on RSW of AA5182 alloy with a thickness of 1.2 mm. According to Kucza et al, the alumina (Al_2O_3) was the main oxide layer but right at its surface, regions of magnesia (MgO) formed. They presented a schematic illustration of oxide layers at the surface of AA5182 considering different processing and storage conditions (Figure 2.2). A range of surface oxides were obtained and the main factors affecting surface oxides were the final annealing (no details of time and temperature were given) and storage conditions (3 months in a humid area with relative humidity in the range of 20 – 85 % and temperature in the range of 2 -25 °C).

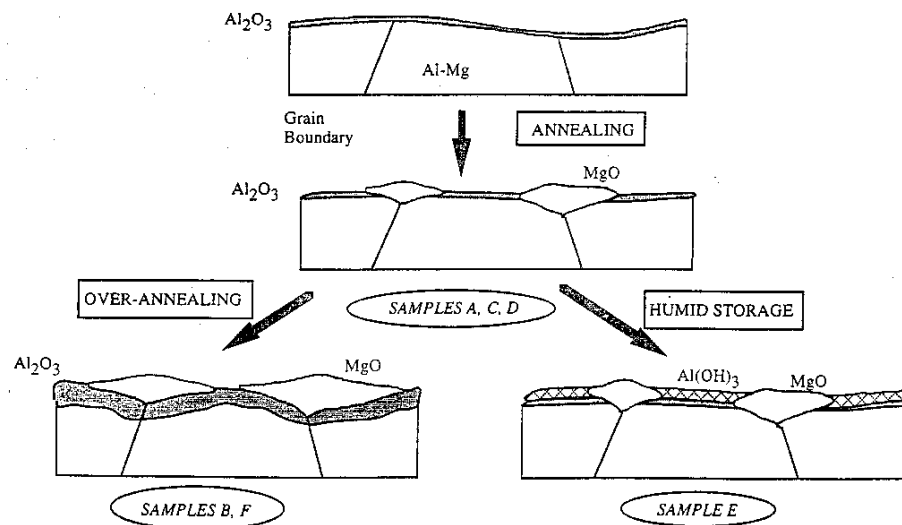


Figure 2.2: Schematic illustration of oxide growth of aluminum alloys (AA5182 in particular) from Kucza et al [37].

Kucza et al [37] also found that the range of weld current for acceptable joint quality was influenced by the surface condition. They reported that various thermal treatments (such as final annealing or heating before rolling) which develop MgO moved the required welding current to higher values. On the other hand, the oxide enriched by hydrated alumina (due to humid storage) allowed lower welding currents.

Ikeda et al [9] performed RSW on mill finished AA5182 of sheet thickness 1.0 mm with radius tip electrodes. They found that, with consecutive welding, electrode face was partly covered with MgO which localized the current conduction and hence affected the nugget formation. Ikeda et al also reported that the presence of MgO on the worn electrode face deteriorate the joint shear force and hence the electrode life. Ikeda et al [9] tried to suppress the formation of MgO on electrode face by coating the aluminum alloy worksheet with Chromate after removing the oxide layer from the sheet chemically. They found an optimal coating thickness that achieved extended electrode life and reliable joint quality. However, effect of the formation of MgO on the electrode face on the electrode pitting rate was not discussed. Also, how the bare surface behaved in terms of electrode pitting after removing the oxide layer chemically was also not reported.

So, the oxide layer at the AA5182 aluminum alloy surface can include alumina (Al_2O_3) and magnesia (MgO), both of which have high resistances to electrical current [40]. The oxide layer thickness on as-received surfaces is considered to be relatively thick and it is not possible to produce aluminum surfaces in large-scale manufacturing operation (such as automotive body fabrication) without this thick oxide layer. Current can only flow in RSW through the cracks in this layer which resulted in metal-to-metal contact between the contacting surfaces [5, 22, 26, 29, 31, 33, 41 and 42]. According to Patrick et al [33], the cracking of the oxide layer is essential for current flow in RSW. Patrick et al attributed this cracking of the hard brittle oxide layer to the deformation at the asperity tips but no details were available about the local contact stress and bending stress that developed in the oxide layer. Also, neither Patrick et al nor any other research have explained exactly how and where this cracking of the oxide layer occurs at the interfaces, this is particularly important at the E/W interface since it influences electrode pitting.

It is mentioned above that the oxide layer cracking results in metal-to-metal contacts essential for current flow during RSW. Although these contacts reduce the electrical resistance, they are very small in size and few in numbers [29, 31]. During the passage of current through these spots, the current density becomes very high and causes constriction resistance [43]. Since the oxide layer on as-received aluminum worksheet is relatively thick, the electrical resistances across the E/W and FS interfaces are essentially constriction resistances only [29-33, 44]. This constriction resistance causes the high heat generation at the FS needed for RSW but, at the E/W interface, it causes early degradation of the electrode tips.

Several studies [31, 33, 44-46] have shown the effect of oxide layer thickness on the contact resistance of the interfaces. Theory was proposed by Sun [44] and by Patrick et al [33] that the electrode deterioration mechanism would be different for thick and thin oxides on the aluminum sheet (Figure 2.3). However, for both these cases, they accounted the oxide layer on the worksheet surface and high weld current as the main reason for electrode deterioration. According to their explanation, when electrode was brought in contact with the worksheet with thick oxide layer, it caused non-uniform fracture in the oxide layer at very few spots, creating only few small areas for current conduction. When current was applied, it was forced to flow through these scattered points of constriction, this resulted in excessive localized heating resulting in both local melting and copper-aluminum alloying. When the electrode was separated from the worksheet, both pitting and pickup occurs caused aggressive electrode erosion. In this case, electrode degradation occurred vary rapidly until a stage was reached where good current distribution though the interfaces was not achieved.

However, when electrode brought into contact with a sheet with thin oxide layer, many current conduction spots would be established and uniformly distributed in the entire contact. In this case, the current conduction will be uniform compare with that of the thick oxide layer. Initially, only micro-pickup of aluminum occurred on the electrode face. As welding continued, alloying started gradually and copper-aluminum intermetallic were formed and would eventually transfer onto the aluminum sheet hence pitting of electrode. In this case, the electrode erosion occurred slowly and gradually until the stage was reached where good current distribution through interface was not achieved. Surprisingly, these works did not

provide any experimental evidence for the electrode deterioration rate. Thus, although the theory remained plausible, it needed to be examined in a detailed research investigation.

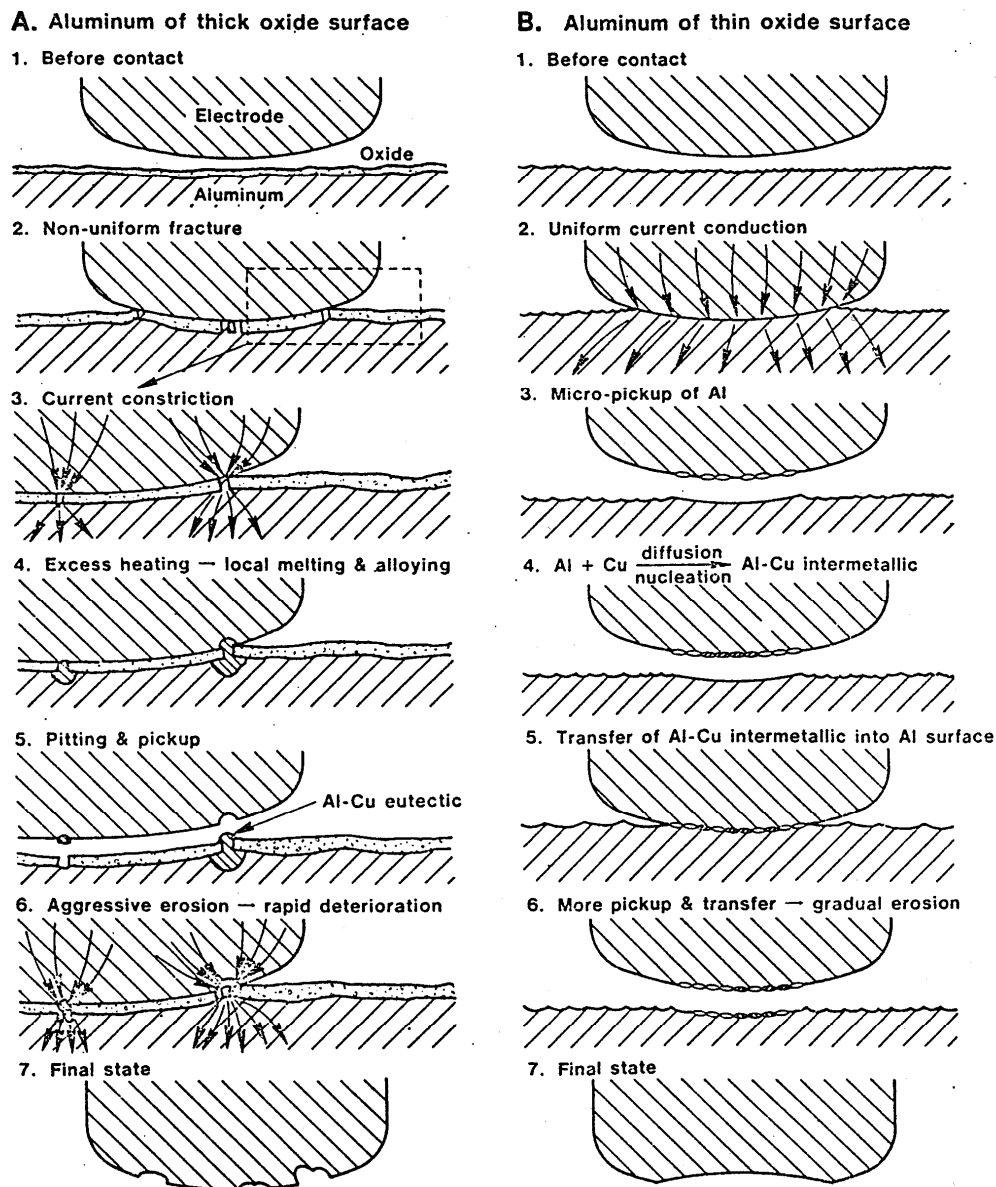


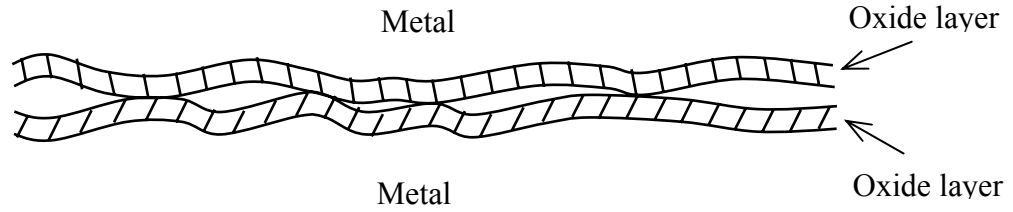
Figure 2.3: The differences in material transfer mechanisms for thick and thin oxide layers according to Patrick et al [33]. The oxide layer thickness was exaggerated to permit a view of the mechanisms.

2.2.2 Removal or Cracking of the Surface Oxide Layer

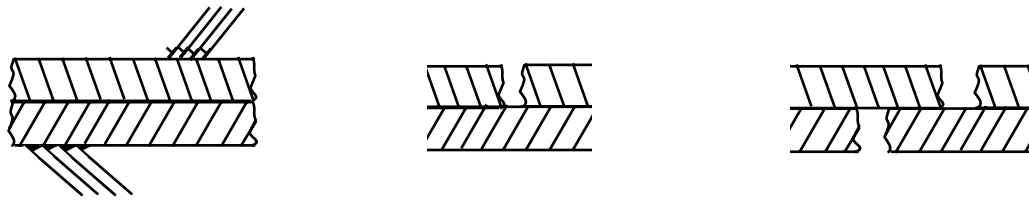
There are several ways and mechanisms that individually or simultaneously contribute to the removal or breaking of the oxide layer in RSW of aluminum alloys. Surface treatments were investigated in a number of studies [30, 33, 45, 47-49]. These surface treatments included chemical treatment of the worksheet surface and abrading or scratching the sheet surface. All these methods showed some improvement in reducing contact resistance at the E/W interface. However, most of these treatments were performed on both side of the sheet and thus reduced the electrical contact resistance at the FS as well. The reduction of contact resistance at the FS caused a reduction in nugget size and consequently in weld strength. The lack of understanding of the RSW process demonstrated by the application of surface treatments to both sides of the aluminum sheet clearly showed a need for research. An obvious approach would be applying surface treatments only to the aluminum surface at the E/W interface.

Rivett [49] studied the effect of sheet composition on electrode life of several aluminum alloys (2117, 3003, 5182, 6009, and 6010). Rivett performed several electrode life tests and a metallurgical investigation for each alloy. He found that the number of acceptable welds obtained for 2117, 5182, and 6010 aluminum alloys were primarily governed by the surface oxide layer of the alloy rather than the substrate composition. From electron spectroscopy for chemical analysis (ESCA), he found that scratching and chemical cleaning decreased the thickness of the oxide layer compared with an as-received surface. He claimed that the decrease was greatest for a chemical cleaning process performed on a particular aluminum alloy (AA5182). However, all these treatments were performed on both side of the worksheet and the contact resistance was measured for FS only which showed a drop in that contact resistance due to the treatments. The study by Rivett suggested the possible effect of oxide layer thickness and continuity on RSW. However, at the time (in 1980) the focus was on the faying surface rather than the E/W interface and thus he did not measure the electrical contact resistance at the E/W interface and was not able to link this resistance to the pitting of electrode and joint quality.

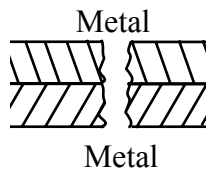
The load applied to the electrode and the resulting contact pressure is an important parameter in reducing the electrical contact resistance at the interfaces. However, applied load alone was not enough and required two basic conditions to be satisfied [50, 51]. Strain at and just below the worksheet surface due to high contact pressures caused by high loads was considered as one of the mechanism for oxide layer cracking of the aluminum surface. For example, Mohamed et al [50] proposed that if the hardness of the oxide layer was higher than that of the base aluminum alloy, the applied normal load would cause dislocation movement of the alloy material in lateral direction which ultimately would cause oxide layer fracture. Mohamed et al showed that in solid state bonding of high purity aluminum, where hardness of the oxide layer (1800 HV) was two orders of magnitude higher than aluminum (15 HV), the oxide layer fractured in brittle manner under the normal load. He also mentioned that since oxide layer was presented on every aluminum surface, the metal-to-metal contact would not be established until the cracks on both surfaces aligned together and the base metal extrude through them (Figure 2.4). Although this work of Mohamed et al [50] was for high purity aluminum which did involve RSW directly, the loading condition which established the metal-to-metal contact represents the tribological interaction of the FS when during squeezing process of RSW.



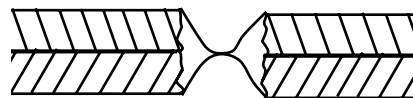
(a) Original Interface



(b) Fracture of brittle oxide layer (no metal-to-metal contact)



(c) First requirement: aligned oxide layer cracking



(d) Second requirement: metal extrusion through cracks (metal-to-metal contact)

Figure 2.4: Schematic illustration of metal-to-metal contact formation at the FS interface from Mohamed et al [50].

Some studies [29, 31] had suggested that significant shear stress at the interfaces along with the contact pressure could reduce the electrical contact resistance. James et al [29] calculated the shear stress at the E/W interface for 5xxx series coated aluminum sheet. They speculated that the ratio of the shear stress to normal pressure could become high enough to exceed the coefficient of friction and cause significant macroscopic slip near the periphery of the interface. They however, did not actually include any friction on their model and did not attempt to measure the amount of slip. Crinon et al [31] suggested that a small amount of sliding at was more effective in reducing the electrical contact resistance than the heavy axial load. They showed that even if shear stress was not present at the faying surface (FS), an induced sliding (by twisting the contacting sheets for a small degree under load) reduced the electrical contact resistance of that interface quite significantly. Although, these studies considered the effect of slip at the interfaces, attempts to measure the amount of slip were not found. Also, consideration of the effect of slip, at either the E/W or the FS interface, on the electrode degradation behaviour was not found in the literature.

2.2.3 Surface Roughness

When two surfaces meet each other and load is applied to press them against each other, the asperities are deformed as they make contact with each other. It has long been established that the actual or real area of contact between two metals is usually much smaller than apparent or nominal area of contact [97]. However, within the real area of contact, there are only small areas of direct metal-to-metal contact as a consequence of the oxide layer [26, 50, 52]. Studer [52] proposed five different regions within the contact zone of two surfaces covered with oxide layer (Figure 2.5). For aluminum alloys in RSW, region A and B were considered likely to be the only conduction paths for electric current. [29, 31, 33, 52].

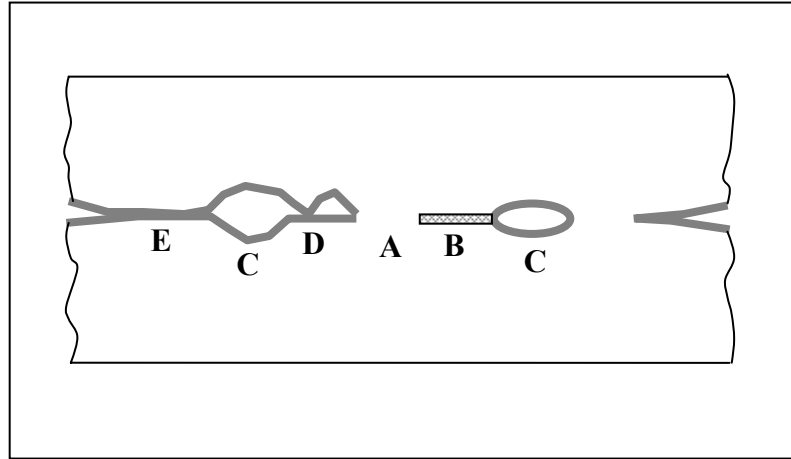


Figure 2.5: Schematic of different contact regions between two surfaces from Studer [52].

Region A was the actual metallic contact without any oxide film. Region B was the area where a mixed metallic contact and an oxide film were present. Region C showed an air gap between the two surfaces and thus a lack of contact of any kind. Finally, Region D and E showed contacts with oxide layers between them.

Roughening the worksheet surface and/or electrode tip was quite effective in reducing the electrical contact resistance at the interfaces [22, 30-33, 45, 47, 53-54]. Most of these works focused on the contact resistance of the FS and not the E/W interface. James et al [29] found the effect of worksheet roughness on the electrical contact resistance at the E/W interface. They used coated and abraded worksheet surface (AA5754) of Ra values 0.36 μm and 0.76 μm respectively. At a load of 6 kN, they reported a drop of resistance from about 100 $\mu\Omega$ for coated surface to about 10 $\mu\Omega$ for the abraded surface. Patrick et al [33] used polished radius electrode to measure the electrical contact resistance of different surfaces of 6xxx aluminum alloy with a load of 2.75 kN. They reported a drop of E/W electrical contact resistance of 2.97 m Ω for mill finished surface which had roughness in the range of 0.33 – 0.76 μm . to 0.11 m Ω for a belt sanded surface of roughness value of 1.2 μm .

In all these works, deformation at the asperity tips, as mentioned earlier, was one of the factors that helped increasing region A and B for more established metal-to-metal contacts. The ideal topography would be one that contained a high asperity peak density so that both uniformity and adequate breakdown could be achieved [33]. However, most of these works

attributed removal of oxide layer due to scratching as the only way to create lower electrical resistance. Crinon et al [31] investigated the effect of both oxide layer and surface roughness on the contact resistance of aluminum. They used 2 mm thick 5xxx series aluminum alloy and produced three different values of oxide layer thickness: 5 nm by precision grinding, 20 - 100 nm by oxidizing specimens in air at 300 °C and 200 - 2000 nm by oxidizing specimens in boiling water for 5 minutes. Samples were prepared with centre line average (Ra) surface roughness values of 0.03, 0.31 and 1.02 μm . The larger Ra roughness denoted larger asperities with tips of smaller radii. They found that the thicker oxide layers had a reduced contact resistance when they were on the rougher surface and that the thinner oxide layers gave a high contact resistance when on a smooth surface. Thus, large asperities with small tip radii were the most effective in breaking up oxide layers and thus reducing contact resistance.

2.2.4 Lubrication of the E/W Interface

In general, aluminum autobody parts undergo several processes (rolling, stamping, etc.) before being spot welded. These processes involve several lubricants that contaminate surface of those parts. No detailed research was found that investigated the effect of lubricant on RSW and/or electrode life. However, some research [22, 30, 32] did suggest even faster electrode degradation when those lubricants were present on the worksheet surface during RSW of aluminum alloys.

Sugimura et al [55] worked with some usual industrial lubricants (oils and waxes) to see their effect on contact resistance for some metals but not aluminum. They found that for each metallic contact, there was at least one suitable lubricant that reduced the electrical contact resistance. Although their work was not specifically related to RSW and was not for aluminum, it did suggest that lubricants might reduce the contact resistance at the E/W interface. This might help reducing heat generation at the E/W interface and hence might extend electrode life.

2.3 Electrode Degradation Mechanisms

It was presented in the previous section that a high electrical resistance at the FS was required for good quality weld while it was not required at the E/W interface, since it could result in early failure of electrode tip and inconsistent weld strength and/or structural consistency. This section will present an overview of the high heat generation at the E/W interface and resulted electrode degradation mechanism. For galvanized steel, the degradation mechanisms appeared to be electrode deformation, alloying, and surface pitting [78]. Unlike steel, the electrode deformation does not appear to be a major factor in RSW of aluminum alloys. Instead, alloying between electrode and worksheet and subsequent loss of material from the electrode was considered as the main degradation mechanism [33, 56-59]. Dilthey et al [56] performed metallurgical investigation of this phenomenon at the E/W interface. They concluded that the high electrical contact resistance at the E/W interface caused high heat generation which resulted in local diffusion between electrode and worksheet material. This diffusion led to alloying between aluminum (worksheet) and copper (electrode) to form new Cu-Al intermetallic phases. The rate of diffusion was subject to the high temperatures of the E/W interface and increased even more with high welding pressure. They also proposed that the diffusion started from the very first weld. After the diffusion weld was formed, the material transfer sequence follows one of three possible scenarios (Figure 2.6).

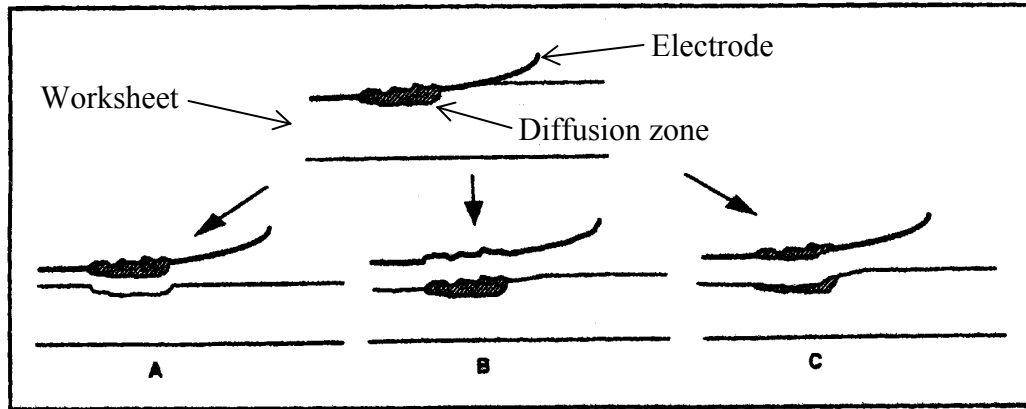


Figure 2.6: Material transfer morphology by Dilthey et al [56]. Case A represents a situation where the intermetallic Cu-Al phase remained stick to the electrode and is known as ‘pick-up’. Case B represents a situation where the intermetallic Cu-Al phase breaks from the electrode and remains with the worksheet and is known as ‘pitting’. Case C is a situation where both pick-up and pitting happened partially and simultaneously. In all cases, subsequent welding with the same electrode would cause further current concentration and enhance the material transfer and thus electrode degradation.

Further research on electrode degradation was conducted using AA5182 with a sheet thickness of 1.5 mm [57-59]. Metallurgical details of electrode degradation mechanism and their influence on electrode life was explained. Lum [57] performed three electrode life tests on this alloy using spherical tip electrodes. These tests included obtaining carbon imprints of electrode at different stages of the tests, and metallurgical analysis after specific numbers of welds with the same electrode. Joint strength measurements were also performed by subjecting the spot welds to an increasing shear force until they failed (Figure 2.7). Electrode life was defined as the weld number when the strength fell below 80% of the initial value [57, 59].

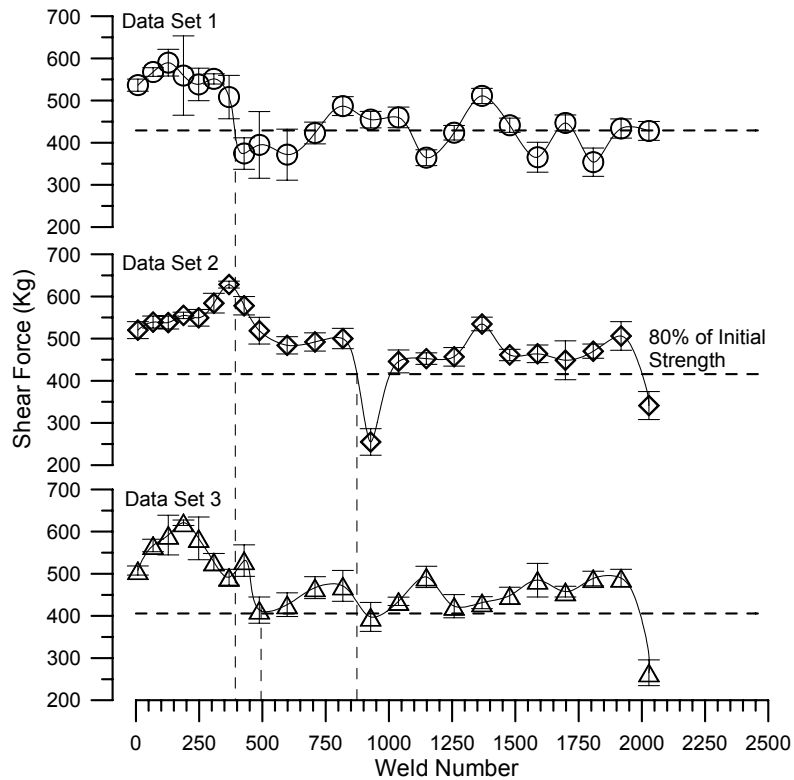


Figure 2.7: Shear force versus weld number for RSW of aluminum sheet [59].

The joint strength tests indicated a tip life ranging from 400 to 900 spot welds for nominally identical electrodes with all process variables held constant. Data sets 1 and 3 had similar values for life whereas set 2 had a much longer life. Lum [57] explained this apparent inconsistency as a consequence of the inherent scatter in the fatigue wear (pitting) of the electrode tips and other uncontrolled variables such as humidity [59]. However, despite the large variation in electrode life, distinct patterns were found in the tests. Based on his findings, electrode life was divided into four stages and the variation of joint strength can be explained in term of contact area at the E/W interface and pitting of electrode (Figure 2.8) as follows:

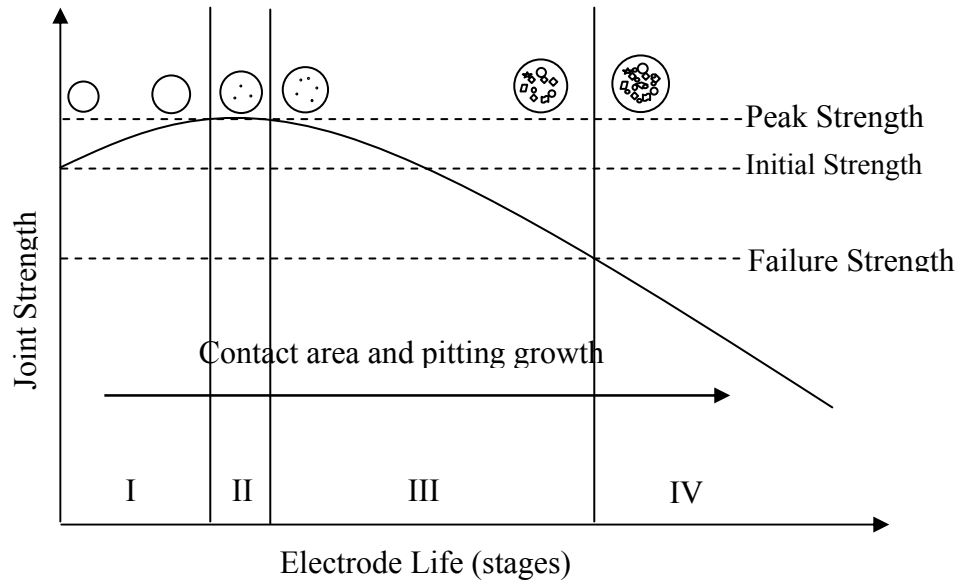


Figure 2.8: Schematic illustration of the four-stages of electrode life; correlating the joint strength with contact area between electrode and worksheet and pitting of electrode.

- Stage I:** The contact area grows slowly without any significant pitting, and joint strength increases.
- Stage II:** Joint strength reached maximum as contact area continue to grow with incipient pitting of electrode.
- Stage III:** Joint strength starts decreasing as the contact area continues to grow but, at the same time, the pitting of electrode become significant and continues to form large cavities.
- Stage IV:** Joint strength reaches the failure criterion as large cavities appear on the tip surface of electrodes.

Lum et al [59] followed concentrated on studying the electrode pitting with carbon imprints taken at different stages during these tests. They noted that the pitting (sometimes called electrode degradation) which eventually led to the previously defined tip failure stage, followed four basic steps during RSW of AA5182 (Figure 2.9).

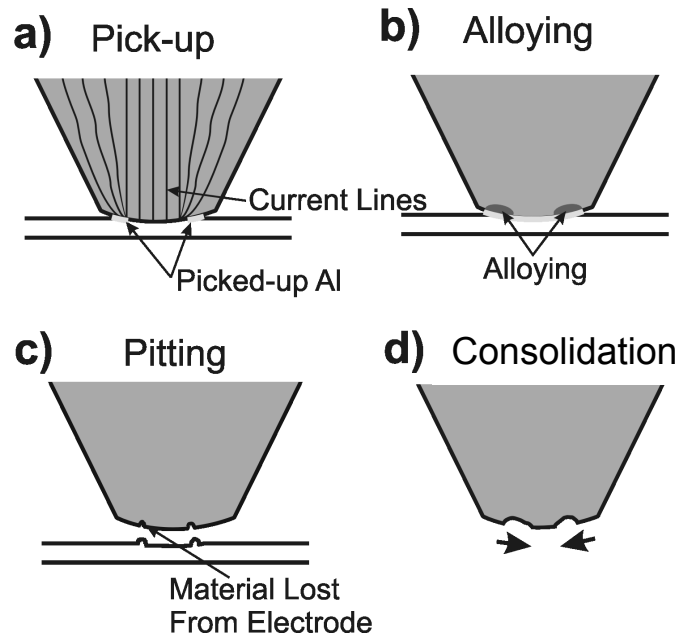


Figure 2.9: Four steps of electrode degradation in RSW of aluminum alloys according to Lum et al [59].

Al pickup: Electrode picked up aluminum (Al) from the first weld as tiny molten drops.

Alloying: Copper-aluminum (Cu-Al) intermetallic compounds were formed at the interface between the Cu (electrode) and Al (workpiece).

Pitting: The breaking up of the alloyed regions, either through transfer of molten Cu-Al mixture or brittle fracture of solidified Cu-Al intermetallic phases, would result in electrode pitting.

Consolidation: Consolidation of the pits into large cavities occurred.

All of the research described above attributed the electrode pitting to high heat generation at the E/W interface. However, these studies did not explain the initiation of electrode pitting or its relationship to nugget growth behaviour.

2.4 Sheet Separation

The term 'sheet separation' in RSW is defined as an opening of the two worksheets at the FS when load is applied and welding is performed. It occurred both due to load effect and thermal effect [6]. The electrode force acts as a lever as outer contact diameter as fulcrum of the lever. During heating and cooling, the expansion and contraction of the fusion zone cause sheet separation. Softer worksheet material as aluminum and/or heavy load which is used for RSW of aluminum alloys enhances the sheet separation [6, 13]. Before squeezing, the FS interface is considered to be one perfectly flat horizontal plane with a large "apparent" contact area. However, on a micro-scale, there are only a few contact spots at the asperity tips that sum to give the "real" area of contact [97]. As the squeezing force is applied, the apparent contact area at the FS interface reduces dramatically [60] because of sheet separation which is a feature of RSW for aluminum alloys. Worksheet separation occurs at the edges of the apparent area of contact and this separation can be used to define a plastic deformation zone and the apparent contact area at the FS interface [60, 61]. Ikeda et al [13] studied the effect of electrode geometry on the electrode life of AA5182 of thickness 1.2 mm and found that severe sheet separation reduced the reliability of the weld joint quality. They also found that electrode geometry was influential on the sheet separation and spherical electrodes produce less sheet separation than flat tip electrodes [16]. Although sheet separation appears to be an important characteristic of RSW of aluminum alloys [16], the present author is not aware of any detailed tribological and metallurgical research efforts that relate this phenomenon to the nugget formation and nugget growth.

2.5 Variability of the Experimental Data

The variability of any experimental measurement involving RSW of aluminum alloys was well known and reported by many [26, 30, 32, 49, 52, 59, 62]. In general, results are often presented in terms of average of the measurements to observe some sort of trends [30, 32, 59]. Thornton et al [30] attempted to find the effect of roughness of electrode tip and worksheet

surface on the contact resistance. They discussed the variability of the data and presented average values.

Usually, this variability is inherent in the process due to the variability of the surface characteristics of worksheet which influence contact resistance directly. This contact resistance is controlled by many factors such as oxide layer, asperity cracking, etc, and difficult to eliminate completely. And therefore, the repeatability of these experiments is limited and standards suitable for one surface could not be suitable for other similar surfaces [26].

Studer [52] reported this sort of variability during the measurement of contact resistance. He described the difficulty of repeating an experiment in these words “it does give an experimenter a sort of feeling of frustration, if, after making a very careful set of experiments on very carefully prepared surfaces, he attempts to check his results with another set of samples prepared in apparently just the same way and he finds that the resistance values are approximately halved or doubled!”

Ivan [59] presented three electrode life tests on AA5182 worksheet using spherical tip truncated electrodes. They found that one of the electrode test results was almost double than the other two tests. He speculated that the variability could be due to the inherent scatter of the electrode pitting behaviour and other uncontrolled variables such as humidity.

In the opinion of the present author, the problem lies in the cascading nature of tribological wear phenomena. The pitting involved in electrode degradation is essentially a wear process. In certain regions of the contact pitting occurs depending on a combination of surface parameters (some experimentally controlled and others not controlled). The pitting then goes on to become progressively worse in this region or stays the same, again depending on a combination of surface parameters. Thus, the initial pitting and the progressive behaviour or cascading is all subject to complex interactions of surface parameters. The result is scatter at an instant in time that depends not just on the current welding conditions but on the cumulative history of welding. The overall statistical variation at an instant in time is unlikely to be Gaussian and thus conventional statistical methods based on Gaussian

distributions often fail to represent the variation properly. The only recourse is to apply conventional statistical analysis but treat the findings with caution and to perform large amounts of testing to try to obtain the full range of possible variation.

2.6 Various Research Approaches

2.6.1 Surface Treatment

As mentioned earlier, surface treatment is always an option for improving weld quality and electrode tip life for RSW of aluminum alloys [30, 49, 62-65]. These include chemical treatment, arc cleaning (the removal of oxide layer from the negatively charged aluminum worksheet by the bombardment of positively charged argon ions), and roughening of the worksheet surface. All of these procedures are related to the tribological features of the worksheet surface and details have been presented earlier in the present chapter.

2.6.2 Welding Parameter Selection

For a given surface condition, the choice of welding parameters can influence the electrode life and weld quality [36, 53, 66-67]. As mentioned earlier, the major parameters in RSW are current, weld time, and force.

Current is an important process parameter in spot welding. As shown previously in Equation 1.1, total heat generation which causes nugget formation is proportional to the square of the current. Obviously, an increase of current, with other variables held constant, causes the temperature at the E/W interface to increase, leading to higher rates of diffusion of aluminum into the copper electrode and increased rates of alloying. It is therefore believed that

electrode life will be maximized with the use of the lowest current that can give enough heat at the FS surface to produce a large, consistent and strong enough weld [6, 53, 59, 68].

Weld time (the time during which current is allowed to pass through the interfaces) is another important process parameter [6, 59, 68]. It is obvious that with excessively long weld times (equation 1.1), more diffusion occurs at the interface of aluminum sheet and copper electrode thus increasing alloying and pitting. Excessively short weld times are also inappropriate because a much higher current is then needed to achieve a suitable weld and thus high temperatures occur at the E/W interface which could cause early failure of electrode [68]. Kimchi and Gould [69] found that for the welding of galvanized steel, intermediate weld times resulted in the longest electrode lives.

The force is also an important parameter which helps creating metal-to-metal contact for the current path during RSW of aluminum alloys [16, 29, 36, 53]. The force during the spot weld process must be sufficient to contain the molten nugget, otherwise expulsion occurs. For aluminum alloys, since the oxide layer is very hard, a high squeezing force is required to crack the layer for better metal-to-metal contacts. However, a very high force can damage the sheet significantly by causing excessive plastic deformation and therefore a balance force is essential for better weld quality [9, 16].

All of the above discussion essentially means that acceptable welds can occur for shorter times with higher currents and/or forces, or longer times with lower currents and/or forces but, for the best results in terms of electrode life, an intermediate time with intermediate currents and/or forces is needed. In the present thesis, the weld parameters are held at "intermediate" values while certain tribological features of the E/W and FS interfaces are investigated.

2.6.3 Electrode Material

One strategy for improving the electrode life is to study novel electrode materials. The electrode material must have low resistance, high thermal conductivity, high mechanical

strength (particularly at high temperature) and resistance to alloying with aluminum [6]. In one study involving spot welding 1 mm thick 5182 aluminum sheet, the electrode materials tested were: Cr-Cu, Cd-Cu, Co-Be-Cu, Te-Cu, and W-Cu [71] where Cr is chromium, Cu is copper, Cd is cadmium, Co is cobalt, Be is beryllium, Te is tellurium, and W is tungsten. The W-Cu displayed the worst performance, with only 5 welds being made before electrode sticking was so severe that the test had to be stopped. The Cd-Cu electrode performed the best, with a life of 300 welds. The electrode material obviously affected the electrode life. Composite electrodes had also been used for spot welding [72]. These electrodes were developed and tested for galvanized steels, but might also find application in aluminum spot welding.

2.6.4 Electrode Surface Coatings

Another approach that received some interest for improving the life of electrodes, involves placing surface coatings on the electrode face. A mixed response regarding the success of this method was available in literature [73, 74]. Ostgaard [73] tried different coatings on electrode tip and found that all those coatings increased the electrical contact resistance at the E/W interface. As a result of the higher interface temperatures, [73] the coatings were very quickly ruined. Glagola [74] attempted RSW of aluminum alloys with nickel plated electrodes. He used several techniques to deposit coating on the electrode tip face and developed one that improved electrode life. To achieve improved performance, the coating must remain adhered to the substrate, continuous and must withstand the thermal and mechanical shock experienced during spot welding [73-75]. The coating should also be smooth and uniform to eliminate stress concentrations at the E/W interface. However, these studies [73, 74] of this approach have been conducted without overwhelming success.

2.6.5 Electrode Geometry

Electrode geometry is an important factor in its life, as shown experimentally by Bowers et al [76] for RSW of galvanized steel. They found that a low truncation angle resulted in a reduced electrode life. In another study by Ikeda et al. [16], electrode geometries were also investigated for RSW of galvanized steel and aluminum. Interestingly, they found that a larger truncation angle resulting in an increased electrode life for RSW of aluminum because face enlargement was delayed. Ikeda et al also found that flat tip electrodes damage sheet surface significantly and hence spherical electrodes were recommended. In general, a truncated electrode with large truncation angle and a spherical tip was recommended [16, 76-78]. Such electrodes were used in the present thesis.

2.6.6 Re-dressing the Electrode Tips

For RSW of sheet steel, it is very common to perform tip dressing in which the electrode tips are machined to restore them to almost the original condition [78]. This involves using a cutting tool and reshaping the surface of the electrode and thus maintaining constant contact diameter. This is used in RSW of steel because tip "mushrooming" is a major problem. However, in RSW of aluminum, the problem is not mushrooming but alloying and the resulting pitting. The large scale removal of electrode material using a cutting tool may be an unnecessarily drastic procedure for the RSW electrodes used for aluminum. Aerospace manufacturers re-dress their electrode tips frequently, once every 10 or 20 welds [80]. Recently, Ivan et al [57-59] published their work on periodic re-dressing of the electrode using a scotch-brite wheel during RSW of aluminum alloys. They showed longer electrode life with periodic re-dressing. They also reported that frequency of the re-dressing was an important factor for longer electrode life.

2.6.7 Simulation with Finite Element Analysis

In RSW it is very difficult to experimentally observe the nugget formation and weld pool behaviour during the welding [60]. However, various techniques can be used to evaluate the joint properties and microstructures after the weld being completed. These include mechanical testing such as joint strength measurement, hardness testing and metallography and high resolution microscopy such as SEM, XRD. All of these techniques and evaluation are used for already completed weld nugget and very little is known about the start of welding when the melting and/or diffusion begin at the interfaces along with pitting and nugget growth.

Finite element analysis (FEA) allows a simulation of the complete weld process and weld growth can be examined at any stage. For RSW of steel, FEA has been successfully applied [84, 87-88, 99] but for RSW of aluminum alloys, FEA is still not well established. Several assumptions were used to simulate the RSW of aluminum alloys [60-61, 83, 85]. Because of the loading mechanism and weld schedule (squeezing, current, hold), RSW is represented as an incrementally coupled electrical- thermal-mechanical process [60-61, 83-88, 90-91]. In some FEA investigations, flat tip electrodes are used and it is assumed that the contact area at the interfaces remains constant. However, for spherical-tipped electrodes which are often used for RSW of aluminum alloys, the contact area changes due to plastic deformation [61, 84] and this effect has to be considered in the FEA.

There were some studies [60-61, 83] that used spherical electrode for the finite element analysis of RSW of aluminum alloys. Sun et al [61] developed a coupled electrical-thermal-mechanical model using finite element method. The developed the model using 2-inch radius truncated electrodes and 2 mm 5xxx aluminum worksheet. Axisymmetrical model was developed with the help of commercial finite element code ABAQUS. Sun et al accounted the model suitable for predicting contact area change at the interfaces, electrode displacement, weld indentation, residual stresses and sheet separation. They showed that the plastic strain could be used to indicate the contact diameter at the E/W interface. However, their model mainly concentrated on the welding behaviour during the current phase of the RSW process.

Few details were presented on the mechanical behaviour of the interfaces during the squeezing of the worksheet between electrodes before the passage of weld current. Also, Sun et al did not give the stress distribution due to squeezing which is likely to be important in understanding the pitting behaviour of electrode and nugget growth. Also, Although, Sun et al allowed slip to occur at the E/W interface, no detail was available about this formulation or coefficient of friction.

Chang et al [83] used spherical tip truncated electrodes on AA5182 worksheet of thickness 1.5 mm. They simulated effect of electrode pitting by using pre-drilled electrodes by using several electrodes with several pre-drilled diameter at the centre of the tip. They used another commercial software ANSYS for the analysis and accounted the model for contact area change, current distribution, and temperature analysis. Chang et al found FEA as a useful method for predicting effect of electrode pitting during RSW of aluminum alloys. However, their study mainly focused on the thermal behaviour during the weld current. Chang et al did not present any details about the mechanical behaviour of the interfaces before the start of weld current.

Zhang et al [60] also used 50 mm spherical tip standard electrodes on pre-treated AA5754 sheet with a thickness of 2.0 mm. Instead of using conventional quarter model which consist of upper electrode and upper worksheet only, they used an axisymmetric half-model which showed both the upper and lower electrodes and both worksheets. A commercial FEA software package (ABAQUS) was employed that permitted elastic-plastic analysis. Zhang et al calculated the contact area change at the interfaces, equivalent plastic strain, and residual stress histories for various input conditions. They showed that the equivalent plastic strain at the interfaces was a good indicator of the actual plastic deformation at the interfaces. They determined the contact area at the E/W interface and the sheet separation at the FS interface. Zhang et al showed the plastic strain distribution of their model after the initial mechanical loading with a weld force of 7 kN before applying any weld current (Figure 2.10). Unfortunately, the details of the stress distributions at the interfaces during squeezing were not presented.

Interestingly, none of these researches analyzed the effect of mechanical behaviour during squeezing on the heat generation at the interfaces at the start of weld current. It is important to explain the interaction of the interfaces after loading and before the current is applied in order to explain the details of electrode pitting and nugget growth.

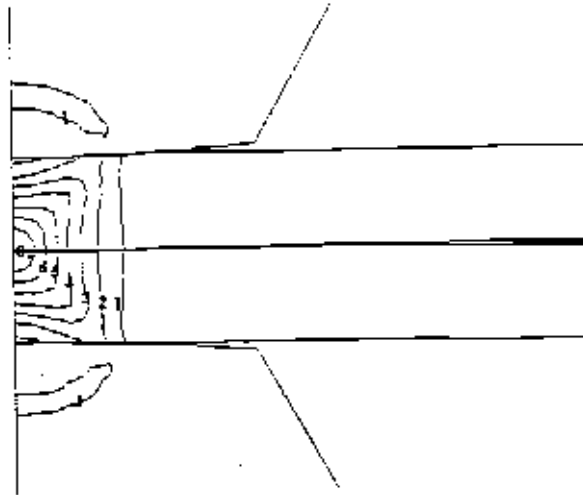


Figure 2.10: Plastic strain distribution (after squeezing only) defining the contact area at the interfaces [60]. Min (1) 2.20×10^{-3} , Max (8): 27×10^{-2} , Inc: 3.54×10^{-3} .

2.7 Concluding Remarks

The present chapter reviewed some work related to RSW of aluminum alloys. It was found that, in case of aluminum alloys, tribological characteristics of the E/W and FS interfaces are likely to play an important role in electrode life and weld quality. However, although the literature presents metallurgical details of electrode degradation mechanisms, there are some approaches that are still incomplete.

For example, the breaking of oxide layer was essential for RSW of aluminum alloys but the location of this cracking and resulting heat generation behaviour at the E/W and FS interfaces

was not available. This, in turn, is very important to explain pitting and nugget growth patterns during the RSW of aluminum alloys.

Most of the FEA related to RSW of aluminum alloys concentrated on the behaviour of the process during weld current. Details of the mechanical behaviour of the interfaces, during the squeezing of worksheet by electrode before the application of weld current, were not available. A complete FEA simulation of the mechanical loading of RSW that includes friction at the interfaces was required.

Also, as mentioned earlier, opportunities exist to find a lubricant that can extend the electrode life without delaying the RSW process and this can provide a practical method for the industry to extend electrode tip life.

Chapter – 3

3 Materials and Methods

RSW of aluminum alloys is the main subject of the present thesis. The main objective is to relate electrode degradation and nugget formation during RSW of aluminum alloys to the tribology of the E/W and FS interfaces. Following from the investigation of the tribology, a way to improve the electrode life without altering the actual RSW sequence was proposed. As discussed earlier, aluminum alloys are gaining popularity due to their weight saving advantage and corrosion resistance property. The present research uses an aluminum alloy that is very popular in automotive industry for auto body and reinforced inner parts [16, 37]. Thus, there is a strong practical foundation. As a result, a broad range of experimental and analytical approaches were taken in an effort to find results that could lead to improvements in electrode life.

Extensive RSW experiments were performed on different worksheet surface conditions to evaluate the effect of tribological surface characteristics on electrode tip life. Several other short run experiments were designed to analyze and understand the problems in details. In addition to experiments, finite element analysis was conducted to explain some of the experimental findings related to the contact mechanics of the interfaces. Details of the materials used in this work, experimental procedure adopted, equipment and tools used, and the approach to the finite element analysis are presented in the following sections.

3.1 Materials

All welding and other experiments were done on samples made from sheet of aluminum alloy 5182 (AA5182) supplied by ALCAN International. The sheet was supplied in mill finished condition in two different sizes of 1.8 x 1.0 m and 2.0 x 1.55 m with the rolling direction identified. The nominal thickness of the sheets was 1.5 mm with chemical composition as shown in Table 3.1. Although, there was no apparent difference in the appearance of the two surfaces of an individual sheet, the upper surfaces as received in the skid were designated as the “top” because there might be some slight differences between them and the corresponding “bottom” surfaces. For the sake of consistency, the E/W interfaces were always made with the top surfaces while the FS interfaces were always made with the bottom surfaces.

Table 3.1: Chemical composition of AA5182.

Element	Weight %
Mg	4.71
Mn	0.32
Fe	0.19
Si	0.08
Cu	0.05
Cr	0.01
Zn	0.01
Ti	0.02
Al	Balance

All welding experiments were performed using MIL–W–6858D standards [79] and samples for welding were cut out by metal shears in two different sizes of strips with the longer

dimension in the direction of rolling (Figure 3.1). From these strips, standard welding coupons for spot welding and conditioning (Figure 3.2), overlapped samples for joint shear force measurement (Figure 3.3) and other samples were made.

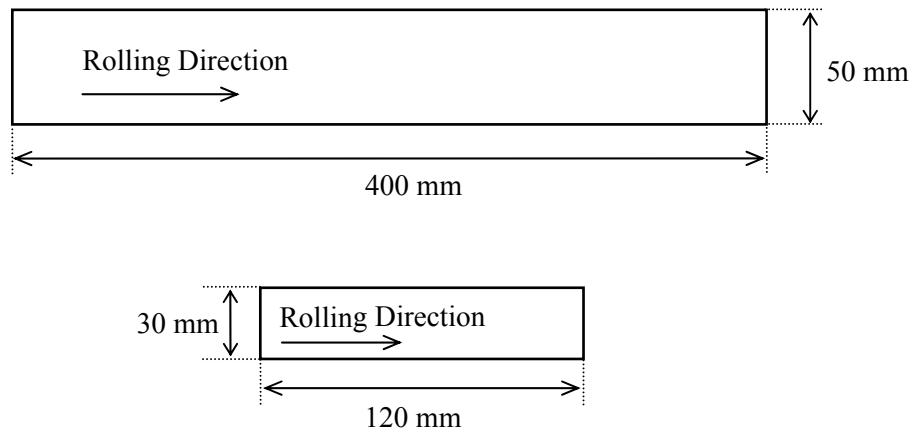
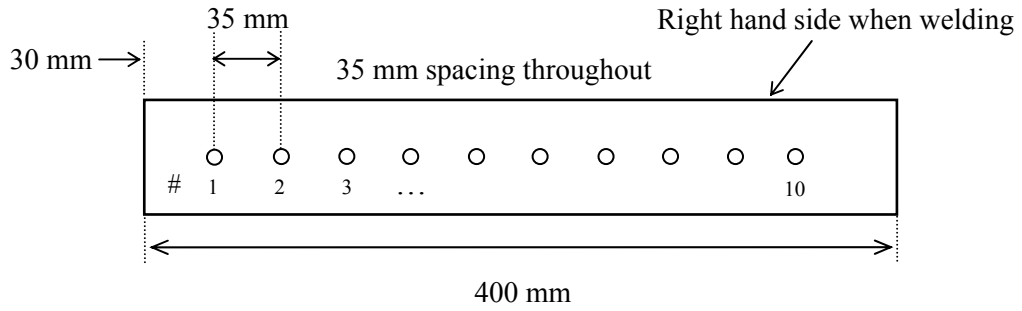
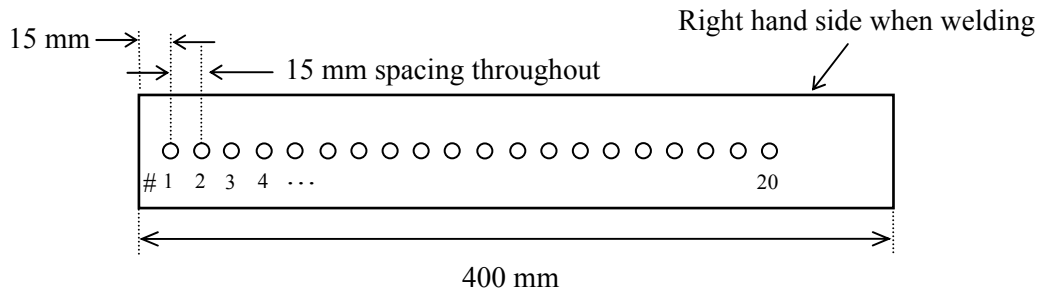


Figure 3.1: Dimension and orientation of sheared strips used for sample preparation



(a)



(b)

Figure 3.2: Geometry of weld specimens and orientations for welding (a) 10-weld standard coupon and (b) conditioning coupon.

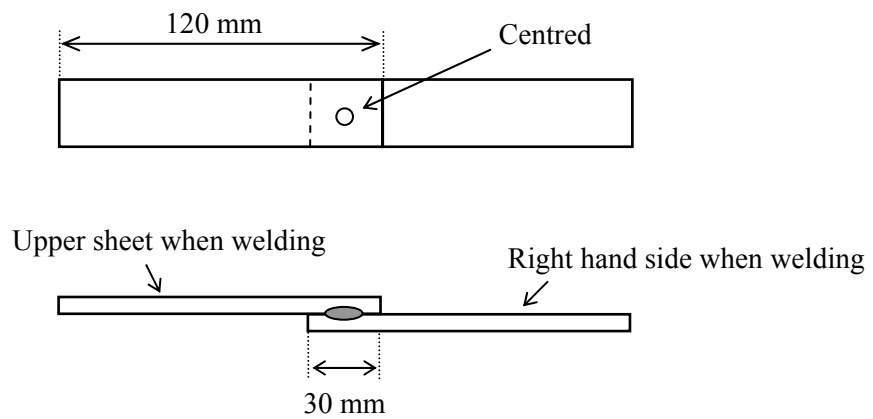


Figure 3.3: Geometry and orientation of overlapped specimen for joint shear force measurement.

The electrodes used in the present thesis were all Class I Type made from material C-15000 which is a copper base alloy containing 0.15 % zirconium [6]. These electrodes were truncated cones as shown in Figure 3.4. The contacting surface was spherical with a radius of 50 mm and a face diameter of 10 mm.

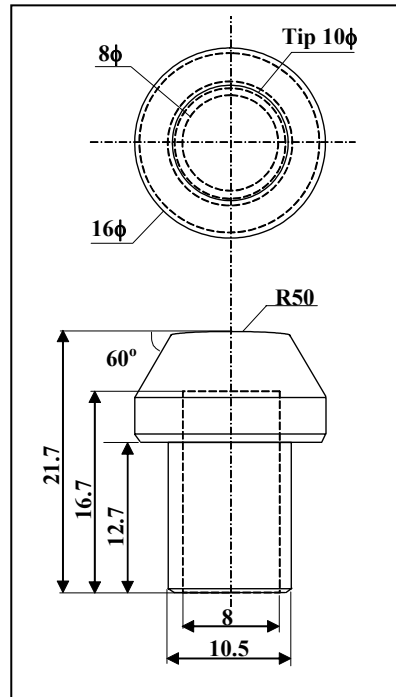


Figure 3.4: Electrode geometry (all dimensions in mm).

3.2 Equipment

Spot Welder: All welding experiments were conducted using a 170 – kVA medium frequency direct current (MFDC) spot welding machine (custom made for University of Waterloo by Centerline Ltd, Windsor, Canada). It is a pedestal type spot welder capable of producing a 60 kA secondary current (Figure 3.5). The weld force can be controlled in a two stage process with low initial ‘tip closing’ force followed by a higher welding force. The force was applied by an air-over-oil cylinder capable of producing up to a maximum of 22.7

kN. The same welder was used for clamping specimens and applying load for contact resistance measurements.

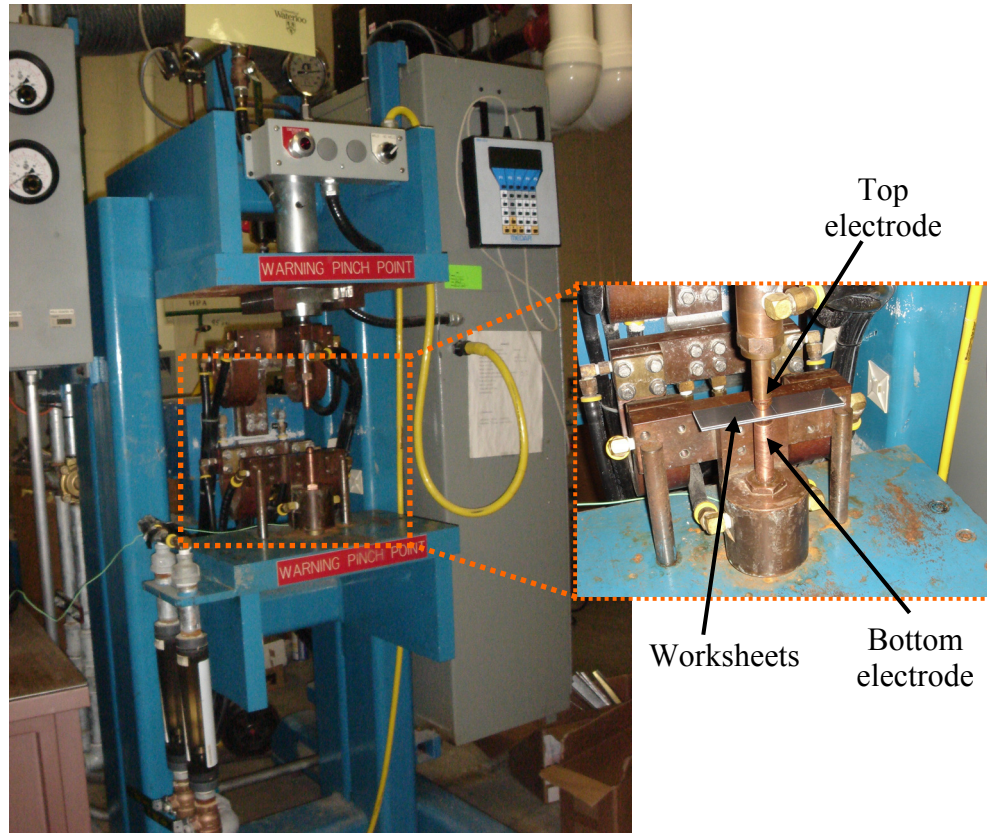


Figure 3.5: MFDC Resistance spot welder used in the present study.

The weld controller used with the spot welder was a Medar Med Weld 3005 Integrated Weld Control capable of storing 31 separate weld schedule. The Weld controller converts the three-phase AC to single phase high frequency DC current in three stages [109]. The output MFDC current remains essentially constant. The peak current and the RMS current are almost similar in intensity as compared to the low frequency AC or DC systems. A typical current waveform of the MFDC spot welder is presented in Figure 3.6. The small window is showing the actual DC current wave form obtained during RSW from the above spot welder and controller.

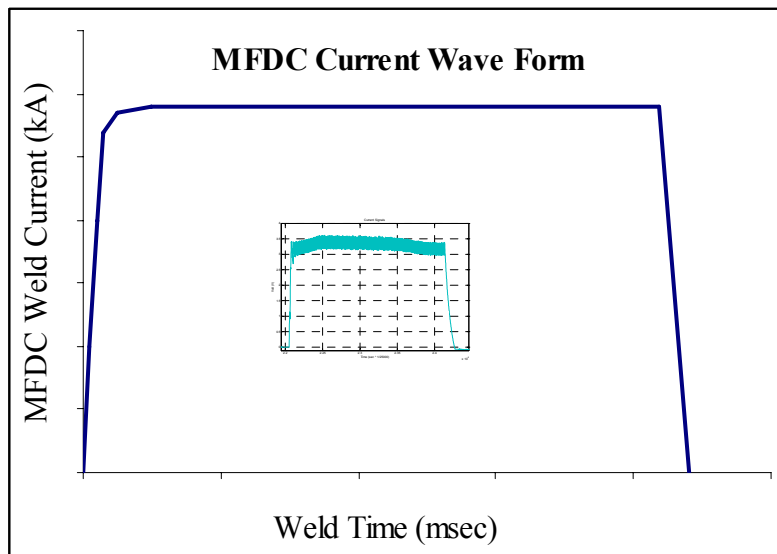


Figure 3.6: Typical current wave-form of the MFDC spot welder.

Weld Force Gauge: For weld force calibration before any experiment, a Digital Hydraulic Weld Force Gauge (Tuffaloy Products, Greer, SC) was used. This gauge was capable of measuring weld force up to about 13 kN (3000 lbs) with an accuracy of 1%

Ohm-meter: All contact resistance measurements were conducted with a low resistance ohm-meter (DLRO 10X) manufactured by AVO International Ltd. It can apply measure current automatically or a current selection can be selected manually in the range of 11 μA to 10 A. The resistance, in the range from 0.1 $\mu\Omega$ to 2 k Ω , was calculated by measuring the voltage across the terminals.

Surface Profilometer: The values of centerline average roughness (R_a) were obtained with a direct contact profilometer Surtronic 3+ Roughness Checker manufactured by Taylor-Hobson Ltd, Leicester, UK. Also, a non-contact optical profiler (WYKO Surface Profiler, Veeco Metrology Group, USA) was used to measure R_a values and to obtain 3-D images of regular and polished electrodes.

Joint Shear Force: For joint shear force measurements and any other tensile testing, an Instron tensile testing machine, (Model-4206, Canton, USA) was used. This machine is capable of applying loads up to about 147 kN.

Microscopy and Surface Analysis:

An optical microscope and a stereoscope were used for general observation of the surfaces, weld nugget and the carbon imprints at different magnifications.

For high resolution images and chemical analysis of both electrode and worksheet surfaces, scanning electron microscopy (SEM) (using model JSM-840, JEOL USA, Inc.) and electron dispersion X-ray spectroscopy (EDX) were performed in the Department of Mechanical and Mechatronics Engineering at the University of Waterloo.

The X-ray Diffraction (XRD) analysis was used for quantitative and qualitative analysis of different intermetallic phases on electrodes and sheet surfaces. This analysis was done in the Department of Chemistry at the University of Waterloo using a D-500 Powder X-Ray Diffractometer manufactured by Siemens Germany. The angles used for analysis were in the range of 20° to 80° with step size of 0.05° per second.

Electron Spectroscopy for Chemical Analysis (ESCA) was used for characterizing the oxide layer on the aluminum surfaces. This analysis was also done in the Department of Chemistry, with ESCALAB 250 (VG Scientific, East Grinstead, UK). Specimens used in this analysis were 6 mm x 6 mm and were taken from the same aluminum sheet.

3.3 Welding Parameters

Six welding parameters values were used for most of the experiments of the present thesis (Table 3.2). The definitions of the welding parameters were given previously in Section 1.1.2 of the present thesis. The values were selected to be typical of those likely to be used for the

AA5182 sheet material of 1.5 mm thickness. The weld frequency, squeeze time and hold time were not as influential on weld shear strength and so could be set easily. However, the other three parameters had a significant influence on the weld strength and differed depending on the particular aluminum alloy used and its thickness. A three dimensional region (weld lobe) exists that defines the range of acceptable values of force, current magnitude, and current time. These values are acceptable if they give a weld nugget that is large enough to provide a high enough level of shear strength.

For AA5182 sheet, data values, that were needed to define the weld lobe, existed in the MASc thesis of Lum [59] who followed the guidelines set out in MIL-W-6858D [79]. The present author followed the guidelines and performed a small series of spot welds (using the spot welding machine described subsequently in the present chapter) with various values of force, current magnitude and current time and then peeled the welds apart to determine the nugget size. This small series of spot welds were performed to check the results of Lum and fortunately gave very similar results. Thus, the weld lobe determined by Lum was used to give typical values for the central part of the lobe as listed in Table 3.2. In a very few experiments of the present thesis, current magnitude and/or current time were changed (and this was indicated when it occurred) but otherwise the values in Table 3.2 were used.

Table 3.2: Welding parameters for RSW of AA5182.

Welding Parameters	
Force	6 kN
Current magnitude	29 kA
Weld rate	20 spots per minute
Squeeze time	25 cycles*
Current time	5 cycles
Hold time	12 cycles

*1 cycle = 16.67 ms

3.4 Surface Preparation

The tribological surface characteristics of the worksheet were the main focus of the present research. In the specimen preparation, the surfaces were modified by mechanical procedures (grinding or abrading) and by chemical procedures (applying boundary lubricants that interacted chemically with the surface). The main response of the surface to the modification procedures was to change both surface roughness and oxide layer geometry (thickness and consistency). Both of these responses had a significant influence on electrode tip degradation and weld shear strength.

3.4.1 Mechanical Procedures

The top of the aluminum sheet had four surface roughness values that were produced manually by different methods. They were obtained by leaving the worksheet surface in the as-received condition, grinding the worksheet with silicon carbide emery paper (grit sizes of either 180 or 600), and abrading the surface with an abrasive wheel. A general purpose 3M Scotch-Brite™ CFFB-R cleaning wheel was used which had a diameter of 3 inch and a width of 1 3/8 inch. It had a three dimensional web which contained coarse grade aluminum oxide as the abrasive material. The web was mounted on a Roloc™ mounting system. This type of wheel was ideal for removing surface layer like paint and rust, provide decorative finish of the surface and also good for decorative applications.

To help characterize this procedure, several measurements of the centerline average surface roughness (Ra) were obtained for each sample using a surface profilometer (described subsequently in the present chapter).

3.4.2 Chemical Procedures

Surfaces were prepared to evaluate the effect of boundary lubricants on RSW of aluminum alloys. Various lubricants were applied to the worksheet surface of E/W interfaces (top and bottom) and kept away from the FS interface (Figure 3.7). The lubricants were applied on the surface with cotton wipes and then allowed to “soak-in” for various times (10 – 30 minutes) depending on manufacturer’s recommendations. However, one of the lubricants (designated as L6 in subsequent sections of the present thesis) was an exception since it settled quickly and formed a solid layer which becomes harder with time and thus experiments were performed within 2-4 minutes of applying this lubricant on the aluminum surface. After the soak-in period, the lubricated surfaces were wiped with soft tissues to leave a very thin, uniform layer. A number of the lubricants applied to the as-received surface to modify the tribology of the worksheet surface associated with the E/W interface.

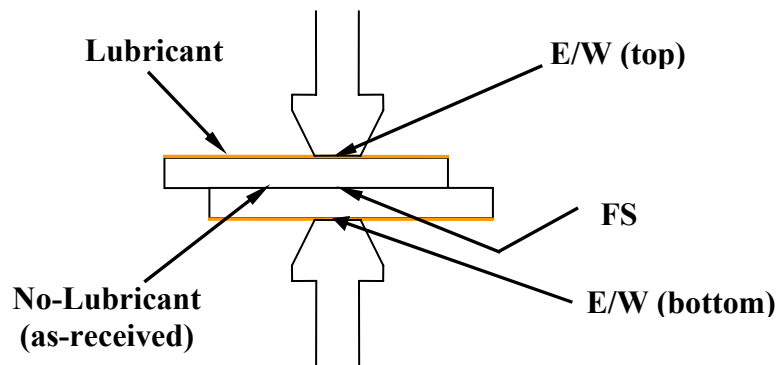


Figure 3.7: Schematic of RSW setup showing the interfaces and application of lubricant.

3.4.3 Omission of Oxide Layer Geometry

The oxide layer geometry was not directly controlled by a surface preparation procedure despite being considered as an input (independent) variable in the experiments of the present

thesis. It was possible to influence oxide layer thickness for the AA5182 used in the present thesis by controlling the time and humidity levels during storage [14, 33, 37]. However, the importance of doing this was not fully recognized at the time the welding experiments were performed and, even if it had been, the oxide layer geometry was further modified by the mechanical or chemical procedures that had been applied.

3.4.4 Overall Comments on Surface Preparation

It was very difficult to obtain good control of the surface input (independent) variables. The mechanical procedures (grinding and abrading) did roughen the surfaces but the result was not very precise or consistent. Similarly, the chemical processes varied depending on the lubricant and acted to further modify the surface roughness. Throughout all of this the oxide layer geometry changed but the specific details of these changes were only known after the mechanical and chemical procedure and the ability to control the changes was not well established.

Thus, the approach of the present thesis involved preparing surfaces by performing the mechanical procedures and by performing mechanical procedures followed by chemical procedures for some surfaces. Then, each surface was characterized in terms of Ra surface roughness and oxide layer geometry (as subsequently described in the present chapter) to give input (independent) variables for the subsequent RSW experiments where weld shear strength and electrode tip degradation were measured and classified as output (dependent) variables. It was considered likely that the difficulty and uncertainty in the present approach had discouraged other research groups from following it. However, the present approach did eventually yield a better understanding of the tribology of the E/W and FS interfaces that led to suggestions for improving electrode life.

3.5 Experimental Procedures

3.5.1 Electrode Life Test

Electrode life tests were conducted on specimens with various worksheet surfaces. The test procedure was as follows.

1. Welding was manually performed (at 20 welds per minute) with clamps and fixtures (that did not conduct significant electric current) were used to locate welds both for standard coupons and overlapped samples.
2. A New electrode was selected and the tip was cleaned by hand with a 3M Scotch-brite brush wheel and then inserted into the welding machine
3. Weld force (6kN) was calibrated using the weld force gauge described in section 3.2 of the present chapter.
4. Twenty conditioning welds at 22 kA were performed (Figure 3.2b).
5. A carbon imprint of electrode was taken at no current.
6. RSW was performed on 5 overlapped specimens (Figure 3.3) for subsequent shear force measurements.
7. RSW was performed to produce a total of 50 spot welds on five 10-weld standard coupons (Figure 3.2a).
8. Step 5 - 7 were repeated till electrode failure (as defined in the next section).
9. Carbon imprints were made of the failed electrode.
10. The electrode and welds were all kept for further analysis.

3.5.2 Electrode Life Criteria

In general, an electrode is said to have failed if the joint strength drops to a certain level of the initial value [59, 71]. In some cases, however, the degradation rate and pattern becomes so abnormal that, even if the joint strength remains in the range, the electrode starts sticking with the work surface and produces an arc with explosion and/or holes on the spot surface. If this stage is reached, the electrode is not safe for operator and considered to have failed [49, 59, 71].

Since the purpose of the present study was to investigate the effect of various tribological surface features, the same failure criterion was set for all surfaces using the as-received surface condition for the initial value. A tip life failure criterion was specified as a “drop in weld shear strength below 3.92 kN” which was about 80% of the initial weld shear strength of the as-received surface condition. A second criterion was also set in which the electrode tip was considered to have failed if excessive sticking (a somewhat arbitrary judgment) or explosions occurred. These allowed a fairly definitive end point for the electrode life tests and permitted a comparison of the influence of different surface conditions.

3.5.3 Carbon Imprint

Carbon imprints of electrode tip surfaces during the electrode life tests were obtained to observe the pitting rate and contact area growth rate. Carbon paper along with plain white paper was placed on a 400 x 50 mm specimen. The whole set is then placed between electrodes. The weld schedule is then turned to ‘no-weld’ mode (meaning that no current was applied) and the rest of the weld schedule was performed including the application of the 6 kN force. The carbon imprints were taken at several stages during the experiments (usually every 50 welds) and then analyzed using a stereomicroscope at a magnification of 7.5X. The diameters of these imprints were measured using the Image-Pro software.

3.5.4 Weld Shear Strength

For weld shear strength measurement, RSW were performed on overlapped (shear test) specimens (Figure 3.3). An Instron tensile testing machine was used to measure the shear force required to break the weld (Figure 3.8). Shims were used to minimize any twisting of samples during the tests [32]. The specimens were mounted with shims and pulled at a rate of 20 mm/min and maximum force was recorded as the weld shear strength.

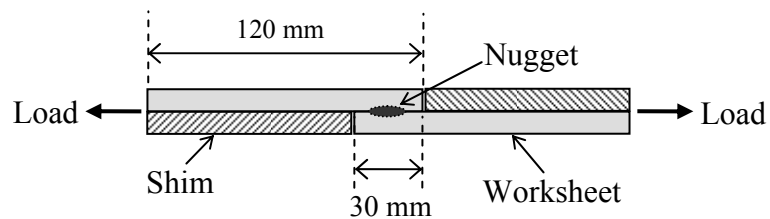


Figure 3.8: Schematic of joint shear force measurement.

3.5.5 Metallography

Metallography was performed to obtain detailed features of some of the particular sections, specially the nugget cross sections. Careful sectioning of the required part was done using either sawing machines or cutting wheels. Specimens were then hot mounted in reinforced bakelite. The samples were then grounded manually with 400, 600, 800, and 1200 grit silicon carbide papers. The next step was grinding automatically using 1200 grit silicon carbide paper. These specimens were then polished with automatic wheels using Struers clothes with 3 micron and 1 micron diamond paste. The final stage of polishing was performed using 0.06 micron silica colloidal solution on the automatic polishing wheel. The polished samples were rinsed with water followed by five minutes ultrasonic cleaning in warm water and then dried with compressed air. Keller's reagent [101] was used for etching; polished surfaces were dipped in the etchant for 10 – 20 seconds and then rinsed with warm water and dried with

compressed air. The specimens were then observed through optical and electron microscopy for detailed analysis.

3.5.6 Electrical Contact Resistance

Under conditions of constant current flow, electrical resistances across the E/W interface were measured for all surface conditions. This is done using the ‘four-point’ method [29] with a particular configuration of connecting current and potential terminals (Figure 3.9). The long strips (Figure 3.1) were cut into 10 equal sizes of 50 x 40 mm and clamped between electrodes with the same welding force of 6kN that was used for RSW. For each specimen, terminals were connected to the same locations to get the consistent measurements. A current of 10 A was allowed to pass from terminal C_1 and C_2 using the digital ohm-meter (as described in section 3.2 of this chapter). The ohm-meter then measured the resistance across the E/W interface by measuring the potential difference across terminals P_1 and P_2 .

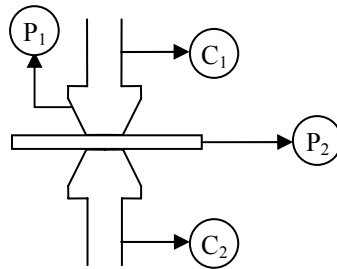


Figure 3.9: Schematic illustration of four-point method for measuring the electrical resistance across the E/W interface.

3.5.7 Contact and Weld Diameters

The E/W contact diameter was measured with the help of Image-Pro software. At the E/W interface, the impression of the electrode on the worksheet was directly measured by viewing the worksheet using stereomicroscope. Two measurements were obtained across the impression and the average was recorded as the contact diameter between electrode and worksheet (Figure 3.10). At the FS, the contact diameter after squeezing was measured by placing carbon paper between the worksheets and applying the weld force (6 kN) using the spot welding machine. Again, two measurements were obtained across the impression and the average was recorded as the contact diameter of the FS after squeezing.

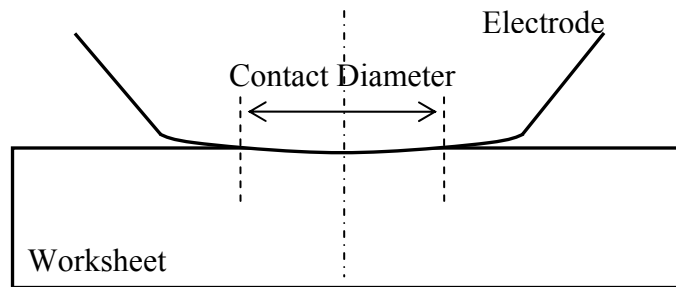


Figure 3.10: Schematic illustration of contact diameter at the E/W interface.

Once the current was passed between the electrodes, a nugget formed at the FS. The nugget diameter was usually somewhat larger than the contact diameter (from the carbon paper). It was measured by pulling the sheet surfaces apart, breaking the welds in tension and then measuring the weld diameter in the same manner as described for the E/W and FS contact diameters.

3.5.8 Statistical Analysis

The various differences between surface roughness and electrical contact resistance of different surfaces were assessed with a statistical analysis (one way ANOVA). This analysis was quite appropriate for analyzing samples from three or more than three groups. Also, another statistical analysis (Student's t-test with a 0.05 significance level) was used to check the significance of the difference between various dependent and independent variables of samples from as-received and lubricated surfaces.

3.5.9 Peltier Effect

A common phenomenon that is observed during RSW using direct current is known as peltier effect. Peltier effect is a phenomenon where a creation of heat difference occurs from an electric voltage [110]. When two dissimilar metals connected to each other at two junctions, the flow of current through these junctions drives a transfer of heat from one junction to other; the junction with the lower voltage cools off while the junction with the higher voltage heats up [110]. In a typical RSW set up using direct current, one electrode kept at positive volt while the other electrode kept at zero volt. In this case, the E/W interface (junction) with positive volt experience high temperature than other electrode due to peltier effect. The result is a faster electrode degradation of positive electrode than other electrode as shown by other work [59]. Since, the positive electrode degraded faster, the emphasis is generally given to that electrode. In the present thesis, all results were presented for upper electrode which was used as the positive electrode.

3.6 Finite Element Analysis

Finite element analysis (FEA) of the mechanical loading during the squeeze part of the RSW schedule and before the application of the current was performed using a commercial FEA code (ABAQUS, Hibbit, Karlsson & Sorensen Inc., Pawtucket, RI) [93]. A complete axisymmetrical was employed which consisted of both upper and lower electrodes and the two worksheets. This model had an advantage over the generally used ‘half-model’ which consisted of only upper electrode and upper worksheet. In the half-model, the sheet-to-sheet contact is updated using pre-set criterion regarding stress and pressure distribution without knowing how friction and slip at the FS interface might influence the behaviour [60]. This limitation was avoided by using the complete model. Also, this model was appropriate for the current study because it better represented the actual situation that during RSW, only the upper electrode was allowed to move down by the spot welding machine while keeping the lower electrode fixed and hence presented actual force and boundary conditions.

It was possible to represent all essential features of the RSW squeeze process in the FEA model. A uniform pressure, equivalent to the load, was applied on the upper electrode while the bottom electrode was fixed for axial (z-direction) displacement. It was observed through the data monitoring process during RSW that the load reach the peak value (6kN) after about 5 cycles (83.3 ms) and remains constant for the next 20 cycles (thus giving a total squeezing time was 25 cycles or 417 ms). The same loading equation (Figure 3.11) was used for the FEA model and this was important to present the similar squeezing condition.

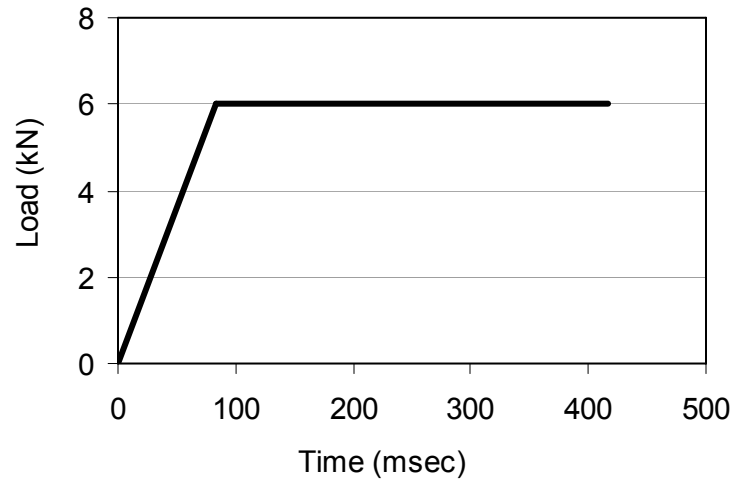


Figure 3.11: The load application during squeezing.

Stress-strain data for worksheet material (AA5182) was obtained using standard tensile tests [107] of five specimens. The general mechanical properties for both electrode material (C15000) and worksheet (AA5182) used for FEA model are given in Table 3.3 [94]. Since electrode indentation into the worksheet was extensive, an elastic-plastic model was needed and required mechanical properties in terms of true stress and plastic strain. These data values were obtained using the following procedure [93] and presented in Table 3.4.

1. Several data points were selected from the nominal stress-strain curve of the material (A linear interpolation was used within ABAQUS® and so a number of data values had to be used to obtain accurate results).
2. Each of these data points were then converted into true stress and true strain values using Equation 3.1 and 3.2.
3. Once the true strain was obtained for a given data point, it was decomposed into elastic and plastic strain as shown in Figure 3.12.

4. Finally, the plastic strain was calculated for the corresponding true stress using Equation 3.3.

$$\varepsilon = \ln(1 + \varepsilon_{eng}) \quad \text{Equation 3.1}$$

$$\sigma = \sigma_{eng} (1 + \varepsilon_{eng}) \quad \text{Equation 3.2}$$

$$\varepsilon^{pl} = \varepsilon - \varepsilon_{eng} = \varepsilon - \frac{\sigma_{eng}}{E} \quad \text{Equation 3.3}$$

where

ε - true strain

ε_{eng} - engineering strain

σ - true stress

σ_{eng} - engineering stress

ε^t - true total strain

ε^{pl} - true plastic strain

ε^{el} - true elastic strain

E - Young Modulus

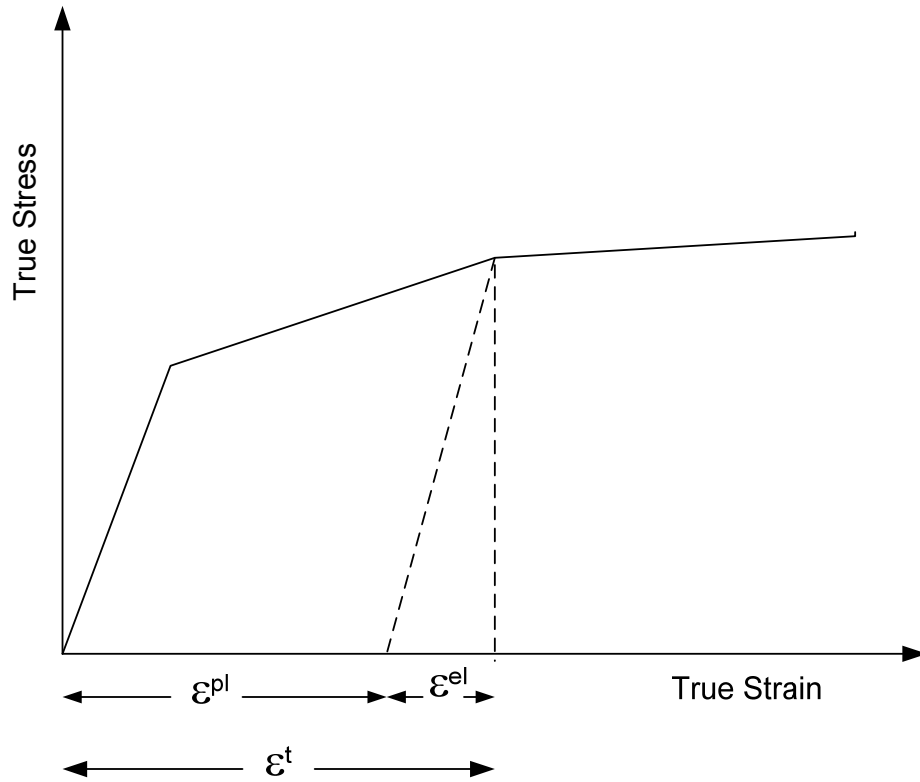


Figure 3.12: Decomposition of total strain into elastic (ϵ^{el}) and plastic (ϵ^{pl}) components [93].

Table 3.3: Mechanical properties of worksheet and electrode materials [94].

Property	AA5182	C15000
Density (kg/m ³)	2660	8890
Yield Stress (MPa)	138	412
Tensile Stress (MPa)	276	445
Elongation (%)	25	16
Young Modulus (GPa)	70.9	129
Poisson's ratio	0.33	0.34

Table 3.4: True stress and plastic strain values for worksheet and electrode

Worksheet (AA5182)		Electrode (C15000)	
True Stress	Plastic Strain	True Stress	Plastic Strain
138.0E6	0.0	412.0E6	0.0
142.0E6	0.008	416.0E6	0.005
188.0E6	0.032	431.0E6	0.021
215.0E6	0.047	449.0E6	0.045
276.0E6	0.096	482.0E6	0.092
315.0E6	0.146	511.0E6	0.136
340.0E6	0.195	516.0E6	0.144
347.0E6	0.227		

Four-node axisymmetric quadrilateral elements were used for both electrode and worksheet (Figure 3.13). No attempt was made to model oxide layer at the worksheet or microscopic deformation of any asperities at the surfaces because to have an accurate representation of these features would require a very large, very fine mesh that would require extensive and advanced FEA procedures to solve.

There were three contacting interfaces; the two E/W interfaces at the top and bottom and the FS interface between the worksheets. At these interfaces, contact pairs were used to ensure that the surfaces would not penetrate into each other [61]. For the contact interaction normal to these interfaces, a “hard” contact behaviour was used which transmitted the contact pressure between the surfaces without any limit on its magnitude [93]. For tangential behaviour at these interfaces, a “finite-sliding” was allowed with a coulomb-friction model. The suggested range of coefficient of friction between the mostly copper electrode and the aluminum alloy worksheet was estimated to be in the range of 0.3 – 0.6, with 0.5 as the most

commonly used value [95-96]. The coefficient of friction could only be estimated in an approximate fashion because it would be somewhat different for each individual E/W contact depending on a number of not that well understood environmental conditions and local surface interactions. Several runs of the FEA were performed with different values of coefficient of friction and it was observed that the entire range of reported coefficient of friction (0.3 – 0.6) provided about same results. Thus, the FEA in the present thesis used a coefficient of friction of 0.5 between electrode and worksheet. At the FS interface, symmetry existed and surface shear stress was not expected. However, a coefficient of friction of 0.8 was assumed, for the sake of rigor, based on other investigations [15, 95].

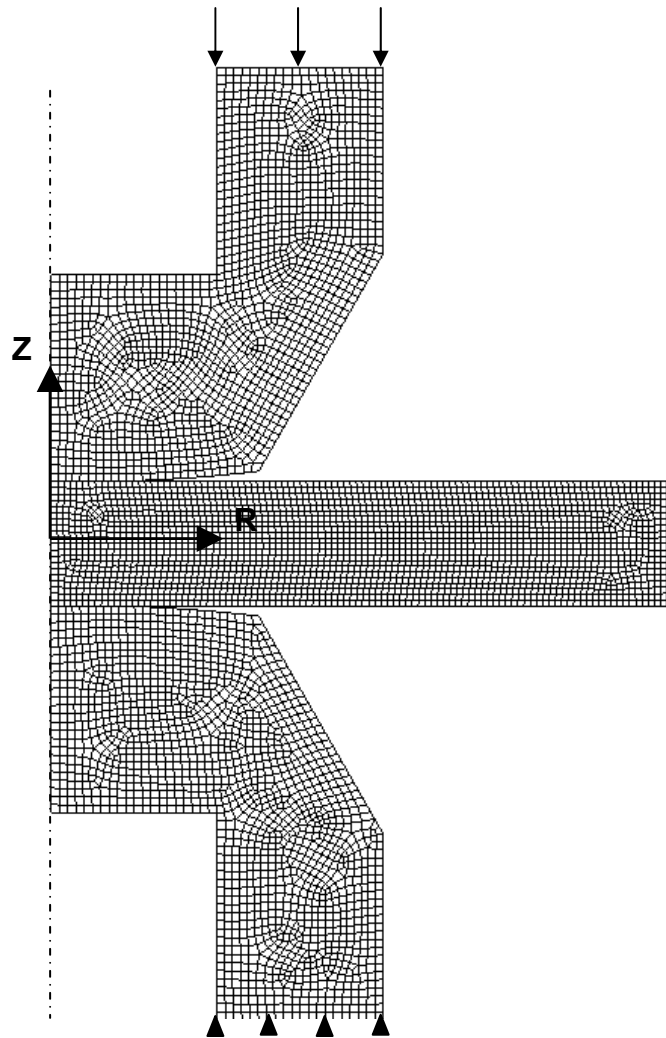


Figure 3.13: FEA mesh and boundary conditions for the axisymmetric representation of RSW during squeezing.

3.7 Concluding Remarks

Since the present study required a complex interaction between several welding parameters, independent and dependent variables, a series experiments were performed to understand these interaction completely. Finite element analysis (FEA) was also employed to understand the contact mechanics of the interfaces. Large amount of equipment was used and large numbers of procedures were employed for detailed analysis. All the main experiments were summarized in Appendix A.

Chapter 4

4 The Electrode-Worksheet Interface

4.1 Introduction

As explained in Chapter 2, the electrical contact resistances at the interfaces (E/W and FS) were the main source of heat during RSW of aluminum alloys and influenced the joint strength as well as electrode tip life. Furthermore, for RSW in manufacturing, tribological modifications could be made to the contacting surfaces of the electrode or of the aluminum worksheet. Since considerable research had been performed regarding modifications to the contacting surfaces of the electrode (Section 6.3 – 6.6, Chapter 2), the present chapter considered some modifications to the contacting surface of the worksheet. Some of the results of the present chapter have been presented by Rashid et al [92].

Thus, at the E/W interface, the contact resistance could be influenced by two main surface features of the chosen AA5182 material (that could be modified by mechanical or chemical treatments as explained in Chapter 3). These factors were the surface roughness (that could directly influence the real area of contact and thus electrical "constriction" resistance) and the geometry (thickness and uniformity/continuity) of the oxide layer. The real area of contact consisted of a large number of small micro-contacts distributed over the apparent area of contact depending on the surface roughness and the elastic-plastic properties of the both interface materials at the asperity tips. The oxide layer was important because it had the inherent material property of being an electrical insulator. Depending on its geometry, the

oxide layer could greatly increase contact resistance. Furthermore, the oxide layer was too thin to influence the deformation responsible for the micro-contacts but this deformation could break up the oxide layer which was brittle compared with the aluminum alloy substrate. Thus, there was likely to be a complex interaction of surface roughness and oxide layer geometry on electrical contact resistance and consequently on RSW.

A series of experiments were performed to investigate the influence of both surface roughness and oxide layer geometry on not only the electrical contact resistance of E/W interface but also the pitting rate of electrodes, and joint shear strength. Detailed metallurgical analysis was also performed to help understand these influences. The specific objective of the present chapter was to characterize the main tribological features (surface roughness and oxide layer geometry) of the AA5182 sheet and their influence on the E/W interface. Based on the findings in this chapter, detailed work on the contact mechanics of the E/W interface, FS interface and effect of boundary lubricants were presented in chapter 5, chapter 6, and chapter 7 of this thesis respectively.

4.2 Results

4.2.1 Experiments

The as-received AA5182 surface had a centerline average surface roughness (Ra) value of 0.32 μm . Two more roughness levels were produced manually to provide a range for this input (independent) variable. The intent was to obtain roughness levels higher and lower than the as-received condition. Specimens were cut in the size of 50 mm x 40 mm and then grinding was performed with two different grades of silicon carbide papers. This grinding was performed manually along the rolling direction and compared with the as-received surface. The Ra roughness was obtained using a direct contact profile meter (described in Section 3.2). Three measurements were recorded on each specimen and the average of them was reported as the Ra value for that specimen. Five such specimens were used for each

surface preparation and the overall average of these specimens gave the characteristic Ra for the particular surface preparation. As expected, the manual grinding of sheet surfaces with two different grades of silicon carbide papers produced sheet surfaces with Ra values above and below those of the as-received surface (Table 4.1). A statistical analysis (one-way ANOVA) indicated that there were significant differences between the roughness (Ra) values for the three different surface conditions ($p < 0.001$). This indicated that these samples were from three different roughness groups.

Table 4.1: Centerline average roughness (Ra) of the contacting surface of the worksheet

Surface	No. Specimens	Total No. of Roughness Measurements	Preparation Method	Ra (μm) avg. \pm std. dev.
smooth	5	15	grinding with 600 Grade silicon carbide paper	0.24 ± 0.02
as-received	5	15	none	0.32 ± 0.02
rough	5	15	grinding with 180 Grade silicon carbide paper	1.08 ± 0.06

Electrical contact resistance of these specimens was measured using the four-point method with a load of 6 kN (as described in Section 3.5.6). The contact zone was carefully selected to avoid regions where the direct contact profilometer had touched it for roughness measurement because the small amount of surface damage caused by the profilometer might influence the measurement. To avoid any variability of the electrode tip surface, the same pair of electrodes was used for all these specimens. Furthermore, through preliminary experiments, it was observed that the electrical contact resistance remained same after the first 10 – 20 measurements (Figure 4.1). Therefore, twenty conditioning measurements were

performed with the pair of electrodes before using them for actual measurement of the above mentioned specimens.

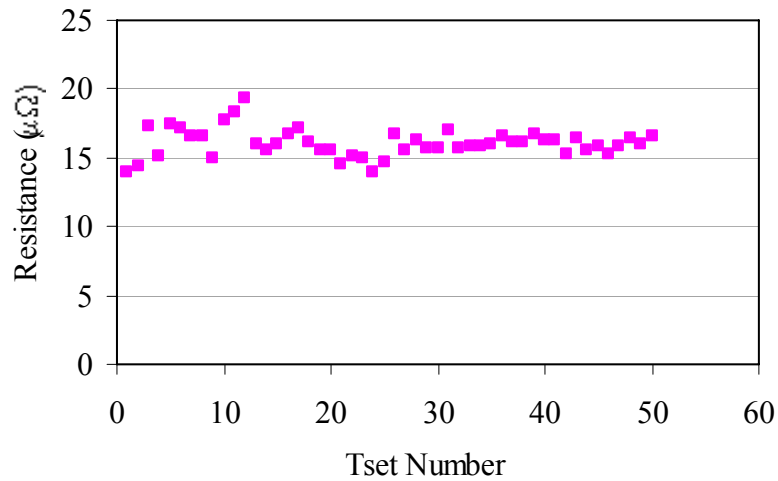


Figure 4.1: Electrical contact resistance variation during successive measurements with the same electrode pair.

4.2.2 Electrical Contact Resistance of E/W Interface

The sheet surface roughness associated with the E/W interface had a very clear effect on the electrical contact resistance at this interface (Figure 4.2). Smooth surfaces showed higher average contact resistance ($9.1 \mu\Omega$) than the rough surfaces ($7.2 \mu\Omega$).

Interestingly, James et al [29] performed similar electrical resistance measurements with the same load on 2.0 mm thick abraded AA5754 sheet ($R_a = 0.76 \mu\text{m}$). The AA5754 was a 5xxx series aluminum alloy with Mg as the main alloying element (making it similar to the AA5182 used in the present study) but, before the abrading procedure, their AA5754 had a silica-containing coating (70 nm thick) which they reported as being an electrical insulator.

In spite of these differences, James et al reported a range of electrical contact resistance values (10 – 12 $\mu\Omega$), as shown in Fig. 4.2 that was in quite good agreement with those of the present study.

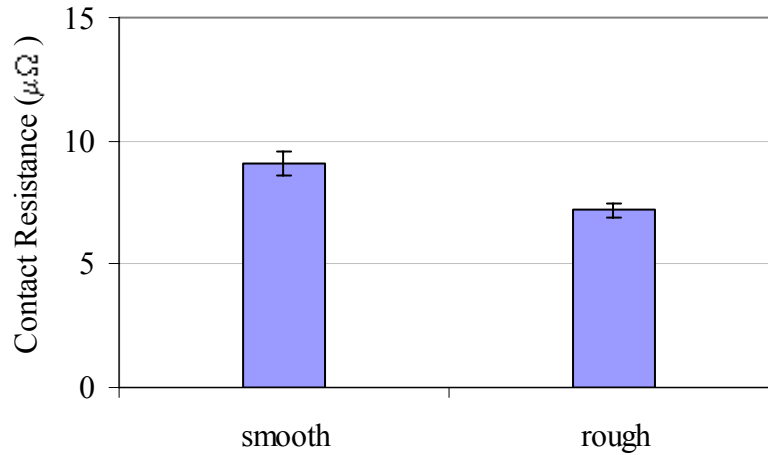


Figure 4.2: Electrical contact resistance at the E/W interface for rough and smooth surfaces.

It is now appropriate to define briefly the concept of real and apparent (or nominal) contact area before discussing these results. In reality, no engineering surface, no matter how carefully prepared, is perfectly flat. There will always be asperities on the surfaces particularly metallic surfaces [97, 108, 111]. When two such surface brought in contact with each other, it is the tips of the asperities that initially carry the load. The sum of the area of all such asperity which carries the total applied load is the “real” contact area. The number of such load carrying asperities depends on the applied load and mechanical properties of the surfaces. In contrast, the total area circumference by all edges of the apparent contact is defined as “apparent” or nominal contact area. In general, the real contact area is much smaller than the apparent contact area [97, 108].

The trend shown above for the roughness was not expected. If the contact involved predominantly elastic deformation because the real area of contact would be lower for the rough surface and thus electrical contact resistance higher. However, if the contact involved predominantly plastic deformation, the real contact area would approach the nominal one and the electrical contact resistance would be independent of surface roughness. Thus, finding higher electrical contact resistance for the smoother surface suggested that there was some other influencing factor.

As mentioned earlier (Table 4.1), the as-received sheet surface had a roughness level in between the rough and smooth levels. With its roughness value, the contact resistance of as-received surface was expected to be between the smooth and rough surfaces but this was not found. Instead, the average electrical contact resistance of the as-received surface ($11.6 \mu\Omega$) was higher than both the ground surfaces (Figure 4.3). The likely explanation for this finding was the lack of damage to the existing oxide layer because surface grinding was not performed. An estimate of the number and size of the constriction points (metal-to-metal contact) is presented in Appendix B.

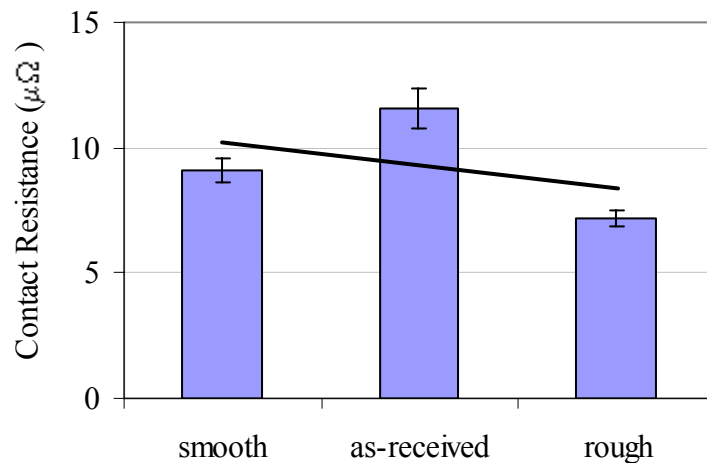


Figure 4.3: Electrical contact resistance at the E/W interface for as-received and ground surfaces.

Statistical analysis (one-way ANOVA) indicated that there were significant differences between the electrical resistance values for the three different surface conditions ($p < 0.001$). The finding that the as-received surface had a higher electrical resistance was almost certainly a consequence of its more uniform oxide layer whereas the ground specimens both had their oxide layer damaged to varying extents by the grinding process thus reducing its insulating effect.

4.2.3 Effect of Surface Abrasion on Electrode Degradation

Welding experiments were performed to investigate the effect of surface roughness on the electrode degradation and joint shear strength. 10-weld standard coupons (Figure 3.2 a) and overlapped specimen for joint shear force measurement (Figure 3.3) were used for these welding experiments. Once again, both as-received and ground surfaces were prepared for these experiments but this time there was only one type of preparation of ground surfaces. Since large number of samples was required for welding, the grinding was performed with the help of rotating wheel of scotch-brite. Samples were held against the rotating wheel and grinding was performed along the rolling directions. This surface was designated as the "abraded" surface for the remainder of the present thesis to differentiate it from the hand-ground surfaces of Section 4.2.1. Also, the increases in Ra value from that of the as-received surfaces were relatively small compared with the previous hand-grinding procedure (as shown subsequently). The intent was to investigate the effect of abrasion by performing the experiments on abraded and as-received surface of nearly same roughness. For all of the present experiments, only the surface condition of the worksheet at the E/W interface was altered while the FS interfaces were in the as-received condition.

The Ra roughness of the contacting worksheet surface and the electrical contact resistance of the E/W interface were measured before welding following the same procedure as described in the previous section. Twenty specimens of the same size as described in section 4.2.1 were

used for each surface condition (Table 4.2). The electrical contact resistance had a sample-to-sample variation which was similar to that found by other investigators [30, 52]. However, within one set of experiments where measurements were obtained with the same pair of electrodes and samples were prepared from the same sheet, the results were consistent with resistance had much less scatter.

Table 4.2: Ra values and electrical contact resistance of as-received and abraded surfaces.

Surface	Roughness avg. \pm std. dev. (μm)	Electrical Contact Resistance avg. \pm std. dev. ($\mu\ \Omega$)
as-received	0.33 ± 0.05	16.3 ± 3.0
abraded	0.39 ± 0.04	13.9 ± 2.9

The electrical contact resistance of the as-received surface was higher than that of the abraded surface (Student's t-test, $p = 0.01$). In the previous section, a large increase in the average surface roughness from that of the as-received specimens ($0.32\ \mu\text{m}$ to $1.08\ \mu\text{m}$) resulted in a large drop in the average electrical contact resistance ($11.6\ \mu\Omega$ to $7.2\ \mu\Omega$ respectively). In the present section, the average Ra of the as-received surfaces ($0.33\ \mu\text{m}$) was not much less than that of the abraded surfaces ($0.39\ \mu\text{m}$) and, as expected, it caused a little lower but fairly large drop in electrical contact resistance from $16.3\ \mu\Omega$ to $13.9\ \mu\Omega$ respectively. Thus, the results of the present section were fairly consistent with those of the previous section.

To observe the effect of these surface conditions on electrode pitting and joint strength, RSW was performed using the same welding parameters and weld schedule mentioned in Table 3.2. For each surface condition, 100 spot welds were performed and each 100 spot welds was divided into four sets. Each set consist of taking carbon imprints of the electrode at no current

followed by 5 spot welds on overlapped specimens and then 20 spot welds (10 on each of two 10-weld standard coupons). After set 4 was completed, carbon imprints were taken and finally five overlapped specimens were welded. For each surface condition, a fresh pair of electrode was used and conditioning of electrodes was performed using the standard procedure before actual spot welding.

After 100 welds, the carbon imprints of positive electrodes were quite different from those taken at the start of welding and indicated that considerable pitting had occurred (Fig. 4.4). For the as-received surface that had a higher contact resistance, pitting occurred earlier and the contact area increased more.

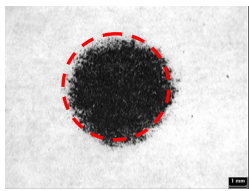
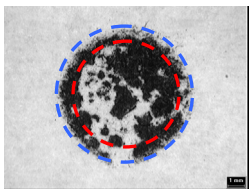
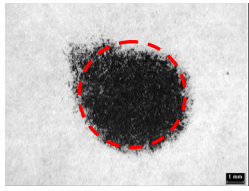
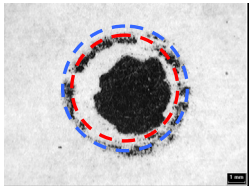
Surface Condition	Positive Electrode		Start of pitting	Contact area growth (%)
	Start	After 100 RSW		
as-received			25 -50 spots	26
abraded			50 -75 spots	17

Figure 4.4: Electrode tip pitting as measured by carbon imprints.

Also, the pitting was more extensive and occurred sooner for the as-received surfaces than for the abraded surfaces. It was considered likely that the higher electrical contact resistance of E/W interface which caused more heat generation and hence more alloying, pickup and/or pitting.

This higher heat generation at the E/W interface and consequent faster pitting rate of electrode subjected to as-received surface was also supported by the growth of the contact area between electrode and worksheet. It was observed that, for both these surfaces, there was hardly any change in the contact area before the start of pitting. However, once the pitting started, the contact area growth accelerated with pitting rate. The contact area growth between electrode and worksheet for as-received surface was much higher than abraded surfaces (Figure 4.4).

Abrading the contacting surface of the worksheet at the E/W interface also resulted in a slightly decrease of the initial joint shear force of the welds compared with the as-received surfaces (Figure 4.5). All these results followed the usual trend of electrode life (Figure 2.8), in that the joint strength increased initially to reach a peak value and then started decreasing. It was considered important to note that during all these welding, the FS interface was kept same along with the welding parameters and only the worksheet surface at the E/W interface was subject to change as an independent variable.

Although, the initial joint shear force of abraded sheet was slightly lower than that of as-received surface, it was still well above the acceptable joint shear force of this material [79]. Furthermore, with continuous welding, the difference of joint shear strength of these surfaces decreased and reached same value at the end of 100 spot welds. At that stage, from these results, it was not clear that which surface would provide better electrode life. However, the faster pitting rate of electrode associated with as-received surface suggested an early failure of the electrode. This aspect of the RSW process, i.e. electrode pitting rate and electrode life was discussed in details in chapter 7 of this thesis. From the current results, it was clearly observed that abrading the worksheet surface brought change in electrical contact resistance of the E/W interface which affected the electrode pitting rate.

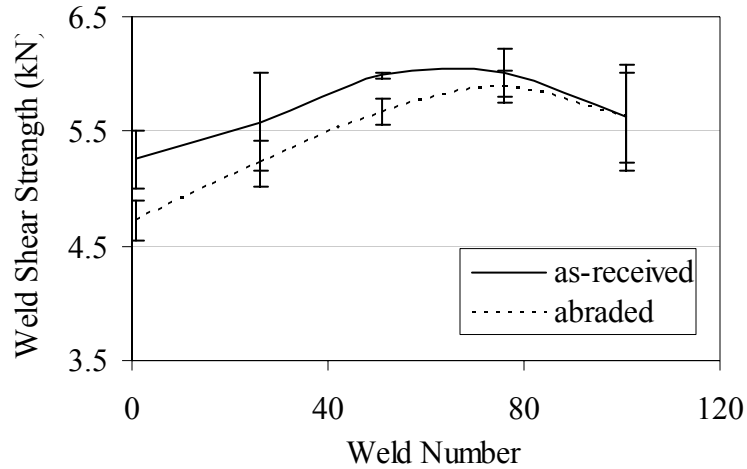


Figure 4.5: Joint shear force comparisons for as-received and abraded surfaces.

4.3 Discussion

As discussed earlier (chapter 2), the real area of contact between two mating surfaces has a direct influence on the electrical contact resistance at the E/W interface. In elastic or elastic/plastic contact, the real area of contact is always less than the apparent area of contact. However, if the deformation is fully plastic, then the real area of contact approaches the apparent area of contact. Thus, the first step in any technical discussion of the tribology of the E/W interface must begin with a determination of the extent of plastic deformation. Also, it must be recognized that the oxide layer on the aluminum worksheet surface has a higher elastic modulus than the substrate and acts as an electric insulator. As a result it may influence surface deformation and electrical resistance.

In the present work, all other factors were kept constant and only the contacting surfaces of the worksheet were ground or abraded to determine the effects on electrical contact resistance and weld shear strength.

4.3.1 Effect of Surface Roughness

Initially, and in accordance with some of the literature [97], it was thought that surface roughness at the E/W interface would influence the effective electrode life because the real area of contact would decrease with increasing surface roughness and thus the electrical contact resistance would *increase*. However, the electrical contact resistance decreased with increasing surface roughness and this might have been a consequence of plastic deformation making the real and apparent areas of contact equal and the drop in resistance could be related to damage of the oxide layer on the aluminum caused by the grinding/abrading process and/or the more extensive bending/cracking of the oxide layer that re-formed on the rougher surface when the substrate sustained extensive plastic deformation.

The first step then was to estimate the extent of plastic deformation. The elastic properties of the surfaces (aluminum and copper alloy) along with the surface geometry were given in Chapter 3. These values were used in the following set of Hertzian contact equations to calculate the average contact stress (σ_{avg}) assuming pure elastic deformation and perfectly smooth surfaces as follows:

$$\frac{1}{E'} = \frac{1}{2} \left(\frac{1 - \nu_A^2}{E_A} + \frac{1 - \nu_C^2}{E_C} \right)$$

$$a = \left(\frac{1.5 F R}{E'} \right)^{1/3}$$

$$\sigma_{avg} = \frac{F}{\pi a^2}$$

where R = radius of the spherical electrode tip
 E_A = elastic modulus of the aluminum worksheet
 ν_A = Poisson's ratio of the aluminum worksheet

E_C = elastic modulus of the copper alloy electrode

ν_C = Poisson's ratio of the copper alloy worksheet

E' = reduced elastic modulus

F = load

a = radius of the contact

The resulting value was $\sigma_{avg} = 716.1$ MPa and since this value was almost equal to the hardness of the aluminum surface (784.8 MPa) as measured with a Vickers indenter (50 kgf), extensive plastic deformation was expected reaching almost to the surface. It was interesting to note that the Vickers hardness values increase when the test was performed with lower loads because the oxide layer, although thin, had much higher hardness than the bulk aluminum. Thus, it was not entirely clear what hardness was appropriate for estimating the extent of plastic deformation in the above comparison with the average Hertzian contact stress. It was considered likely that a lower value would be more appropriate and if so, the plastic deformation would be more extensive.

For a contact with extensive plastic deformation, the real and apparent contact areas would be virtually identical. Thus, the only link between electrical contact resistance and surface roughness were considered likely to be related to how the oxide layer was deformed in the contact. The rougher surface might subject the oxide layer to more deformation during the plastic deformation of the aluminum substrate and thus promote oxide layer cracking a reduction in electrical contact resistance. Alternatively, the more extensive grinding/abrading process performed on the rougher surface might have damaged the oxide layer leading to a drop in contact resistance. In either case, the oxide layer geometry during the RSW process was an important consideration as subsequently discussed.

4.3.2 AA5182 Oxide Layer Composition

It was observed that the electrical contact resistance of the as-received surface was higher than the ground and abraded surfaces. The main reason for the high contact resistance of as-received surface was likely to be the different geometry of the oxide layer. All those ground surfaces were prepared within 2 hours of experiments and were expected to have fresh, thin, and uniform oxide layer [29] while the as-received surface was untreated and would have thicker perhaps less uniform oxide layers.

Aluminum alloys are known for the presence of alumina (Al_2O_3) on their surfaces. This layer is very hard and non-conductive [40]. The 5000 series aluminum alloys, which are very popular for auto body applications, contain high amount of Mg as their main alloying element which has the affinity to absorb oxygen at high temperature to form magnesium oxides. Depending on the manufacturing and other high processing temperature, the Mg at the surface of the aluminum alloy could segregate from the bulk material to form MgO [33, 100]. Also, fresh surface of AA5182 may have thin and uniform alumina, but with different processing and storage conditions, the oxide layer on the as-received aluminum surface could become non-uniform with the possibility of other oxides like MgO [37].

Mg was the major alloying element of AA5182 and was expected to be distributed homogeneously in the alloy. As expected, It was observed that the Mg content on the polished and as-received surfaces of AA5182 were 4.6% and 4.7% respectively which were very close to the nominal value of 4.5% often given for this aluminum alloy AA5182 and to the 4.7% value provided by the manufacturer. However, for the as-received surface, the Mg content varied over the surface. SEM micrographs showed that there were several spots on the surfaces which were not consistent with the general surface morphology and appeared bright in contrast (Figure 4.6). Chemical analysis (EDS) of some of those spots revealed different chemistry than the general base matrix (Table 4.3). These bright spots appeared rich in Mg and O (sp-1 and sp-2) while the base surface had less Mg content than the alloy composition (sp-3, sp-4, and sp-5). It appeared from these results that, some of the Mg at the

surface was segregated from the base and produced MgO rich spots on the surface and hence made the surface oxide layer non-uniform in terms of its composition.

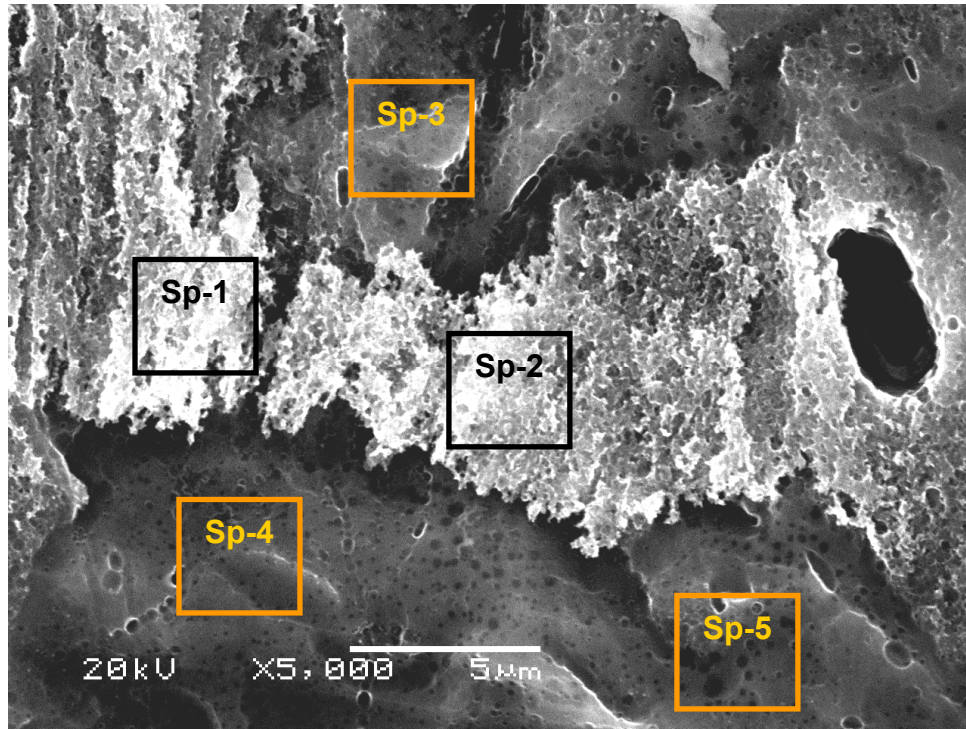


Figure 4.6: Surface morphology of AA5182 showing non-uniform bright spots.

Table 4.3: Chemical analysis (EDS) of as-received surface of AA5182.

Wt %	Sp-1	Sp-2	Sp-3	Sp-4	Sp-5
Al	88.3	88.2	96	94.8	96.2
Mg	6.4	5.5	3.8	3.9	3.5
O	5.3	6.3	0.2	1.3	0.3

Additional continuous chemical analysis (line scan EDS) across such non-uniform spots on the surface of AA5182 confirmed their high Mg and O content (Figure 4.7 and 4.8). It should be mentioned that the oxygen signals were less intense but this was due to the fact that the oxide layer on aluminum surface was very thin (in the range of few nano meters) and SEM has difficulty analyzing such thin surface layers and also has difficulty obtaining data for light elements such as oxygen. However, while performing the analysis on the same surface in the same condition, the difference in oxygen intensities was large enough to indicate that those spots had higher amounts of oxygen and suggested the formation of an MgO oxide which made the oxide layer of AA5182 non-uniform in terms of composition.

The presence of a somewhat higher Mg content and relatively high signal for oxygen in the bright spots clearly indicated the segregation of magnesium from the base metal and the likely formation of MgO dispersed over the sheet surface. These results provided direct evidence for the schematic representation proposed by Kucza et al [37] for the surface oxide layer of AA5182. However, the sizes of these Mg and O rich spots were much smaller than depicted in the schematic of Kucza et al and only a very small fraction of the surface area was appeared to be covered by such spots.

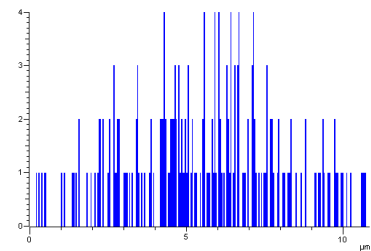
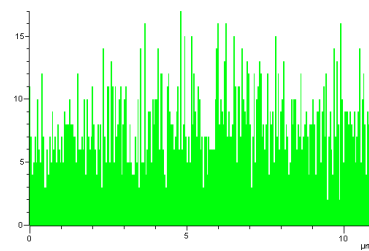
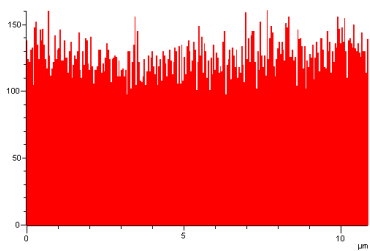
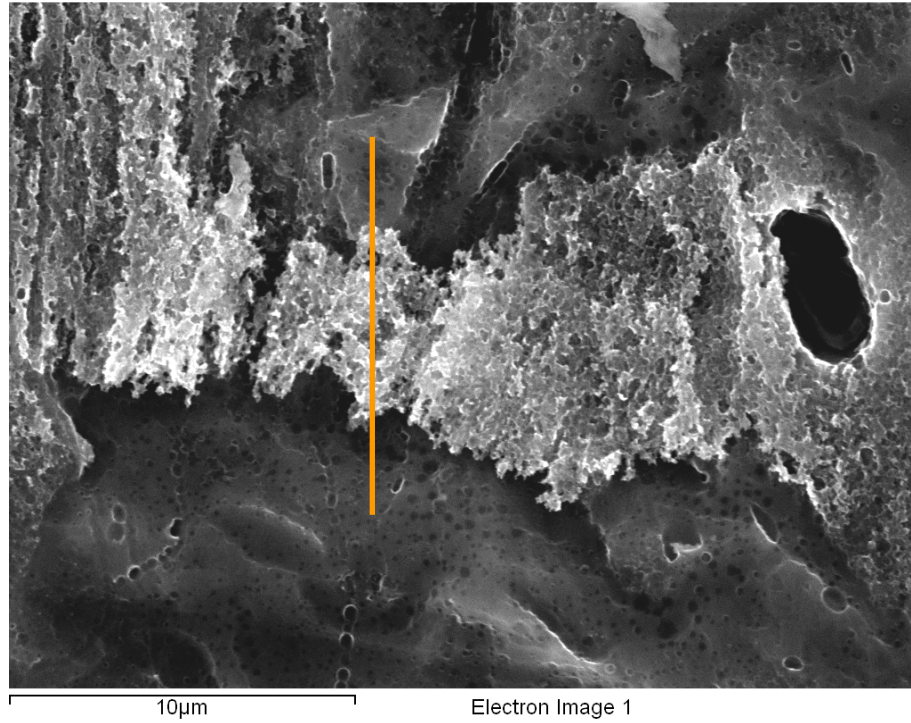


Figure 4.7: Line scan chemical analysis (EDS) analysis of non-uniform spots showing intensities of Aluminum (Al), Magnesium (Mg), and Oxygen (O).

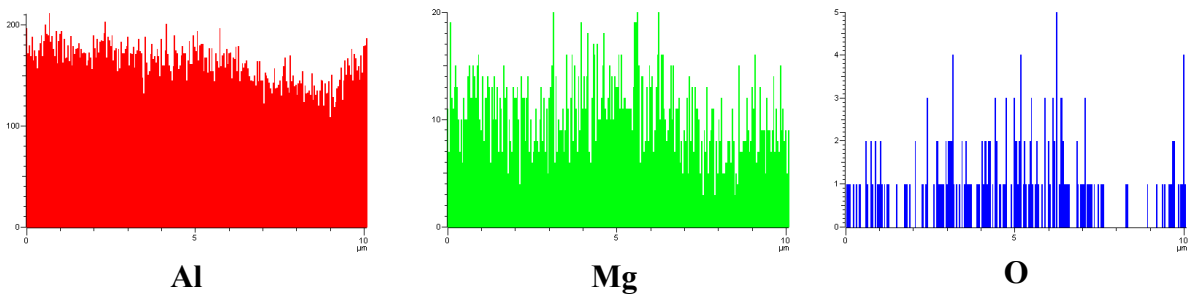
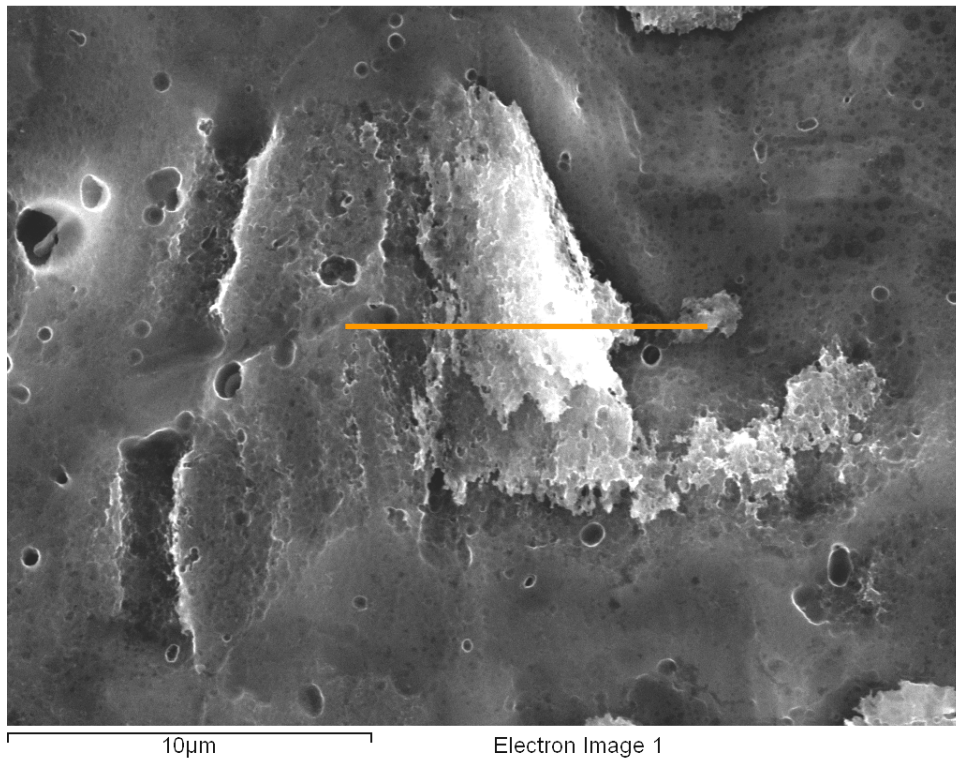
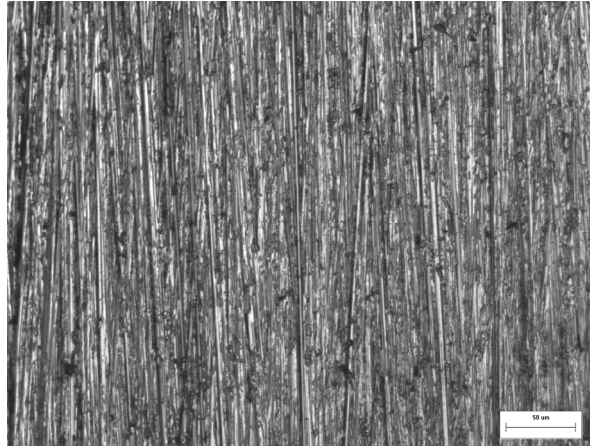


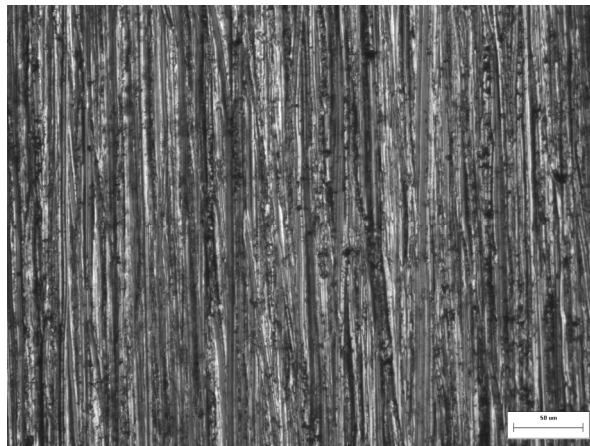
Figure 4.8: Line scan chemical analysis (EDS) analysis of non-uniform spots showing intensities of Aluminum, Magnesium, and Oxygen.

4.3.3 Effect of Grinding/Abrading on the Surface Oxide Layer

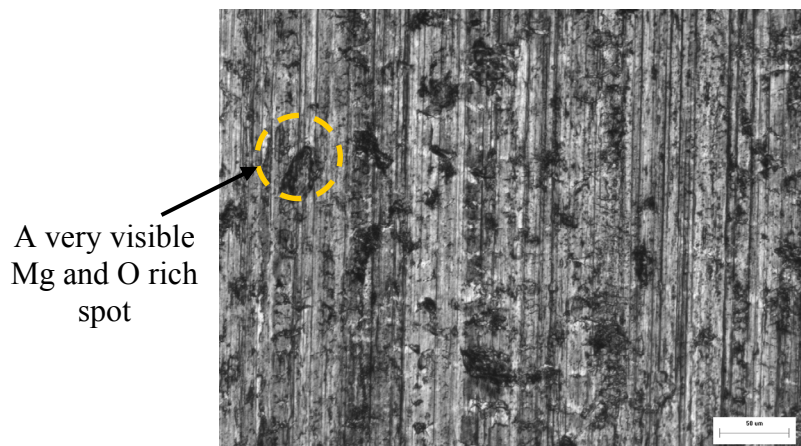
It was expected that the as-received surface would have a relatively thick and non-uniform oxide layer compared with surfaces subjected to grinding or abrading. This was confirmed both by general surface appearance and chemical analysis of these surfaces. Optical microscopy of these surfaces confirmed that grinding and abrading of the sheet surface almost removed (or reduced the size) the Mg and O rich spots from the as-received surface (Figure 4.9). Chemical analysis of some of those spots on the as-received surface confirmed the presence of high amount of Mg and O. It was also observed that those Mg and O rich spots were not uniformly distributed on the entire area of as-received surface and some area on the surface had fewer spots than others; an area of more visible Mg and O rich spot is presented here. The maximum size of the Mg and O rich spots on the as-received surface was about in the range of 30 μm . Although on the surfaces subjected to grinding and abrading, those Mg and O rich spots were not very visible as compared with as-received surface, they were visible at some places in the range of 3 – 5 μm . Chemical analysis of these surfaces revealed that the as-received surfaces had higher amounts of oxygen than surfaces subjected to grinding or abrading whereas the intensities of aluminum on the as-received surfaces were the lowest (Figure 4.10). Since all these samples were prepared from the same sheet and analyzed in the same condition, the difference in amount of oxygen was high enough to believe that the as-received surface had relatively higher amount of oxygen than surfaces subjected to grinding or abrading.



(a) grinding with 600 silicon carbide emery paper



(b) abrading with a scotch-brite wheel



(c) as-received

Figure 4.9: Effect of grinding and abrading on the surface oxide layer of AA5182.

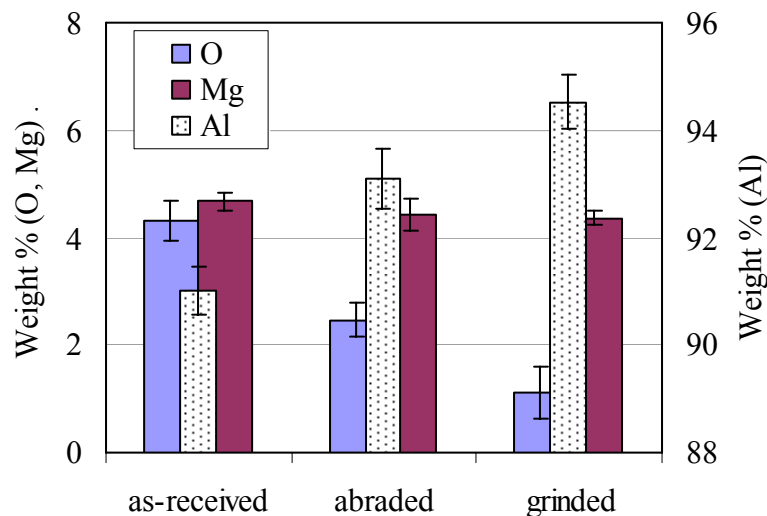


Figure 4.10: Chemical analysis of as-received, ground, and abraded surfaces of AA5182.

Since oxygen was not an alloying element of AA5182, it was likely to have come from the environment during the formation of surface oxides. High amount of oxygen in the surface layer of as-received surface clearly indicated a thicker and concentrated oxide layer on this surface compared with the surfaces subjected to grinding and abrading. A higher intensity signal for oxygen indicated a relatively thicker oxide layer and this was found for the as-received surfaces. The higher weight % of aluminum on the surfaces subjected to grinding and abrading procedures provided further evidence for a reduction in the oxide layer thickness because there was less oxide and more base alloy. It was also observed that the amount of magnesium was little lower on the surfaces subjected to grinding or abrading (about 4.4% compared with 4.7% on the as-received surface as shown in Figure 4.10) than as-received surface. Although this difference was not very significant, a slightly lower value of magnesium on the surfaces subjected to grinding or abrading was likely to be caused by the removal of Mg-rich spots from these surfaces. These findings suggested a less concentrated oxide layer on ground and scratched surfaces with fewer Mg and O rich spots compared with the as-received surface.

4.3.4 Effect of Oxide Geometry and Composition on Electrical Contact Resistance, Pitting of the Electrode and Weld Strength

As shown in the previous section, the as-received surface of AA5182, in addition to alumina (Al_2O_3), had some Mg and O rich spots, strongly suggesting the formation of MgO that were scattered over the surface. These spots were very small and covered only a small fraction of the surface. The grinding/abrading process reduced the size of these spots and was likely to have reduced the thickness of both the alumina and the MgO oxide layers.

Both of these oxides (Al_2O_3 and MgO) were ceramics [40] and as such they were electrical insulators with properties as presented in Table 4.4. Presence of these oxides made the surface of AA5182 non-conductive for electrical current. However, the oxide layer on ground and abraded surfaces appeared to have thin oxide layer without any significant amount of MgO.

Although, it was not possible to produce an aluminum surface in air without an oxide layer, grinding or abrading the surfaces and performing the experiments within two hours would have provided a surfaces with oxide layers that were thinner and more uniform in composition compared with as-received surfaces. For this reason, all surfaces that were either ground or abraded, irrespective of their roughness level, had lower electrical contact resistance of E/W interface compare with as-received surfaces.

Both these oxides (Al_2O_3 and MgO) were known to have effect on RSW of aluminum alloys in terms of electrode life and weld shear strength [33, 9, 100]. It was observed that, a thin oxide layer on the abraded sheet surface resulted in slow pitting of electrode compared with the electrode subjected to as-received surface which had thick and complex oxide layer. This observation was quite consistent with the suggested electrode pitting mechanism for thick and thin oxide layer of aluminum surface [33]. Also, in terms of weld shear strength, although, the weld shear strength of as-received surface was initially a little higher than that of abraded surfaces, it deteriorate quickly and the two values became almost equal at the end of 100 spot welds. This was more likely due to the presence of more MgO on the electrode face subjected

to as-received surface than that of abraded surface. For AA5182, with continuous welding, electrode face was found to be covered partially with MgO which was responsible [9] to localize the current conduction and deteriorated the weld shear strength.

Table 4.4: General properties of oxide layer (Al₂O₃ and MgO) and bulk of AA5182 [23,40]

Properties	Alumina (Al₂O₃)	Magnesia (MgO)	bulk AA5182
Electrical nature	Insulator	Insulator	Conductor
Mechanical nature	Brittle below 1100°C	Brittle below 1000°C	Ductile
Melting temperature (°C)	2050	2800	638
Heat Capacity (J/kg-K)	880	940	904
Thermal conductivity (W/m-K)	60	39	123
Coefficient of Expansion (1/K)	7.4×10^{-6}	12×10^{-6}	22×10^{-6}
Volume resistivity (Ω-cm)	$> 10^{15}$	$> 10^{15}$	5.6×10^{-6}
Application	High temperature electrical insulator, Refractory in furnaces, High voltage insulator	High temperature electrical insulator, Refractory in furnaces, Insulation for thermocouples	Container ends, Autobody structure, brakes, and parts

4.4 Concluding Remarks

The influences of surface roughness and oxide layer geometry on the electrical contact resistance of E/W interface, pitting of the electrode and joint shear force were determined in a series of experimental studies. A summary of these observations is given as follows.

Changing the worksheet surface roughness by grinding and abrading damaged the surface oxide layer which resulted in decrease of electrical contact resistance at the E/W interface. Extensive plastic deformation of the worksheet occur during RSW which make the real and apparent contact area almost identical thus the effect of surface roughness was more related to the damage of oxide layer. Oxide layer of the worksheet surface of AA5182 was non uniform in composition with presence of both aluminum and magnesium oxide regions. Grinding and/or abrading the worksheet surface reduced the oxide layer thickness and made it more uniform in composition by removing the magnesium oxide. These factors decreased the electrical contact resistance of the E/W interface compared with the as-received surface, thus reducing heat generation and the associated pitting of the electrode surface during RSW.

Heat generation and resulting pitting of the electrodes increased with increasing electrical contact resistance that was measured across the E/W interface prior to any welding. This conclusion meant that pitting and ultimately life of an electrode could be predicted from such electrical resistance measurements.

Chapter 5

5 Contact Mechanics at the E/W Interface

5.1 Introduction

In the previous chapter, the E/W interface was examined in a series of experiments. The electrical contact resistance at the E/W interface was found to be an important variable in terms of electrode tip life and the quality of the weld. The oxide layer on the aluminum alloy (AA5182) was non-uniform and it seemed to have an influence on the electrode pitting rate. Understanding of the influence of this layer on RSW was considered very important in attempting to improve electrode life and weld quality. The present chapter provided a detailed investigation of the contact mechanics at the E/W interface. Experiments were conducted to observe the surfaces after contact, some conclusions were drawn and then finite element analysis (FEA) was used to further explore the contact mechanics.

Experiments were conducted to observe the pitting behaviour during successive RSW and the electrode indentation into the worksheet, both before and during welding. A more detailed study of the contact mechanics during the squeeze period (before the weld current was applied) was performed using FEA. Finally, the link between contact mechanics in the squeeze period and electrode pitting was established.

5.2 Experimental Investigations

As discussed earlier, high heat generation at the E/W interface cause local melting resulting in alloying, pickup and pitting of electrodes. The following sections explore the contact mechanics of the E/W interface starting with the pitting behaviour of the electrodes during RSW of AA5182 and the contact mechanics of the E/W interface.

5.2.1 Electrode Pitting

Purpose

These experiments were performed to observe the electrode pitting behaviour during the early stage of electrode life which was usually in the range of 50 – 100 spot welds for the as-received surface of AA5182 [59].

Materials and Methods

RSW was performed on the standard welding coupons described in Figure 3.2 using the welding parameters listed in Table 3.2. Several sets (more than three) of 100 spot weld experiments were performed using fresh pair of electrodes for each set. No joint shear force measurements were performed and only carbon imprints as described in chapter 3 (section 3.5.7) were obtained to show the pitting of behaviour.

Results and Discussion

It was observed that after about 50 spot welds on the as-received surface, the pitting became clearly visible on the electrode tip and some lumps of material were found on the aluminum worksheet surface. High resolution SEM of a typical contact area on the worksheet surface

after 76 spot welds clearly showed these lumps (Figure 5.1). Chemical analysis (EDS) of the spots showed that they had high copper content (about 30 wt %) thus indicating that they were Cu-Al inter-metallic phases (Figure 5.2). Lum et al [57] presented similar observation after 77 spot welds when using similar electrodes for RSW of AA5182 of thickness 1.5 mm. They presented the observations as pitting of electrode and also used it for pitting progress along with other observations after different spot welds. The result presented here (Figure 5.1 and Figure 5.2) clearly indicated that alloyed material formed between the electrode and worksheet but adhered to the worksheet surface hence creating a pit in the electrode surface.

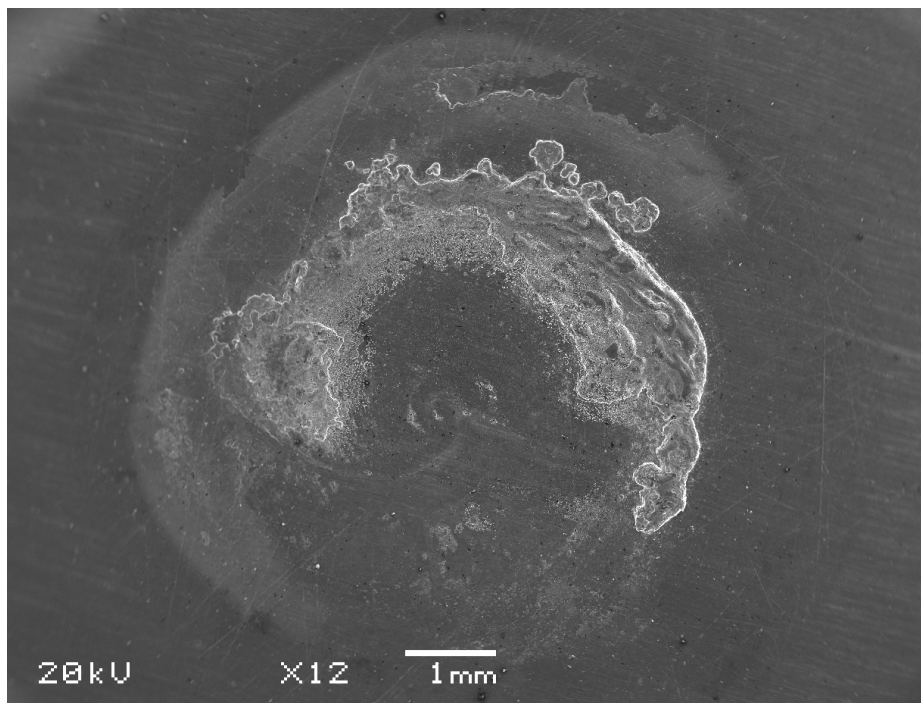


Figure 5.1: As-received worksheet surface with alloying regions indicating electrode pitting.

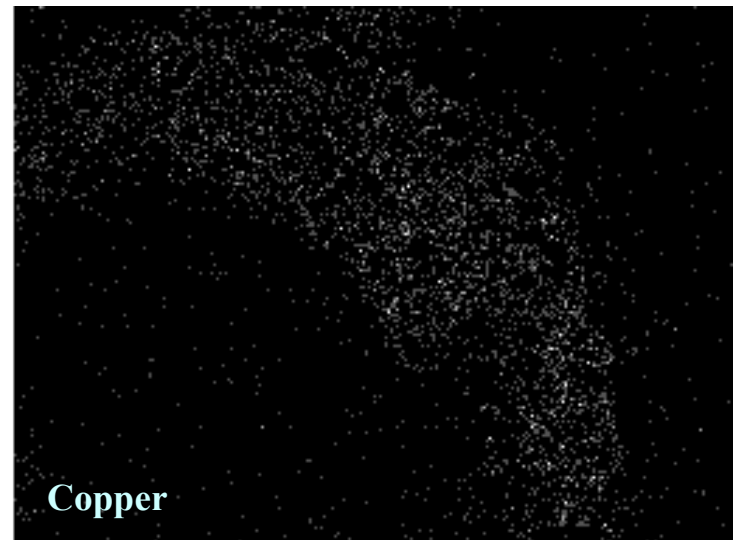
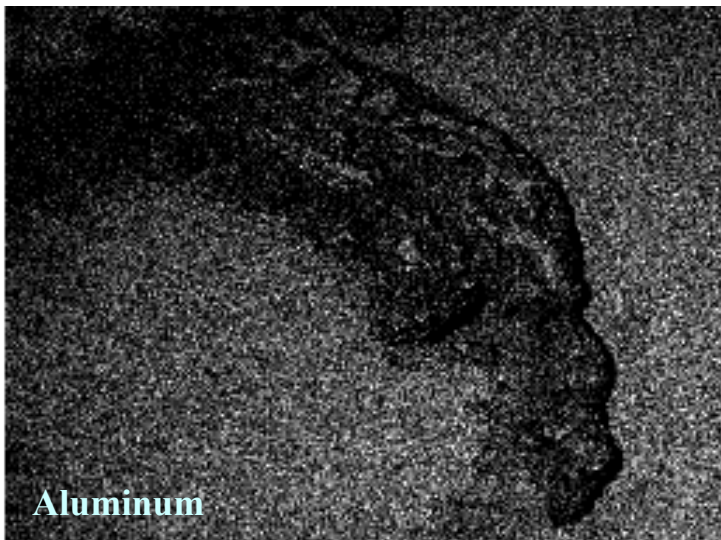
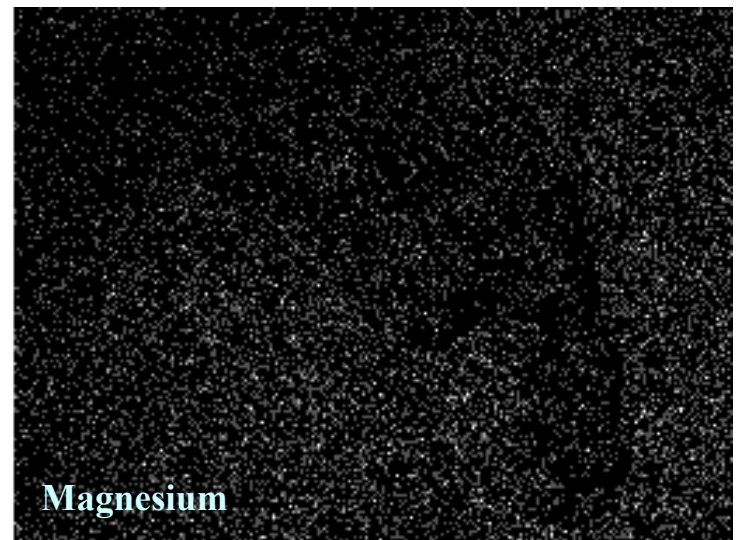
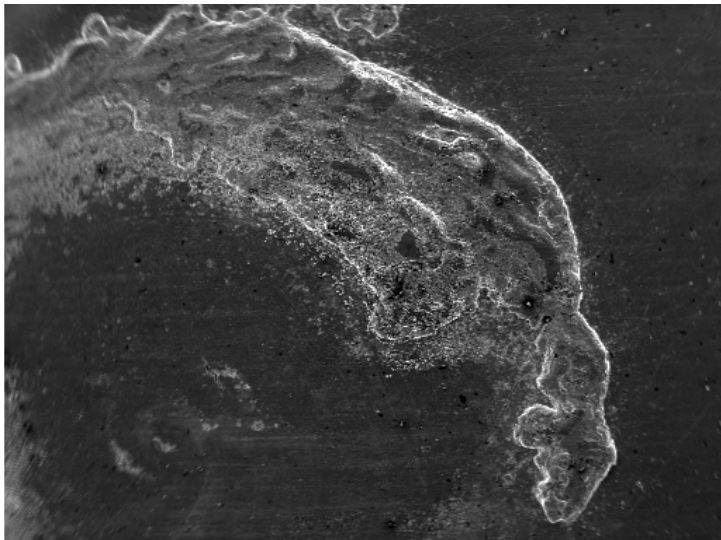


Figure 5.2: Chemical analysis (EDS) of the alloyed spots on worksheet (from Figure 5.1)

One of the most important observations from these figures was the shape and location of these pits that formed early in the electrode life. A similar pitting behaviour of an abraded surface was shown previously (Chapter 4, Figure 4.4). It was observed on the worksheet surface that the transfer lumps were not located at the centre of the contact but seemed to be developing to form a ring around the centre. After getting the shape of the pitting at the start of electrode life, the next step was to further investigate the location of ring-pitting on the surface of electrode tip. This was done by gathering carbon imprints of the electrode tip (see Section 3.5.3 in Chapter 3) at the end of 100 spot welds. These imprints showed the surface topography, contact area and pitting of the electrode. It is important to mention here that all other experiments in which continuous spot welding was performed on standard coupons (including electrode life tests) showed similar pitting behaviour and only typical examples were presented in the present section. As observed on the worksheet surface, the pitting of the electrodes started in a ring around the centre (rather than from the centre) that had a diameter of about 5.0 mm (Figure 5.3). This pattern of electrode pitting was designated in the present thesis as "ring-pitting". Earlier, Lum [59] found similar pitting behaviour under similar welding conditions including electrode geometry and worksheet material and thickness. He reported the diameter of the ring pit as 5.0 mm and accounted high contact resistance and hence high current density at the periphery. However, any detail of the contact mechanics, which is one of the main focuses of the present work, was not presented.

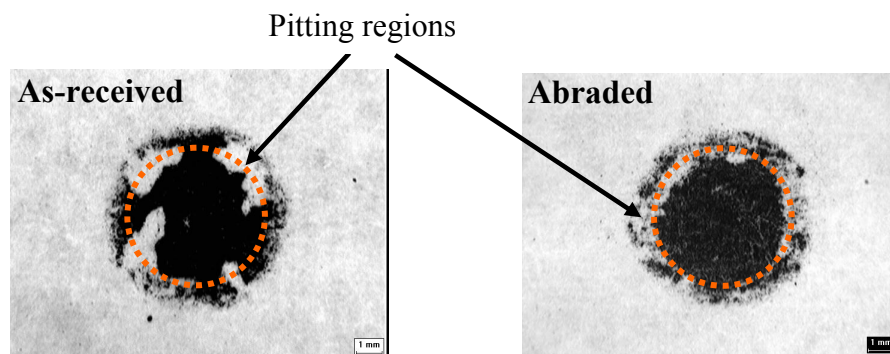


Figure 5.3: Carbon imprints of electrodes, ring-pitting pattern during the early stages of electrodes life for as-received and abraded surface; the dotted circle had a diameter of 5.0 mm and linked the local pitted regions together.

5.2.2 Contact Diameter

Purpose

In a continuing effort to investigate the contact mechanics, it was decided to study the diameter of the contact areas between electrode and worksheet for different current times during the RSW sequence.

Materials and Methods

RSW was performed with different current times (1 – 5 cycles) on the overlapped (shear force) samples (Figure 3.3). Contact diameter was measured as the diameter of indentation produced by electrodes into the worksheet (plastic deformation of the worksheet at the E/W interface) using the stereomicroscope at low magnification and Image-Pro software (see Section 3.5.7). Other than current time, all other welding parameters were kept constant with the values given in Table 3.2 and this included squeezing for 25 cycles (before the current was applied) plus holding for 12 cycles after the current had been applied.

Before any welding was done, five ‘squeezing-only’ tests were performed on similar overlapped samples (i.e. performing the RSW tests for the squeezing cycles only without the application of weld current). The intent of these squeezing-only tests was to obtain the diameter of the electrode-worksheet contact at the end of squeezing and they were each done with a fresh electrode pair to avoid the permanent contact mechanics changes that might have been present in electrode pairs with an RSW history. The subsequent welding tests, involved using five additional electrode pairs and subjecting each of them to a randomized sequence of five different current times (Table 5.1). The welding sequence was randomized so that any progressive and permanent contact mechanics changes from previous RSW would be included in the scatter of the data.

Table 5.1: Randomized sequence of RSW tests involving different current times (note that 1 cycle = 16.67 ms).

Electrode Pair	Test Sequence	Test Number	Current Time (cycles)
A	1 st	A.1	3
	2 nd	A.2	1
	3 rd	A.3	2
	4 th	A.4	4
	5 th	A.5	5
B	1 st	B.1	2
	2 nd	B.2	4
	3 rd	B.3	3
	4 th	B.4	5
	5 th	B.5	1
C	1 st	C.1	4
	2 nd	C.2	3
	3 rd	C.3	5
	4 th	C.4	1
	5 th	C.5	2
D	1 st	D.1	1
	2 nd	D.2	4
	3 rd	D.3	2
	4 th	D.4	5
	5 th	D.5	3
E	1 st	E.1	5
	2 nd	E.2	2
	3 rd	E.3	1
	4 th	E.4	3
	5 th	E.5	4

Results and Discussion

The average contact diameters were plotted against current time (Figure 5.4). The contact diameters of squeezing-only test were considered to have current times of zero. The scatter in the data from the squeeze-only tests was the lowest and, in retrospect, it might have been better to have a fresh electrode pair for each test involving RSW. However, the scatter in the RSW tests was not very much larger (particularly at the higher current times) and this

suggested that permanent and progressive changes in contact mechanics from previous RSW were indeed quite small when 0-4 previous RSW were performed.

During the weld, the contact diameter increased with the current time. This increase in diameter was most pronounced during the first cycle as had been found by others [17, 81]. Specifically, it was observed that the contact diameter between electrode and worksheet after first current cycle was 7.65 ± 0.16 mm and this was about the 57% of the total change that occurred after 5 cycles. This change in diameter was very close to the numerical simulation results presented by Sun et al [61]. However, they predicted a distinct change of slope after the second current cycle whereas the present experiments showed a change in slope after the first current cycle. Thus, the present results suggest that there might be a minor flaw in the numerical analysis of Sun et al.

Interestingly, it was observed that the contact diameter at the end of squeezing was 5.0 ± 0.06 mm which was also the location of the ring-pitting of electrodes. This observation suggested a relationship between the ring-pitting and the contact diameter before the weld current was applied.

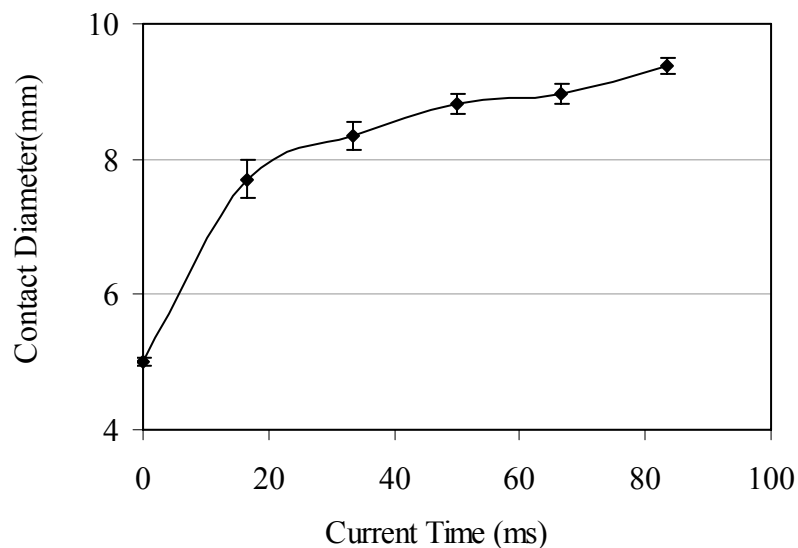


Figure 5.4: Contact diameter between electrode and worksheet for different weld times in ms (note that 1 ms = 0.06 cycles)

The increase in contact diameter was almost certainly caused by the heat generation and resulting thermal softening [97] of the aluminum sheet. Due to the high electrical contact resistance of aluminum alloys, the overall resistance at the beginning of the current time was very high but dropped sharply after about quarter of the first current cycle [17, 25, 41, 80]. Thus, it was considered likely that the high heat generation in the beginning of the weld current caused a rapid initial thermal softening and hence the initial increase in contact diameter. Once the contact area started growing, both current concentration and consequently thermal softening along with contact pressure dropped [61] so that the rate of contact area growth declined.

5.2.3 Effect of Squeezing on the Worksheet Surface

Purpose

While measuring the contact diameter after squeezing (at weld time zero) using the stereomicroscope, it was observed that the central part of the contact zone had different topographical appearance than the periphery. Since it was suspected that this topography might be related to the ring-pitting phenomenon, it was decided to study the topography of the worksheet in more detail after the squeezing period of RSW.

Materials and Methods

The as-received worksheet surfaces were relatively smooth compared with the as-received electrode tips that had visible machining marks and centre line average roughness (Ra) values of $1.48 \pm 0.04 \mu\text{m}$ (avg. \pm std dev) as shown in Figure 5.5 but these machining marks soon disappeared as successive RSW were performed.

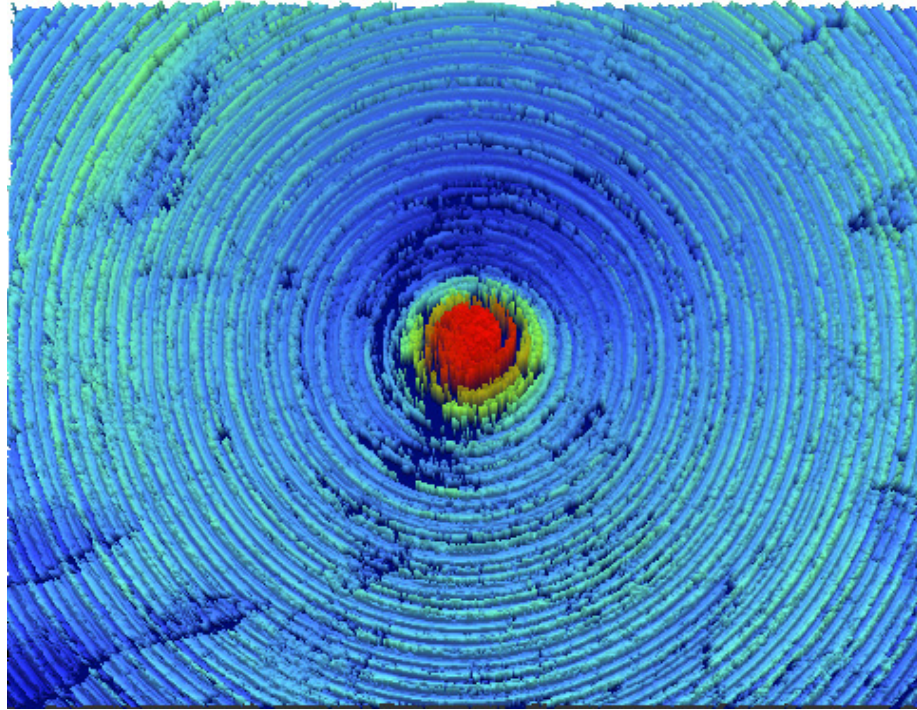


Figure 5.5: Tip surface of a typical as-received electrode showing machining marks ($R_a = 1.48 \pm 0.04 \mu\text{m}$).

Thus, the study of the worksheet topography required more than just using the as-received electrode tips. One approach would have been to use electrode tips that had been subjected to many welds (say 50 - 200) but these used electrodes had considerable variation in both macroscopic and microscopic surface geometry. Thus, it was decided for the sake of precision to produce polished surfaces with a closely controlled geometry and to use them in subsequent testing. Electrode tips were polished using abrasive paper (1200 grade silicon carbide). To accomplish this, the electrodes were rotated in a lathe and the silicon carbide paper was held manually against the electrode tips. Several electrodes (about 30) were polished and radiuses of the tips were measured before and after the polishing using profile projector (Model PH350, Mitutoyo Mfg Co. Ltd., Japan). Only those polished electrodes that retained the as-received radius of curvature (50 mm) were used in the subsequent testing (Figure 5.6). The polished electrodes had a centre line average roughness (R_a) of $0.25 \pm 0.01 \mu\text{m}$ compared with $1.48 \pm 0.04 \mu\text{m}$ for the as-received electrodes.

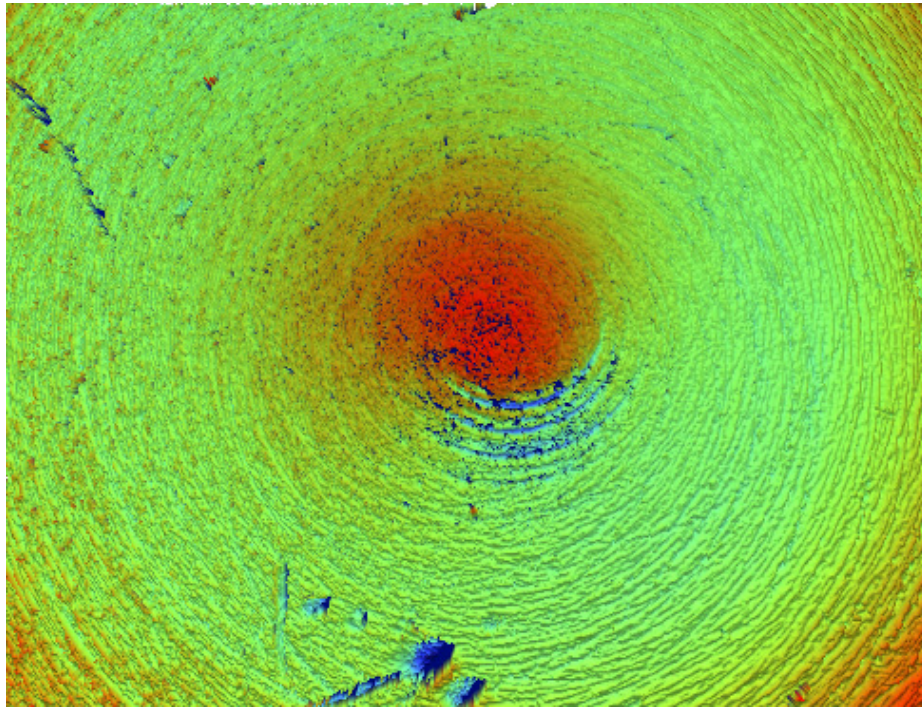


Figure 5.6: Tip surface of a typical polished electrode ($R_a = 0.25 \pm 0.01 \mu\text{m}$) showing faint evidence of the original machining marks.

The squeezing only tests were performed with polished electrodes using the same procedure as described in the previous section for the as-received electrodes. The worksheet surfaces that were produced by contact with both the as-received and polished electrode tips during squeeze only were examined closely using SEM, particularly in the peripheral zone of the contact.

Results and Discussion

In both these cases (polished or as-received electrodes), the contact diameters were in the range of 5.0 mm. When in contact with the as-received electrodes, the contact area on the worksheet surface revealed some aligned circular indentation marks (Figure 5.7). These

indentation marks were very similar in pattern to the fine machining marks found on the electrode tips. However, the machining marks on the electrode tips were the same size across its face (Figure 5.5) whereas the indentation marks on the worksheet surface were much more visible near the periphery than near the centre of the contact. This important observation suggested that the electrode had indented the worksheet with higher pressure at the periphery than at the centre of the contact zone.

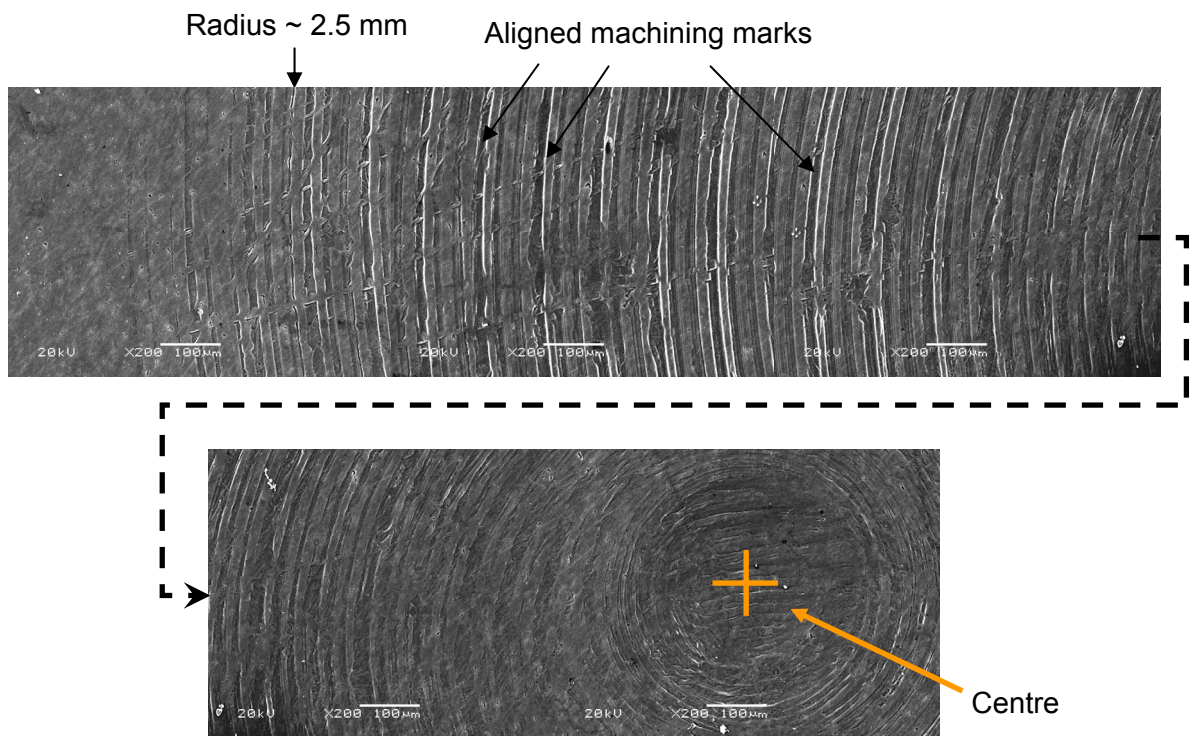


Figure 5.7: A series of SEM micrographs of the worksheet contact area (when using as-received electrodes) from the periphery into the centre after only the squeezing period of the RSW procedure.

Squeezing of the aluminum sheets with the polished electrode tips showed similar loading behaviour to squeezing with the as-received electrode tips. As expected, no machining marks were observed in this case, but it was found that squeezing produced some scratches on the worksheet contact areas. These scratches were more numerous and distinct at the periphery of the contact (Figure 5.8) compared with the interior zone. Furthermore, the interior contact zone appeared very similar to that of the untouched sheet surface outside of the contact.

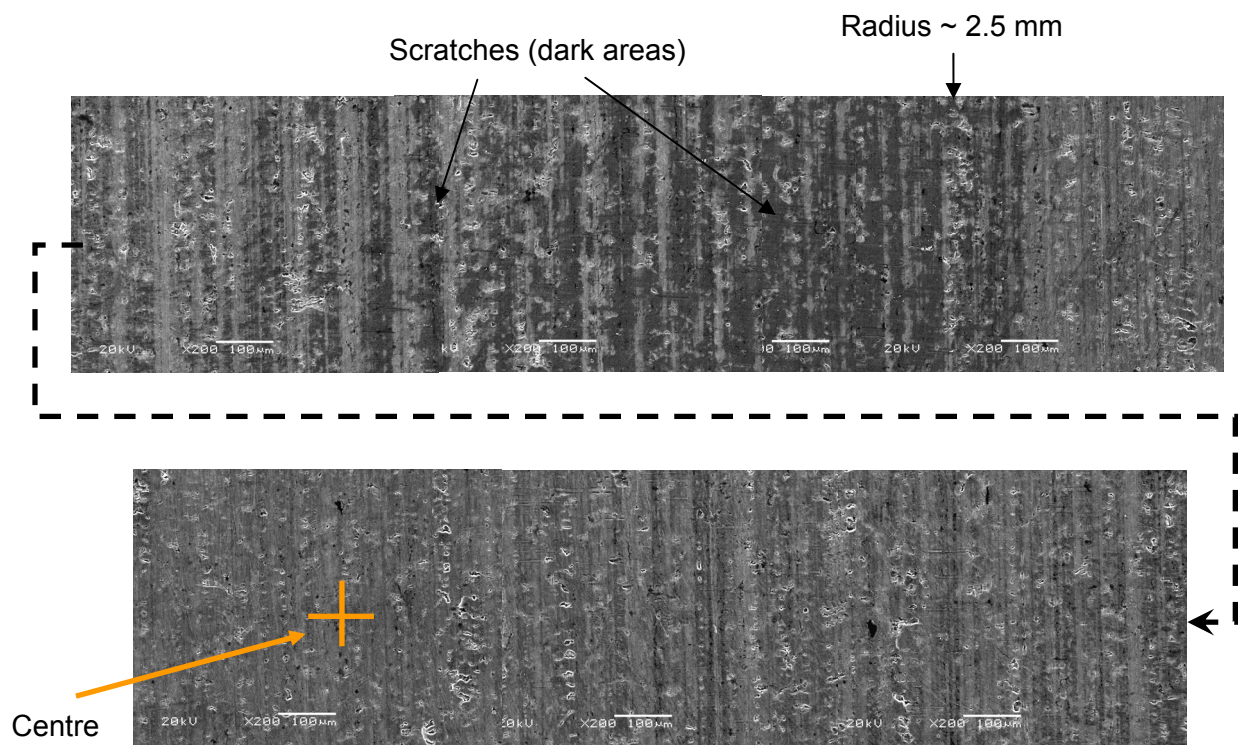


Figure 5.8: A series of SEM micrographs of the worksheet contact area (when using the smooth electrode tips) from the periphery into the centre after only the squeezing period of the RSW procedure.

5.3 Finite Element Analysis (FEA)

To further explore the contact mechanics at the E/W interface, FEA was performed over the squeezing phase of the welding sequence. The objective was to calculate the stress distribution, pressure distribution, extent of plastic deformation, and relative deformation or slip between the surfaces.

5.3.1 Formulation

The FEA model was formulated using all the essential features of the RSW squeeze process and details of this formulation were presented in Chapter 3. A commercial FEA code (ABAQUS) [93] was used for this analysis. There were two sources of nonlinearity in the model; the material nonlinearity due to and geometric nonlinearity. The time varying load function that was applied in the experiments was used in the FEA (Figure 3.10). This load function was applied incrementally by ABAQUS and the size of load increments was automatically adjusted to solve nonlinear problem efficiently [93]. Contact pair surfaces were used at the interfaces in order to permit slip at the interface and they also ensured that the surfaces in contact did not penetrate into each other during the loading [61, 93]. For each of the load increments, ABAQUS performed several iterations to deal with the non-linearity of the material in the contact mechanics problem and the elastic-plastic response of the materials. The results were available at the end of each load increment. To ensure that the mesh was refined enough to give a grid-independent solution; a convergence study [93] was performed (Appendix C) and an adequate mesh density was determined.

5.3.2 Shear Stress Distribution

FEA showed that a high pressure (normal stress) and/or shear stress occurred at the periphery of the E/W contact. The shear stress distribution along the E/W interface showed the highest stress values in the contact range of 4.0 to 5.0 mm diameter (Figure 5.9 and Figure 5.10). No limit for maximum shear stress was used in the model; the maximum shear stress was found to be a little over 80 MPa near the periphery of the E/W interface. Quite interestingly, the

value of the shear stress was not very significant near the centre of the contact. This pressure and shear stress distribution developed frictional shear stress between electrode and worksheet surface. The formulation of the present model allowed finite sliding and used coefficient of friction at the E/W interface for relative motion.

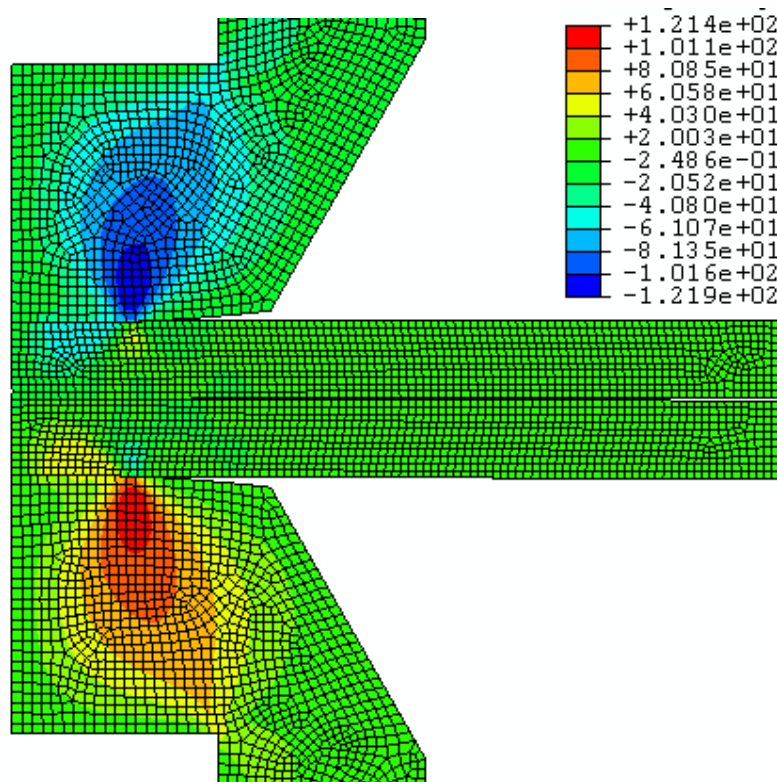


Figure 5.9: Shear Stress (MPa) distribution due to squeezing of electrode into the worksheet; contours showing the shear stress distribution in the entire model.

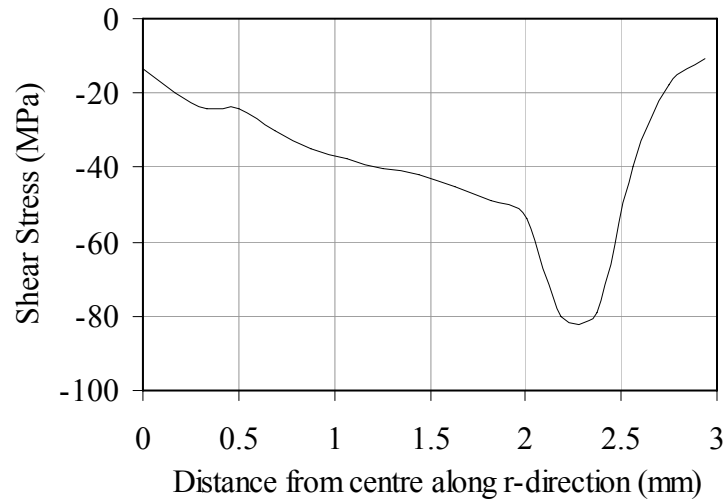


Figure 5.10: Shear Stress distribution along the E/W interface.

The distribution of the frictional shear stress between electrode and worksheet surface had similar behaviour, i.e. the frictional shear stress value was highest near the periphery and not very significant at the centre of the contact (Figure 5.11).

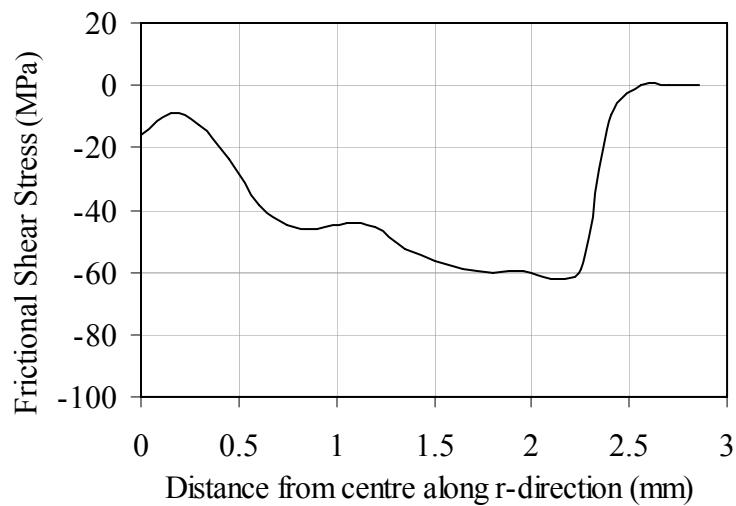


Figure 5.11: Frictional Shear Stress distribution between electrode and worksheet surfaces.

5.3.3 Pressure Distribution

The contact pressure distribution along the E/W interface had similar distribution as that of shear stress, i.e. the pressure started increasing from the centre and reached maximum value near the periphery (in the range of 4.0 mm diameter) and dropped to zero at the end of the contact at 5.1 mm (Figure 5.12). However, this change of pressure (difference) between centre and periphery of the contact was not as significant as in case of shear stress where a significant change was observed (Figure 5.9 – Figure 5.11). The contact diameter at the E/W interface obtained from this pressure distribution was 5.1 mm which agreed well with the experimental value of 5.0 ± 0.06 mm.

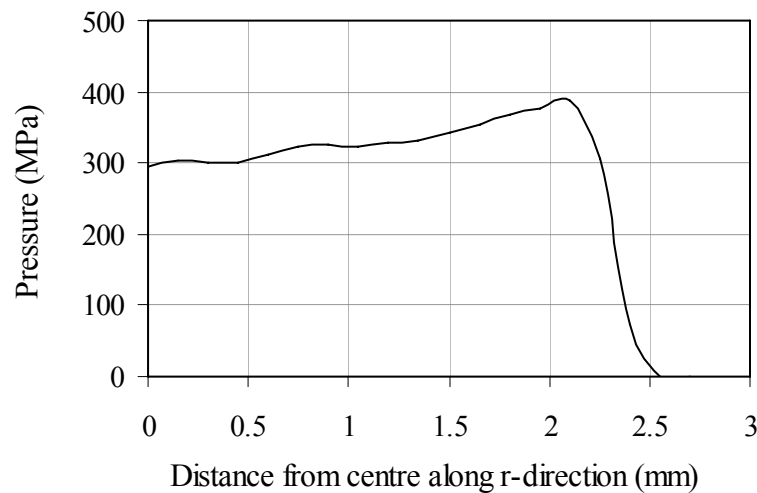


Figure 5.12: Pressure distribution along the E/W interface.

5.3.4 Slip along the E/W Interface

The presence of high shear stress near the periphery could cause microscopic slip in some part of the contact region. As explained in chapter 3 of this thesis, the present model

characterized the tangential behaviour between electrode and worksheet surface by using the coefficient of friction of 0.5. In this case, macroscopic slip would occur at this interface if the ratio of the shear stress (τ) and contact pressure (p) become greater than the value of coefficient of friction (μ). However, the stiffness method (penalty method) used for the formulation of this model connects the surface together with stiff spring and thus allow some relative motion (slip) between the contacting surfaces even if the shear stress to pressure ratio remain below the value of coefficient of friction [93]. In this manner, the stiffness method converges to a solution with less computational efforts and provides reasonably accurate stress distribution and contact shape. The magnitude of this slip, however, is limited to the “elastic slip”, i.e. micro slip and not the macro slip or bulk sliding between contacting surfaces.

The ratio of the frictional shear stress and contact pressure was calculated and plotted as a function of radial distance from the centre along the E/W interface (Figure 5.13). It was observed that the ratio of frictional shear stress and contact pressure was very low near the centre of the contact and reached the highest value at the periphery of the contact.

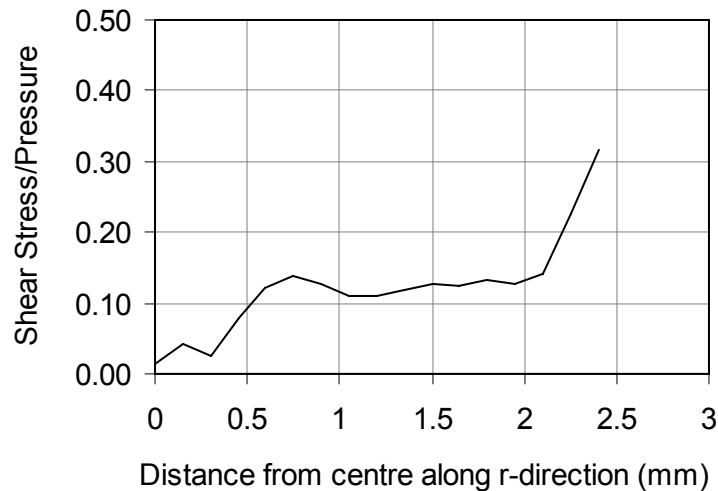


Figure 5.13: Shear Stress as a fraction of Pressure at the E/W interface.

James et al [29] performed an FEA of the contact mechanics in RSW for 2mm 5xxx aluminum alloy sheet with dome-shaped electrode with the radius of curvature of 50.8 mm but apparently did not use contact pair (that would permit interfacial slip). They presented a somewhat similar shear stress to pressure ratio variation over the contact area and speculated that a macroscopic slip occurred near the periphery for a coefficient of friction of 0.4. However, they did not model this directly and they did not present any experimental evidence.

In the present study, although, the maximum value of the frictional shear stress to pressure ratio (0.31) did not reach the value of the coefficient of friction (0.5) used for this model, some micro (elastic) slip was expected to occur due to the method used for this analysis. However, it was quite interesting to observe that the shear stress to pressure ratio was relatively quite higher near the periphery than the central contact zone. Therefore, this micro (elastic) slip was expected to be higher near the periphery than the centre of the contact. Also, as mentioned earlier in chapter 3 of this thesis [95-96], 0.3 was reported as the lowest value of the coefficient of friction for this interface and if this value is considered as true value than some macro slip would occur near the periphery of the contact at the E/W interface. However, the present model selected more realistic value of coefficient of friction (0.5) for this interface and only micro slip was expected. The amount of this micro (elastic) slip or the relative displacement between electrode and worksheet at the E/W interface was calculated and explained as follows.

The relative displacement between electrode and worksheet surfaces in the radial direction (r-direction) was calculated in the following manner. For each node at these surfaces, the displacement was calculated from the time when the load was sufficient to cause contact between the two surfaces until the end of the squeezing phase. The difference of these displacements was the relative displacement or slip between the surfaces at the E/W interface (Figure 5.14). Interestingly, the amount of slip remained insignificant in the central contact zone and only started increasing from a diameter of 3.0 mm. This increase became relatively significant near the periphery; in the range of 4.0 to 5.0 mm. Although this slip was only elastic slip, its value was relatively much higher near the periphery than the central contact

zone. This result was quite consistent with the experimental evidence where squeezing had more effect at the periphery than the centre as shown in Figure 5.7 and Figure 5.8.

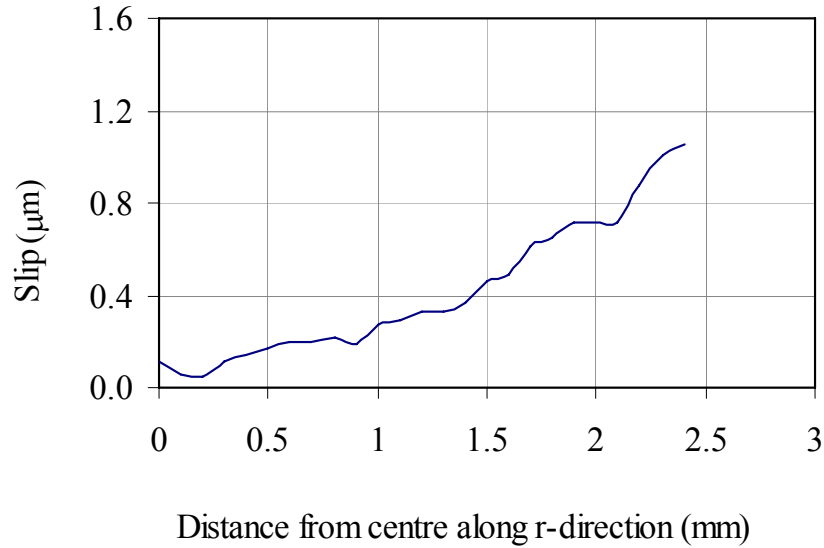


Figure 5.14: The amount of slip between electrode and worksheet at the E/W interface.

In another attempt, the sticking constraints at the interfaces were reinforced by using the Lagrange multiplier method which does not allow any “elastic slip” [93]. However, this method had convergence problem and produced converged solution for the ‘very fine’ mesh and could not converged for the ‘ultra fine’ mesh. However, this mesh size (fine mesh) was also good enough for most variables as shown in Appendix A. The analysis was performed for the coefficient of frictions of 0.3 as well 0.5. Quite interestingly, the frictional shear stress to pressure ratio obtained with this method were quite similar (Figure 5.15 and Figure 5.16) to that obtained with the stiffness method (Figure 5.13). The relative tangential motion (slip) obtained from this method did not show any slip near the centre and only some slip (about 1 µm) near the periphery (Figure 5.17 and Figure 5.18).

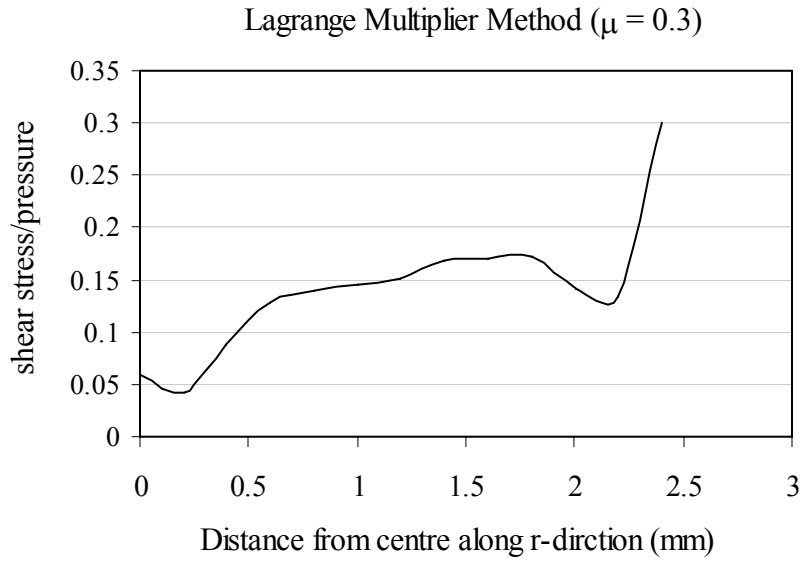


Figure 5.15: Shear stress as fraction of Pressure at the E/W interface ($\mu = 0.3$).

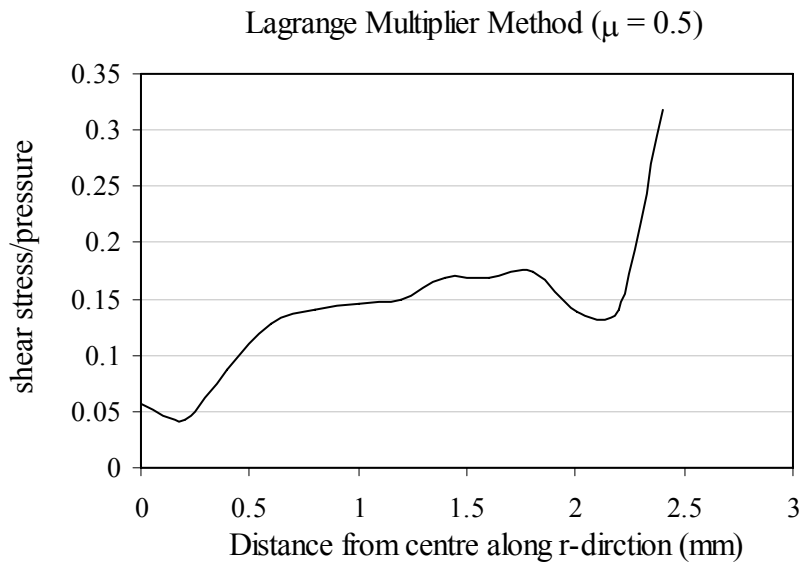


Figure 5.16: Shear stress as fraction of Pressure at the E/W interface ($\mu = 0.3$).

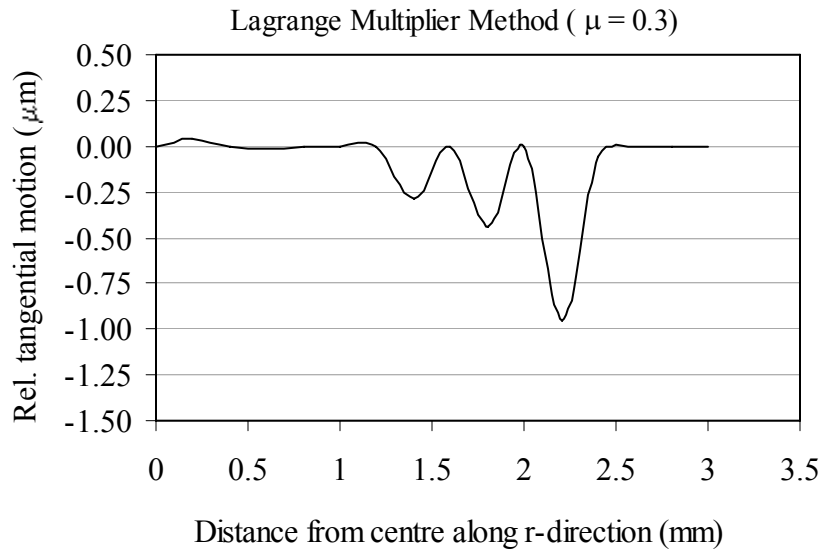


Figure 5.17: Relative tangential motion (slip) along the E/W interface ($\mu = 0.3$).

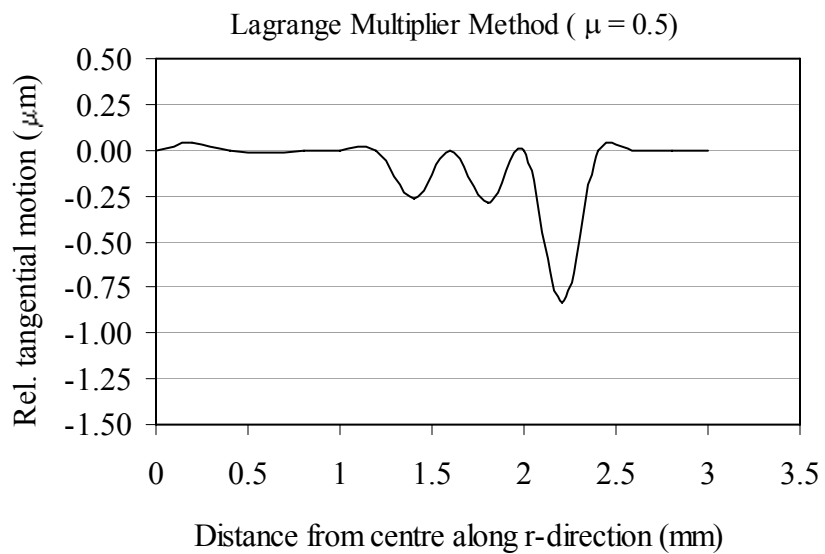


Figure 5.18: Relative tangential motion (slip) along the E/W interface ($\mu = 0.3$).

Although, the slip obtained using both analytical method (Stiffness method and Lagrange multiplier method) were not as accurately presenting the slip behaviour as shown by the shear stress to pressure ratio, all these results were quite consistent in indicating that the effect of squeezing was more at the periphery than at the centre. Also, all these results were very consistent with the physical condition of the E/W interface observed experimentally. All these results and analysis clearly suggested that the squeezing process caused some micro slip only at the periphery of the contact at the E/W interface.

5.3.5 Contact Mechanics at the E/W Interface

Results from the FEA model along with experimental observations explained the ‘Contact Mechanics’ at the E/W interface which provided the true explanation of the ring-pitting of electrodes. During squeezing, high shear stress to pressure ratio at the periphery of the E/W interface caused slip to occur in that zone. That slip would result in significant scratching of oxide layer on the worksheet and established a good metal-to-metal contact zone. Although, there could be some spots in other contact zone where metal-to-metal contacts would established due to surface roughness (asperity tip cracking). However, the size and number of those spots would be very insignificant compare with the scratched zone near the periphery. Current always takes the least resistant path; a bigger area of metal-to-metal contact means less resistance. At the beginning of weld current, the periphery of the contact would provide the least resistance path for current flow from this interface. However, because of the high amount of current, there would always be constriction resistance due to current concentration. This kind of high current density near the periphery of this contact, at the beginning of the weld current, was also predicted by another FEA analysis [83]. The constriction resistance near the periphery would have resulted in high heat generation in this zone. High heat generation near the periphery along with the low melting temperature of aluminum worksheet caused local melting which resulted in alloying, pickup, and pitting of electrodes. A combination of all these effects led towards ring-pitting of electrodes.

At the same time, due to high heat generation at this interface, the base alloy of the worksheet became soft due to thermal softening. High pressure and thermal softening of the worksheet caused electrode to penetrate into the worksheet which resulted in contact area growth between electrode and worksheet. The overall effect was reduced pressure and reduced current density hence low heat generation; the contact area growth rate decreased after first current cycle.

5.4 Concluding Remarks

The experimental results clearly indicated that during squeezing and during the initial weld time, the periphery of the E/W contact area (having a diameter of about 5.0 mm) had the highest contact stress and, in the early electrode life, the most pitting. These results suggested that some significant tribo-mechanics might be occurring in this peripheral region at the time of squeezing before the current flowed and the RSW procedure was completed. This suggestion was very important because much RSW research had concentrated on the complex welding process itself and paid less attention to the “stage setting” contact mechanics.

Results from the FEA along with the experimental observations provided a consistent explanation for the ring-pitting of the electrodes. During squeezing, high shear stress to pressure ratio at the peripheral zone of the E/W interface caused some slip to occur. The slip caused abrasion of the aluminum sheet surface and this might break up the oxide layer on the worksheet thus allowing some direct metal-to-metal contact. The current would take the least resistant path and a zone with metal-to-metal contact means less resistance. Thus, at the beginning of weld current phase of the welding sequence, the periphery of the contact would provide the least resistance path for current flow through the E/W interface. However, the high current density would face a constriction resistance because the regions of direct metal contact would be relatively small and so the local temperatures would climb as energy (or heat) was generated. This heat generation near the periphery, along with the low melting

temperature of the aluminum worksheet, would cause local melting, alloying, pickup, and eventually ring-pitting of electrodes.

Chapter 6

6 Contact Mechanics at the Faying Surface

6.1 Introduction

Contact mechanics at the electrode-worksheet interface was presented in Chapter 5 and provided an explanation for the ring-pitting behaviour of electrode and contact area growth at that interface. In the present chapter, a similar approach was attempted to understand the start of melting, nugget formation, and nugget growth behaviour at the faying surface.

Contact mechanics at the faying surface and resulting nugget growth behaviour were investigated. Again both experimental work and FEA were adopted to understand the interaction at this interface. Finally, a comprehensive understanding of the contact mechanics at this interface was presented.

6.2 Experimental Investigation

High and uniform heat generation at the FS is essential for proper nugget formation. As discussed earlier (Section 2.1), the contact resistance at the FS provides the heating that causes melting to occur at this interface and hence nugget formation. The following sections explore the contact mechanics at the FS experimentally starting with the nugget formation, growth and shape during RSW of AA5182.

6.2.1 Nugget Formation, Growth and Shape

Purpose

These experiments were conducted to monitor the nugget formation at the FS. The intent was to observe the nugget formation behaviour, shape of the nugget during different stages of the melting and nugget growth rate.

Materials and Methods

First step in this regard was to observe the nugget formation. Nugget size was monitored by performing RSW on overlapped samples (Figure 3.3) of AA5182 for different current times (1 – 5 cycles). Other than current time, all other welding parameters were kept constant with the values given in Table 3.2 and this included squeezing for 25 cycles before the current was applied plus holding for 12 cycles after the current had been applied. Three sets of experiments were performed each with three pair of electrodes. Typical nugget cross sections for all these welds were performed using a standard metallographic procedure (Section 3.5.5) up to the stage of manual grinding with 1200 silicon carbide paper and further polishing was not considered necessary to view the nuggets. However, a typical set of these nugget cross-sections were prepared completely up to the last stage of polishing and viewed through optical microscope to obtain a very precise view.

Also, the experiments reported earlier in chapter 5 of this thesis (Table 5.1) to monitor the contact diameter at the E/W interface were used to monitor the joint shear force as well. Since the present chapter deals with the faying surface, it was found appropriate to present the results of the joint share force here in this chapter.

Also, RSW was performed on some overlapped shear force samples (Figure 3.3) using low current magnitudes; the intent of these experiments was to monitor the shape of the nugget at low currents.

Results and Discussions

A typical set of nugget cross section for the various current times showed several interesting features (Figure 6.1). Although smaller, but the nugget seemed to be completely formed after applying the current for 1 cycle. As mentioned in chapter 3 of this thesis, when selecting the welding parameters for the present materials, it was observed that 1 current cycle (16.67 ms) at 29 kA was not enough for proper joint properties. However, the apparent formation of a complete nugget during the first current cycle showed that how difficult it is to monitor real nugget growth pattern for this material. Since 1 cycle was the minimum time that the spot welding machine could apply, it was considered possible that even less than 1 cycle might be sufficient to allow nugget formation.

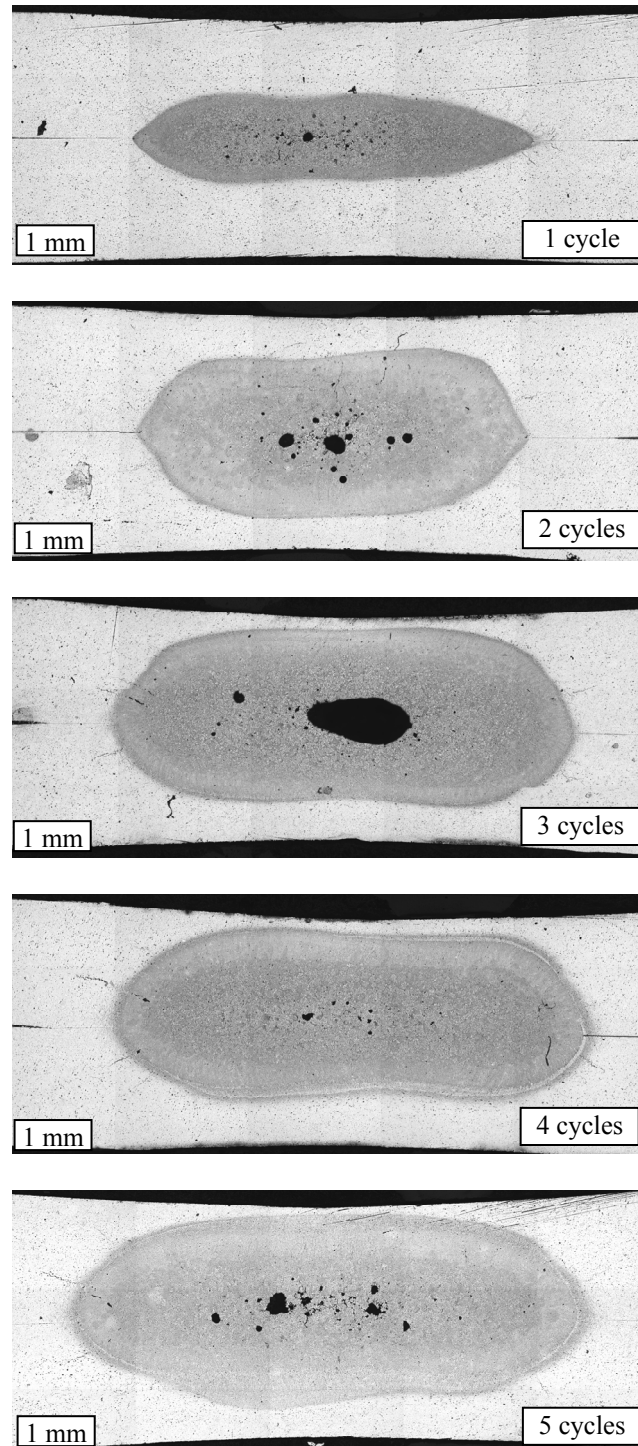


Figure 6.1 Nugget cross-sections showing the shape and nugget growth for different current time (1 – 5 cycles).

The second main finding of these experiments was related to the nugget growth with current time. As expected, the nugget size grew with current time but the growth rate was faster during the 1st current cycle. After that, the expansion of the nugget occurred more slowly. This finding was supported by the joint shear force values measured for the RSW process reported earlier (Table 5.1) and plotted against current time (Figure 6.2).

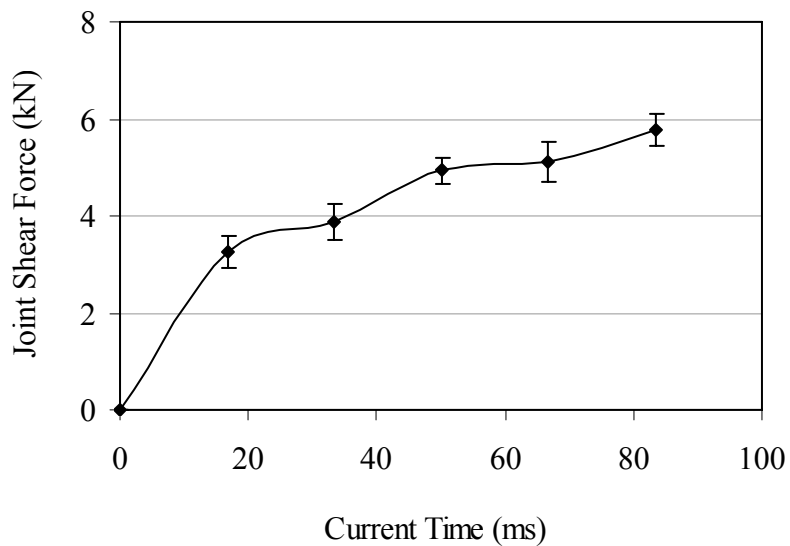


Figure 6.2: Average joint shear strength of RSW when welded for different current time.

Two visible growth rates (slopes) were observed; the growth rate during the 1st current cycle was much higher than the growth rate during the last four cycles. It was reported [52, 82] that during RSW of aluminum alloys, the electrical contact resistance of the FS dropped sharply during the 1st current cycle and remained very low during the remaining current time. Obviously, a high resistance in the beginning would cause more heat generation than during the remaining current time which was the case here. Simultaneously, the good thermal conductivity of aluminum allows very high rate of heat transfer [6] from the FS and did not allow the nugget to grow both in radial and axial directions.

Another interesting observation that can be brought into focus from Figure 6.1 was the shape of the nuggets itself. These nuggets were not exactly elliptical; rather they were elliptical from the two ends but had less height at the centre. The shape gave the indication that two ellipses grew and merged with each other and produced a nugget which had a shape that resembled a doughnut but without a hollow middle section. This shape of weld nugget was very obvious in the beginning (after the first and second current cycle) of the nugget formation but still remained visible at the end of the 5 – cycle. The shape of these nuggets suggested that the melting at the faying surface did not start in the centre; rather it started at an intermediate radial distance from the centre and grew both inwards and outwards. This type of peripheral melting was suggested somewhere else [32, 83, 85, 89] and will be discussed in next section. The growth was more extensive in the inward direction and merged to form a continuous nugget. This general doughnut-shaped nugget was observed for all cases, particularly at lower current times, although there were few minor differences in porosity.

This doughnut shape of the nugget was most obvious at low current; Figure 6.3 shows another typical example of this shape of the nugget when RSW of AA5182 was done for lower current of 20 kA for a current time of 1 cycle.

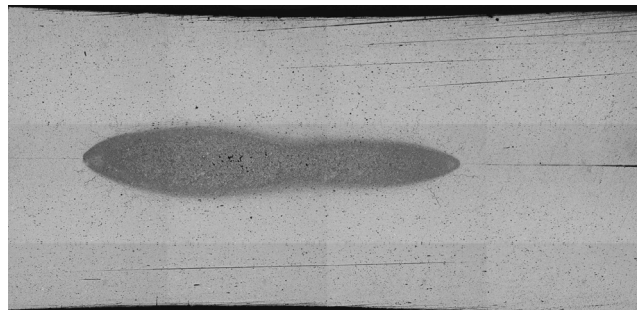


Figure 6.3: Shape of the nugget after RSW of AA5182 with 20kA for 1 current cycle.

6.2.2 Start and Progress of Melting at the FS

Purpose

In general, aluminum alloys require very high current for a successful nugget formation and even for a low current time, the RSW produced a small but complete nugget as shown in Figure 6.1 and Figure 6.3. In this situation, it was quite difficult to locate the start of melting at the FS. Thus, RSW of AA5182 sheets was performed for very low current in order to observe the location of the start of melting and to monitor the nugget growth pattern. A similar approach was taken by Kaiser et al [89] for HSLA steel.

Materials and Methods

Initially, several spot welds were performed using 10 kA and 15 kA on overlapped (shear force measurement) samples (Figure 3.3) for different current time. Spontaneous melting was observed at the FS of these spot welds. A complete set of RSW was then performed on similar overlapped samples using current in the range of 10 kA and 20 kA with an increase of 1 kA; for each current magnitude, the current was applied for only 1-cycle. RSW was also performed on overlapped samples using current magnitude of 10 kA and 15 kA for different current time (1 – 5 cycles) for each current (Table 6.1).

Results and Discussion

The current magnitude (10 – 20 kA) used in these experiments was not appropriate for RSW of AA5182 (the appropriate current for AA5182 was in the range of 27 – 31 kA) and only spontaneous melting was expected. Figure 6.4 shows typical SEM micrographs of the melting process at the FS while performing RSW for low currents and low current time (test sequence 1 – 11, Table 6.1). As expected, the melting occurred at different spots in the contact zone; the size and number of the melted spots increased with increasing current magnitude. It was observed that all of those melted spots were near the periphery of the contact without any significant melting at the centre. For higher currents in this range (15 kA – 20 kA), these spots grew and merged to form a very clear melted ring around the centre.

Table 6.1: RSW test sequence involving different current magnitude and current times (note that 1 cycle = 16.67 ms).

Electrode Pair	Test Sequence	Current Magnitude (kA)	Current Time (cycles)
F	1 st	10	1
	2 nd	11	1
	3 rd	12	1
	4 th	13	1
	5 th	14	1
	6 th	15	1
	7 th	16	1
	8 th	17	1
	9 th	18	1
	10 th	19	1
	11 th	20	1
	12 th	10	1
	13 th	10	2
	14 th	10	3
	15 th	10	4
	16 th	10	5
	17 th	15	1
	18 th	15	2
	19 th	15	3
	20 th	15	4
	21 st	15	5

This melting behaviour suggested that at the beginning of the nugget formation, there was more heat generation at the periphery than at the centre. Even at 20 kA, there was melting in the ring near the periphery while the central portion was still not yet melted completely. Interestingly, the locations of these melted spots (outer diameter) were in the range of 4.0 – 5.0 mm. Thornton et al [32] also suggested initial melting at the periphery of the FS when spot weld aluminum alloy with spherical electrodes. He accounted good contact near the periphery than at the centre for this melting behaviour. Chang et al [83] performed FEA for similar welding conditions and compare it with experiments. Although, his FEA showed elliptical nugget, his experimental nugget appeared similar to those presented earlier. Although he reported high current density at the periphery during the initial stage of the weld

phase, they [83] did not mention this shape in their work. Kaiser et al [89] reported that high current and short current time caused peripheral melting when used flat tip electrode for steel. He believed that the peripheral zone provided good metallic contact and hence the least resistance zone because it deformed easily. Feng et al [85] reported similar observation for RSW of steel with flat tip electrode. He also found good metallic contact at the central region during the early stages of the weld as the main reason for peripheral melting. Although, these works showed peripheral melting, none of the work showed a doughnut shaped nugget presented here neither provided details of the contact mechanics that actually happened at the FS during squeezing process particularly for the RSW of aluminum alloy.

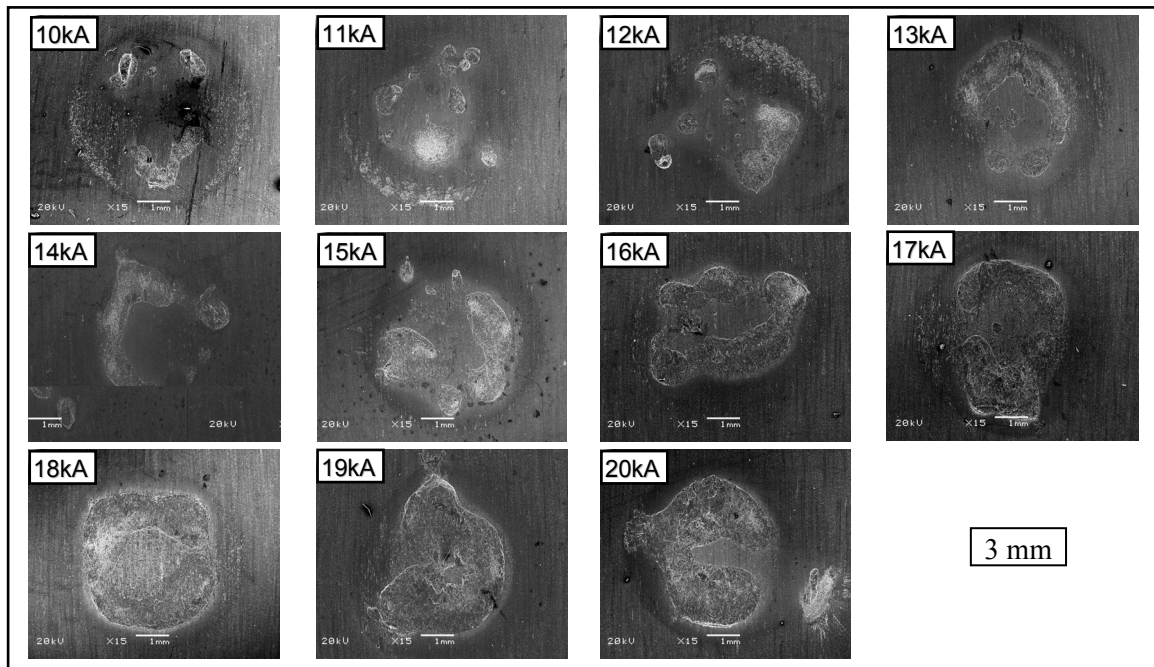


Figure 6.4: SEM micrographs showing heat generation and start of melting at the faying surface spot welded at low currents (10 – 20 kA) for short current time (1 cycle).

Welding for different current times (1 – 5 cycles) at low current of 10 kA and 15 kA showed the melting growth pattern at the FS. Similar behaviour was observed for both these current

magnitude and a very clear observation of melting growth at 10 kA (test sequence 12 -14, Table 6.1) is presented here (Figure 6.5). Once again it was observed that the melting started at the periphery and proceeds inwards with increasing weld time. It was observed that the central portion of the FS was heat affected at the end of 3 cycles; however, there was no melting of the sheet metal. These observations very clearly showed that during the RSW of AA5182, melting at the FS started in a ring near the periphery and proceed inwards from all sides and merge to form a complete nugget with central contact zone melts at the end of nugget formation. A melted spot at the FS means both the high current (I) and high resistance (R) for the required heat generation (I^2Rt). High current concentration caused constriction resistance [29-33, 44] and start of melting near the periphery clearly indicated the current concentration in this zone in the beginning of weld current.

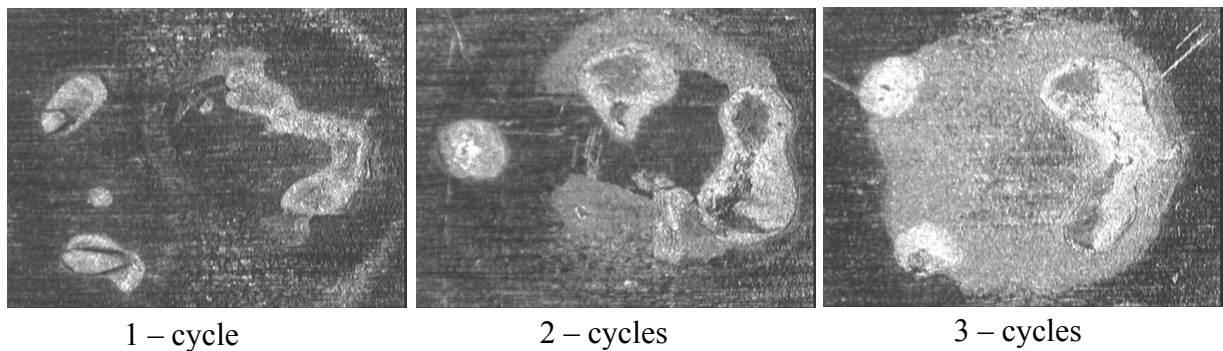


Figure 6.5: Start and progress of heat generation (melting) at the faying surface spot welded at low current of 10 kA for different weld time (1 – 3 cycles)

6.3 Finite Element Analysis (FEA) with Additional Experiments

To further explore the contact mechanics at the FS, FEA was performed over the squeezing phase of the welding sequence. The objective was to calculate the stress and pressure distribution, sheet separation, extent of plastic deformation, and displacement at this interface.

6.3.1 Formulation

Details of the FEA formulation were presented in Chapter 3 of this thesis and a brief description was also presented in Chapter 5. Due to the symmetrical nature of the spot welding setup, significant shear stress and slip were not expected at the FS.

6.3.2 Contact Pressure and Contact Diameter

The pressure distribution at this interface showed the highest values at the centre and dropped to zero at the end of the contact (Figure 6.6). This pressure distribution was typical for RSW of aluminum alloys with spherical electrodes and similar FEA results were reported earlier [61] for the FEA of aluminum alloys with radius electrodes. The pressure distribution was also used to define the contact diameter at this interface which was found to be 5.4 mm.

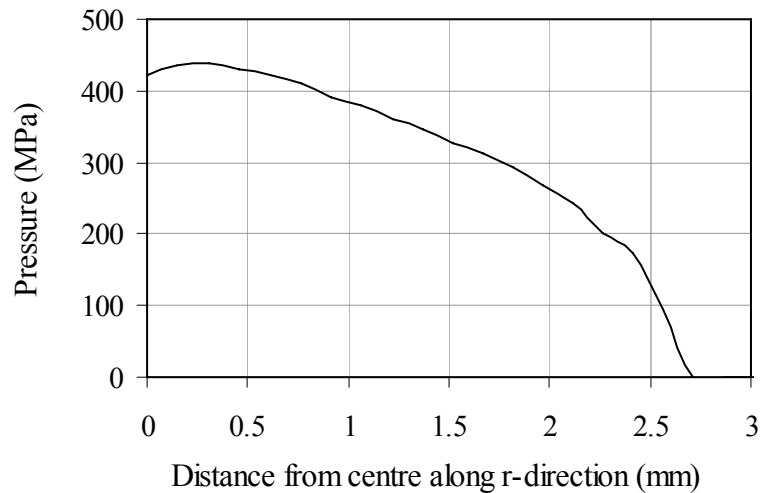


Figure 6.6: Distribution of contact pressure at the faying surface after squeezing.

Experimentally, the contact diameter of the FS after squeezing was measured by placing carbon imprints between the worksheets during squeezing. Five overlapped specimens were used and the contact diameter of the FS was measured as discussed in chapter 3 (section

3.5.7). The average contact diameter of the FS at the end of squeezing was found to be 5.3 ± 0.04 mm.

The contact diameter obtained through FEA showed good agreement with the experimental values (Figure 6.7). Both experimentally and analytically (FEA), the value of the contact diameter of the FS was just a little higher than the contact diameter of the E/W interface. Experimental values showed a contact diameter of FS of 5.3 ± 0.04 mm compare with 5.0 ± 0.06 mm for E/W interface while the FEA analysis found a contact diameter of 5.4 mm at the FS compared with 5.1 mm for the E/W interface. These results showed very good agreement between experimental values and FEA analysis. Other FEA analyses [60-61] showed similar behaviour where the contact diameter of the FS was reported a little higher than that of the E/W interface.

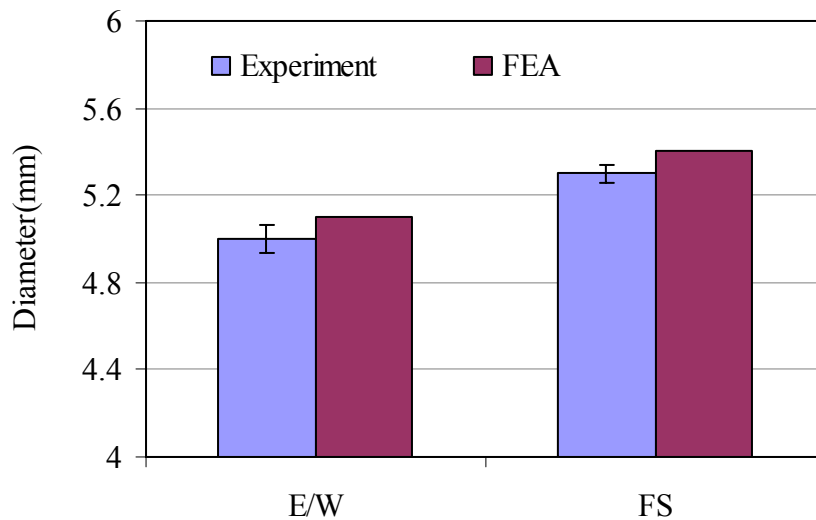


Figure 6.7: Contact diameters of the FS and E/W interface obtained experimentally and through FEA.

6.3.3 Sheet Separation

The most significant of these results was the sheet separation from the end of the contact at the FS (Figure 6.8). As described earlier in chapter 2 (section 2.4), sheet separation is a

typical characteristic that occurs during RSW, particularly during RSW of aluminum alloys [13].

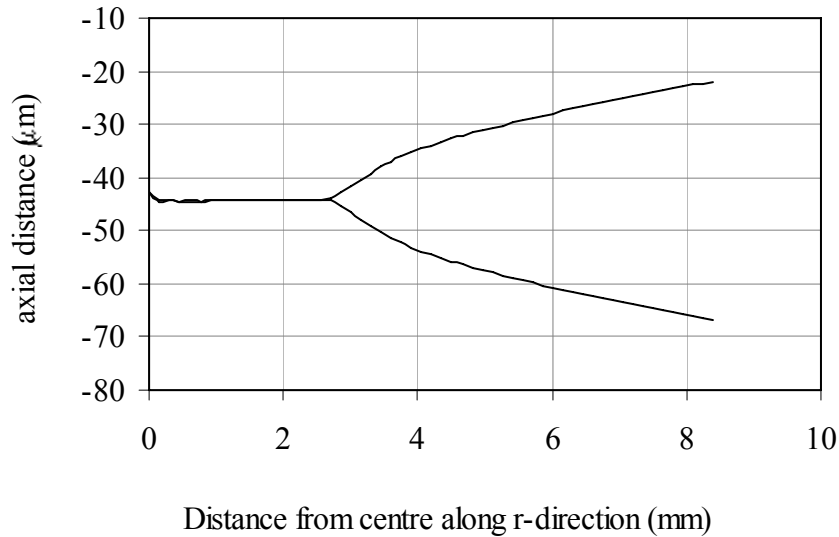


Figure 6.8: Axial position of the two worksheets at the FS showing sheet separation at the end of the contact.

Sheet separation due to squeezing was also observed through experiments. Strips of AA5182 sheets of size 120 x 30 mm (Figure 3.1) were used for these experiments. Two such strips were brought in complete overlap with each other to make a sample. These samples were squeezed between electrodes with the same welding force of 6.0 kN and sheet separation was measured at a distance of 60 mm from the centre (Figure 6.9). Ten measurements were obtained and the average sheet separation (A) was found to be $91 \pm 13 \mu\text{m}$.

The space available around the electrode in the spot welder (Figure 3.5) did not allow measuring the sheet separation accurately anywhere closer than this 60 mm from the centre while the FEA model used sheets that were only 15 mm away from the centre. It can be seen that the slope of the sheet separation (Figure 6.8) was not same thorough out and therefore, an exact comparison of the experimental values with that of FEA results was not possible and is

not discussed here. However, the sheet separation was observed both experimentally and from FEA.

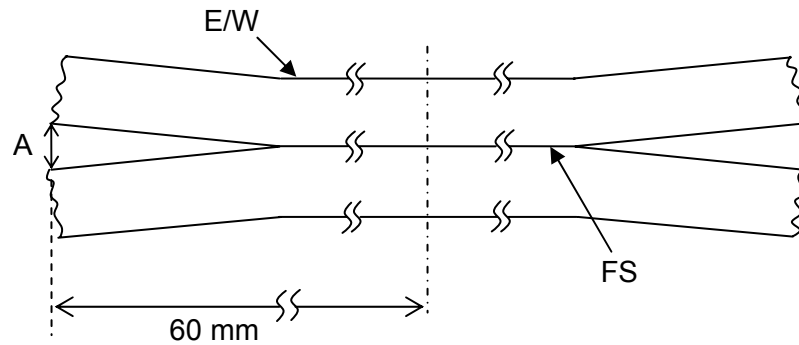
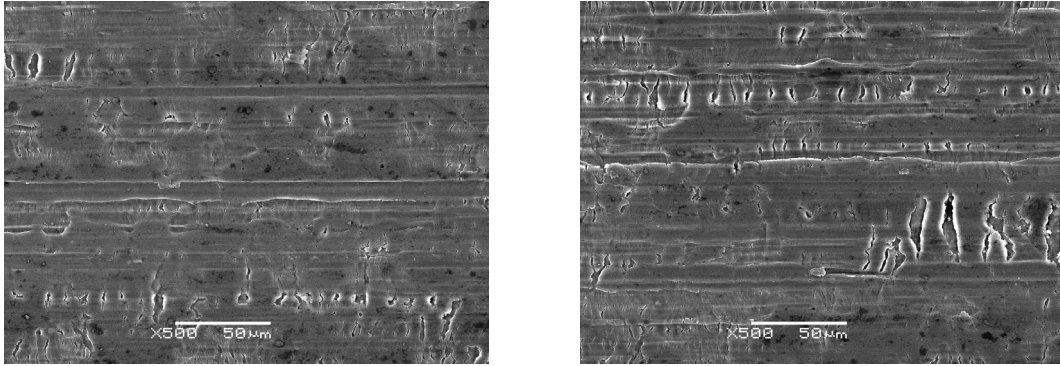
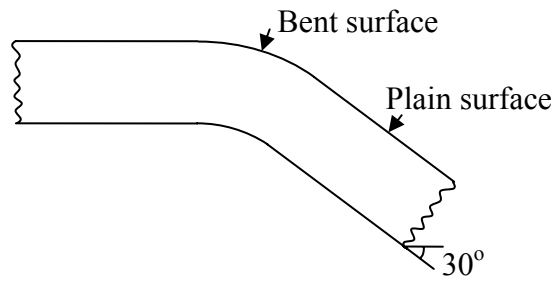


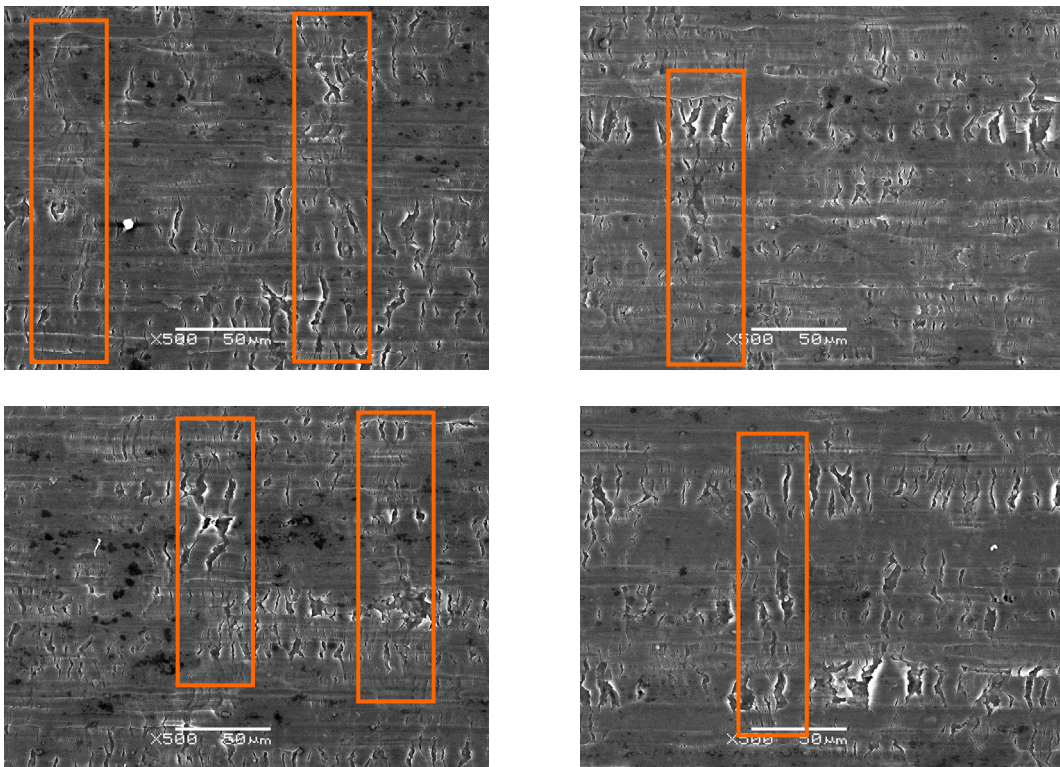
Figure 6.9: Schematic illustration of experimental measurement of sheet separation due to squeezing; the average value of A is $91 \pm 13 \mu\text{m}$.

6.3.4 Effect of Sheet Separation

As mentioned earlier [40, 50-51], oxide layer on aluminum sheet surface was very hard compare to base metal and fractured in brittle manner under straining. Sheet separation, from the end of the contact, acted like bending and although, an oxide layer was not included in FEA, in reality, the bending of sheet from the end of the contact could cause the fracture of hard oxide layer. To evaluate the effect of bending due to sheet separation on the worksheet surface layer, exaggerated bending was produced to enhance the effect of bending. Samples similar to those used in sheet separation measurements were clamped from the centre and force was applied to produce about 30° bend in the sheets. Three such pairs were bended in similar manner. Plain and bent surfaces, taken from the same samples, were observed through SEM and typical micrographs are presented (Figure 6.10). Two significant effects on the bent surfaces were observed; (i) the cracks on the bent surface got enlarged due to bending and (ii) these cracks got aligned at several locations to produce larger cracks. These sort of large and aligned cracks were not observed on the plain sheet surface.



(a) Plain sheet surface



(b) Bend surfaces

Figure 6.10: Effect of bending on surface layer; enlarged and aligned cracks are visible on bent surfaces.

The actual sheet separation during the squeezing had much less bending than the exaggerated bending as shown above and hence the effect of squeezing on the surface layer cracking was not expected to be as obvious as shown in Figure 6.10. However, it was possible to locate such effect, to a lesser extent, on some squeezed samples. FS of all of the specimens used for sheet separation measurements were observed through high resolution SEM at high magnifications and two obvious effect of sheet separation on the surface layer cracking is presented (Figure 6.11). Once again, some significant and aligned cracks were observed along the periphery; importantly, these kind of aligned cracks were not visible anywhere else in the entire contact zone.

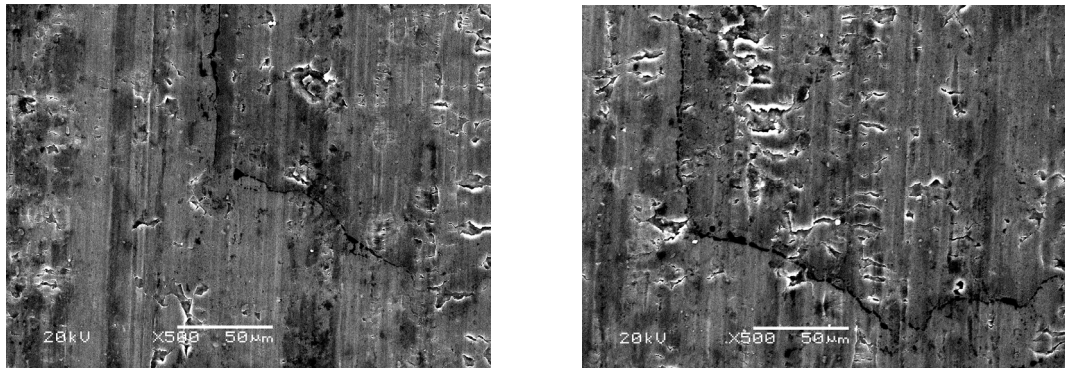


Figure 6.11: SEM micrographs showing the effect of sheet separation on the surface layer of AA5182; visible cracks at the periphery of the contact at the FS

6.3.5 Location of Sheet Separation

Having observed the effect of sheet separation on the oxide layer cracking, it was considered important to monitor the sheet separation locations during the squeezing. Since it takes 5 cycles (83.3 msec) to apply and reach the maximum load during squeezing, it was decided to locate the point of sheet separation during different stages of load increments.

It was observed that the sheet separation started as early as the loading started and the location of sheet separation as well as the amount of sheet separation changed with increasing loads. The initial location where the sheet separation occurred during the early stage of loading was found at a diameter of 4.0 mm. With increasing load, this location moved away from the centre and at full load of 6 kN (after 5 cycles), sheet separation was found at the end of contact at this interface (Figure 6.12). The effect of sheet separation on the surface (oxide) layer cracking was already explained in the previous section. The movement of the location of sheet separation with load indicated that the oxide layer cracking during squeezing started very early. However, with increasing load, contact area at the FS grew and collapsed sheets near the periphery. Interesting to note here that although, the contact pressure dropped to zero at the end of the contact, it remained significant in the range of 4.0 5.0 mm (Figure 6.6). It was believed that in this range, there would be more cracks in the oxide layer and the contact area in this zone would have some significant amount of metal-to-metal contacts.

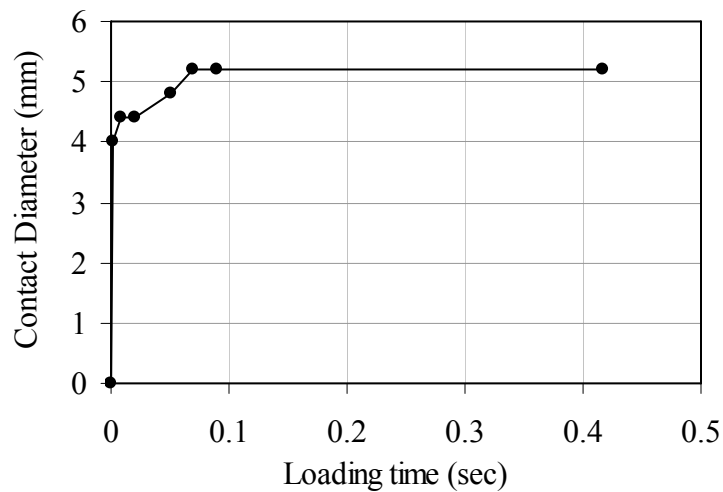


Figure 6.12: Location and movement of sheet separation at different stages of squeezing.

6.3.6 Plastic Deformation Zone

Another result of the FEA that enhances the sheet separation and contact diameter values was the distribution of plastic strain in the worksheet material (Figure 6.13). The size of plastic deformation zone at both the interfaces (E/W and FS) matches well with the contact diameter values. Other studies [60-61] presented similar FEA results for the RSW of aluminum alloys and accounted that plastic strain distribution for contact diameter at the interfaces and sheet separation at the FS.

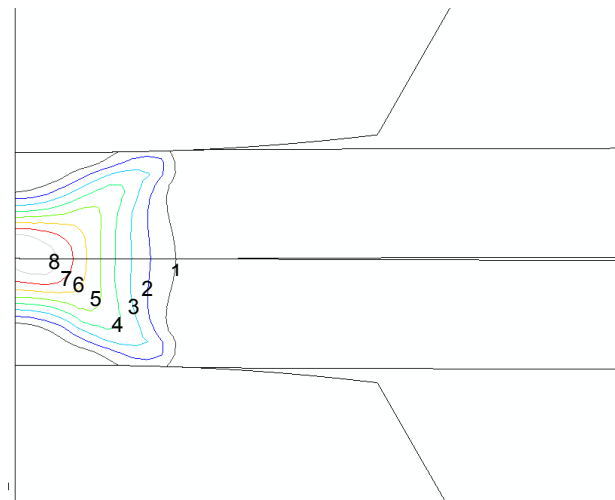


Figure 6.13: Equivalent plastic strain distribution in the sheet. Min (1) – 8.0×10^{-3} ; Max (8) – 3.6×10^{-2} ; Inc – 4.0×10^{-3}

6.4 Concluding Remarks

Through experimental observations and FEA results, the ‘Contact Mechanics’ at the FS could be explained to understand the nugget formation at this interface during RSW of AA5182. It was already mentioned that the current flow through this interface was only possible through metal-to-metal contacts. In the entire contact zone, there could be several cracks at each

surface. However, at the periphery of this interface, there would be exaggerated cracks in the surface oxide layer of both the worksheets due to bending effect of sheet separation. The chances that the cracks from both the sheets would align with each other would be much higher; this is because the two sheets separated from the same point and the bending effect was in a very narrow zone (4 – 5 mm diameter) and hence the chances of metal-to-metal contact would be higher. While in the central contact zone, there could be several cracks on each surface. However, there would be only few spots [50, 52] where those cracks would be aligned to produce metal-to-metal contacts.

The more the area of the metal-to-metal contact the less would be the constriction resistance. At the beginning of the weld current phase of the weld sequence, the periphery of the contact at the FS provided the preferred (least resistance) flow path for the current coming from the E/W interface. This caused current concentration at the periphery resulted in high heat generation and hence start of melting near the periphery. With increasing current time, the melting proceeded in all directions and merge to produce a complete nugget of doughnut shape.

Experimental observations and FEA results were used to explain the contact mechanics at the FS during RSW of AA5182. Start of melting, nugget formation, and nugget growth were studied and explained. These results suggested that the tribo-mechanics that occurred at the FS during squeezing had significant effect on the nugget formation during RSW of AA5182.

Chapter 7

7 Effect of Boundary Lubricants

7.1 Introduction

It was discovered in Chapter 4 that the nature of oxide layer at the worksheet surface of AA5182 was the most influential variables for electrode life during RSW process. Study of contact mechanics (chapter 5 and chapter 6) explained the breaking of this layer for current flow through the interfaces. Several research efforts have been made to alter the tribology of the contact at the E/W interface like periodic cleaning (dressing) of electrode tip [57], electrode coating [73], arc cleaning [64], etc. However, such procedures may interrupt the manufacturing activity that involves the RSW. In the present study, a different but somewhat similar approach was adopted. Most of the results of the present chapter have been published by Rashid et al [102, 103].

Since autobody sheets go through several manufacturing processes (rolling, stamping, etc.) before being placed in the vehicle and different lubricants are used for these processes, so instead of altering the tip surface of electrode, a thin layer of boundary lubricant was placed at one side of the aluminum sheet which touches the electrode (i.e. only at the E/W interface). With the modern manufacturing equipment and expertise, it is quite possible to apply a lubricant to only one side of a component while keeping the other side clean. It could require some modification either in manufacturing steps and/or manufacturing tools or both while preparing the autobody component before being spot welded. However, these changes were not explore and was not the intent of the present work. The strategy behind this approach was

to alter the contact resistance at the E/W interface without altering any feature of the FS, thus altering the tribological sequence of alloying, pickup, pitting and eventually electrode tip failure. This approach has the merits of being simple and flexible and not interrupting the RSW activity and hence more practical for the industry. The focus of the present work was given to investigate the change in electrode life and pitting behavior under similar weld conditions by changing only the surface feature of the worksheet at the E/W interface. The E/W surfaces are studied both physically and chemically and the inevitable scatter of results in this complex process is dealt with using a statistical analysis.

7.2 Electrode Life Experiments

7.2.1 Screening of Different Lubricants

Purpose

Since the present approach was relatively new and not much information was available in literature, an initial screening test, using several lubricants, was performed that contributed directly to the methodology of the present study.

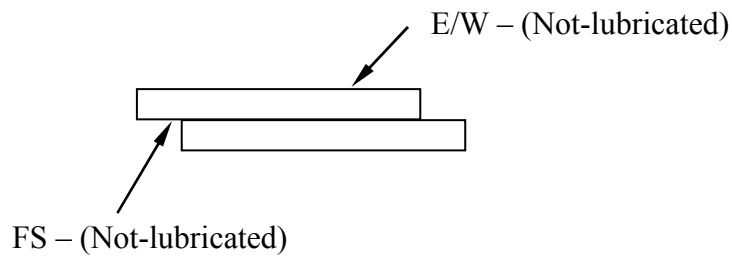
Materials and Methods

The screening test involved RSW on the 10-weld standard coupons (Figure 3.2); one hundred spot welds on each of the lubricated surfaces and as-received surface were performed. Six different lubricants (L1 – L6), that had been developed for various other metal working processes, were used for the screening tests. Lubricants were applied only to one side of the aluminum alloy worksheet that touches the electrode (top and bottom) and kept away from the FS; this condition will hereafter termed as L-surface while A-surface will represent the condition where no boundary lubricant was used at all and all interfaces were kept in as-received condition (Figure 7.1). The methodology to apply these lubricants on the worksheet surface was explained earlier in chapter 3 (section 3.4.2) of this thesis. Since the focus of the

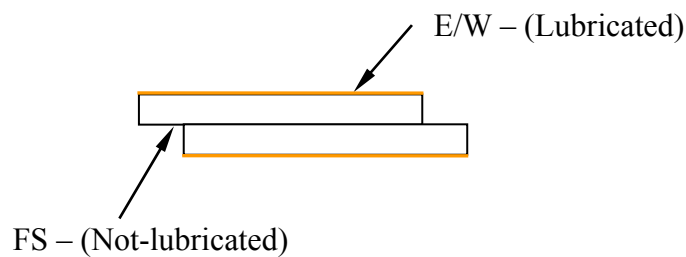
study was about the electrode tip life and E/W interface, two of these lubricants were selected for detailed investigation by considering their influence on the electrode degradation behavior during screening tests which is described as follows.

Table 7.1: General description of the lubricants used for the screening tests.

Symbol	Lubricant (Manufacturer)	Type	Application	Used for
L1	KLIR Cut-2 (Monarch Oil Ltd)	Oil-based lubricant	Cutting Oil	Ferrous and Non-ferrous
L2	HydroDraw®689 (D. A. Stuart Inc.)	Water-based lubricant	Metal- Working/Manufacturing	Ferrous and Non-ferrous
L3	HydroDraw®551 (D. A. Stuart Inc.)	Water-based lubricant	Metal- Working/Manufacturing	Ferrous and Non-ferrous
L4	AOL-70 (unknown)	Dry Lubricant	Chemical coating/Storage	Ferrous and Non-ferrous
L5	CIMTAP® (Milacron Canada Inc)	Oil-based lubricant	Tapping Fluid	Ferrous and Non-ferrous
L6	HydroDraw®625 (D. A. Stuart Inc.)	Water-based lubricant	Metal- Working/Manufacturing	Ferrous and Non-ferrous



(a) A-surface



(b) L-surface

Figure 7.1: Surface conditions of lubricated and as-received samples (a) A-surface, all surfaces are in as-received condition and (b) L-surface, E/W interfaces were lubricated and FS was as-received.

Results and Discussions

Results from the screening tests showed that all these lubricants had some influence on the RSW process and electrode degradation. Optical stereoscopic views of the top (positive) electrodes at low magnification showed that most of the lubricants sustained combustion due to high heat generation at E/W interface (Figure 7.2). It was observed that different lubricants

resulted in different topography of electrodes even though the experiments were performed under same conditions. For some lubricants, electrode degradation occurred even more rapidly than for the A-surface that did not have any lubricant.

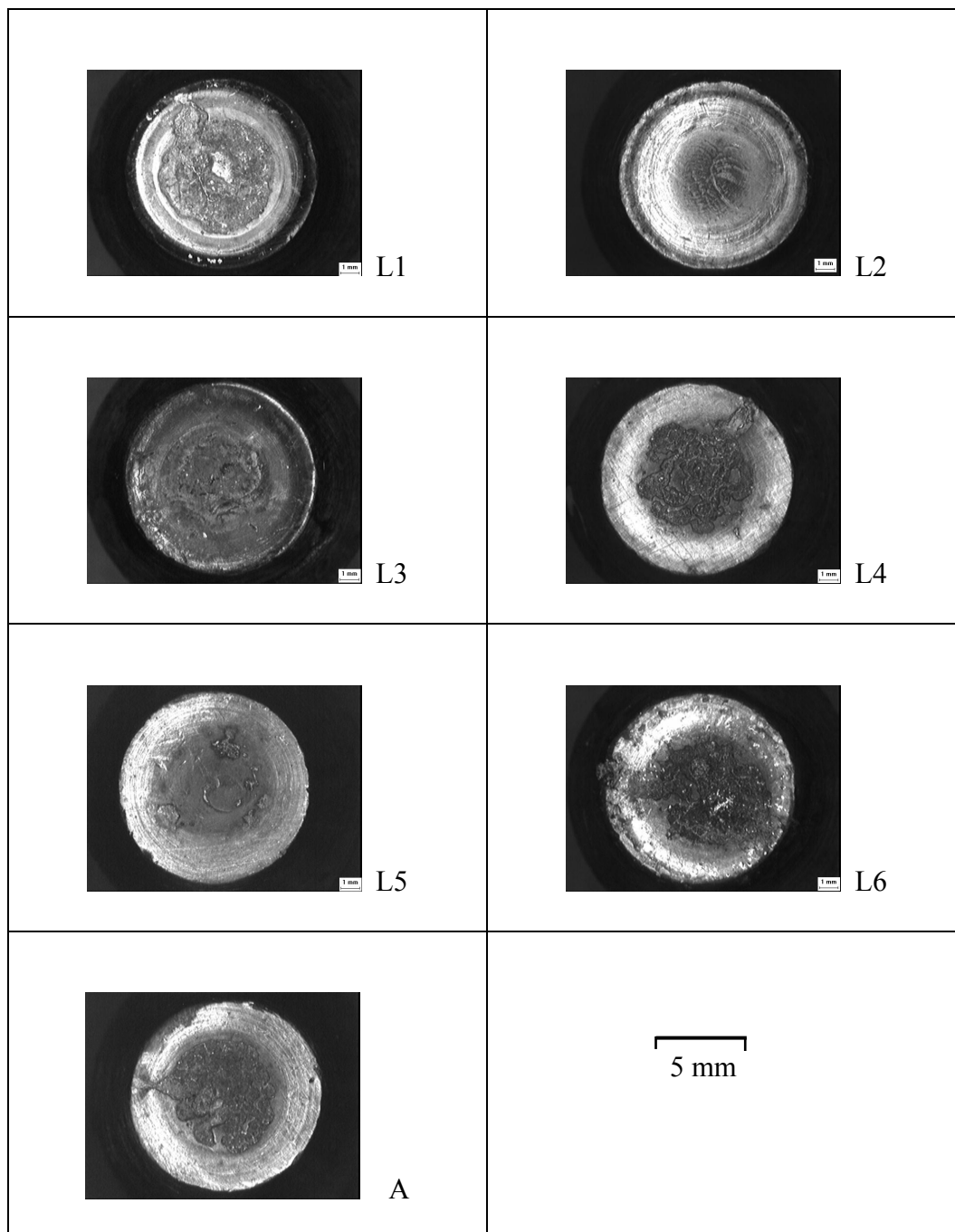


Figure 7.2: Optical stereomicroscope images of the positive electrodes after performing 100 spot welds on different surfaces.

Welding on L2-surface produced an almost clean electrode tip surface while welding on L6-surface showed the heaviest degradation of electrode. Both these lubricants were water based synthetic lubricant used for metal working of ferrous and non-ferrous (including Aluminum) alloys. These two lubricants then selected for further investigation as “good” and “bad” boundary lubricants for RSW of aluminum alloys. Some details of these lubricants are presented here for general considerations

HydroDraw®689 (L2): This is a water-based synthetic lubricant designed for several manufacturing applications such as hydro forming, drawing, and stamping. It is a smooth off-white paste with very low odor and easy to use. This lubricant is suitable for ferrous and non-ferrous materials including aluminum, brass, copper, and galvanized metals. The lubricant can be applied on the surface by pump, spray, dipping, roll coating or by brushing by hand. This is an oil-free lubricant and readily cleanable from parts. This lubricant has good wetting property and provide rust protective film for storage.

HydroDraw®625 (L6): This is also a water-based synthetic lubricant designed specially for hydro forming and drawing applications. It is a smooth light-brown paste with very low odor and dries quickly to form a thin layer of dry lubricant on the surface. The lubricant is suitable for both ferrous and non-ferrous materials including aluminum. The lubricant can be applied on the surface by pump, spray, dipping, roll coating or brushing by hand. This is an oil-free lubricant which could easily remove from the parts by subsequent cleaning operations.

7.2.2 Electrode Life

Purpose

Complete electrode life tests were performed on as-received and lubricated surfaces using the good and bad boundary lubricants that were selected from screening tests. For all these

experiments, only the Tribological condition of the worksheet surface associated with the E/W interface were altered, all other welding conditions including tribology of the FS were kept constant. The objective was to evaluate the effect of boundary lubricants on the electrode life during RSW of aluminum alloy AA5182.

Materials and Methods

Three electrode life tests were performed for each surface conditions; A-surface, L2-surface, and L6-surface. These electrode life tests involved RSW on standard coupons and overlapped samples (Figure 3.3). Details of electrode life test procedure were given in chapter 3 (section 3.5.1) of this thesis. Again, the lubricants were applied only on one side of the worksheet that would touch the electrode (Figure 7.1). The methodology to apply these lubricants on the worksheet surface was explained earlier in the previous section and in chapter 3 (section 3.4.2) of this thesis. These tests also involved joint shear force measurements (section 3.5.4) and obtaining carbon imprints (section 3.5.3) at specific intervals as described in electrode life procedure (section 3.5.1). The results from these experiments were useful both for evaluating electrode life and pitting rate of electrodes. The electrode life criterion was selected as the drop of joint shear force below 80% of the initial joint shear force of the A-surface which was about 3.92 kN.

Results and Discussions

Results of these life tests were plotted as the average joint shear force of five overlapped samples welded in sequence (as described in chapter 3) against the corresponding spot weld numbers. The straight (dashed) line in all these plots represents the failure load at 3.92 kN as described earlier.

The average electrode life for L2-surfaces was found to be 730 welds with a range of 700 – 775 (Figure 7.3) while the average electrode life for A-surfaces was 393 welds with a range of 325 – 435 (Figure 7.4). In case of the L2-surface and A-surface, the declining joint strength defined failure while for the L6-surface, electrode sticking and explosion defined failure. In all three tests with L6, the electrode started pitting at a very early stage. Then, the

electrodes started sticking to the work surfaces and producing explosions so that the average electrode life was only 98 welds with a range of 37 – 198 (Figure 7.5). All these curves followed the four stages of electrode life, i.e. joint shear strength increased initially and reached a peak before drop down to the failure mark (as shown in Figure 2.8) or physically damaged.

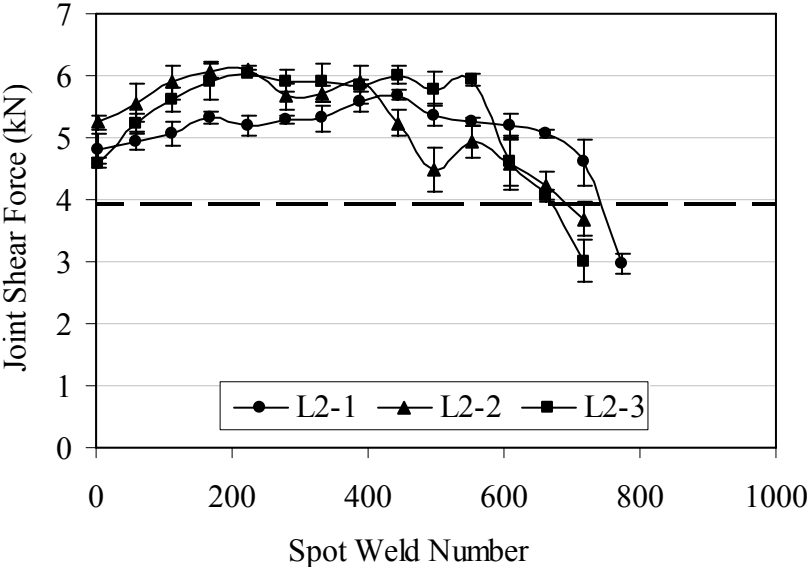


Figure 7.3: Electrode life results for L2-surfaces with horizontal dashed line representing the failure strength.

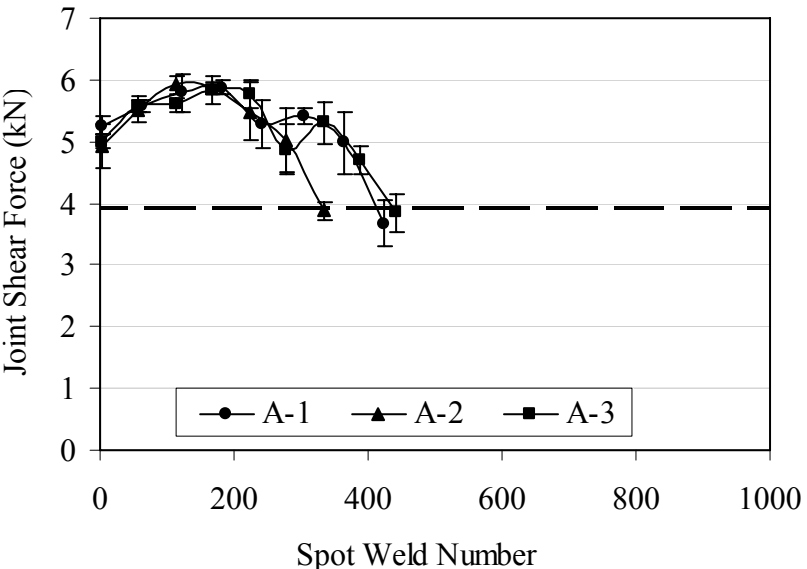


Figure 7.4: Electrode life results for A-surfaces with horizontal dashed line representing the failure strength.

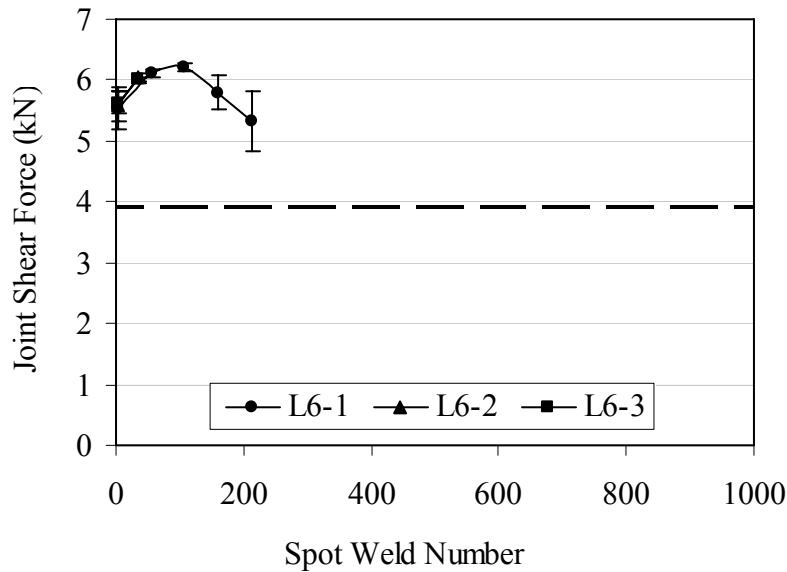


Figure 7.5: Electrode life results for L6-surfaces with horizontal dashed line representing the failure strength.

These results very clearly indicated that the presence of a boundary lubricant on the worksheet surface associated with E/W interface can influence electrode life. Although the results were somewhat scattered which was typical for this type of experiments [30, 52, 62], the electrode life experiments showed that, for the same welding conditions, the “bad” lubricant (L6-surface) caused electrode failure at very early stages, while the “good” lubricant (L2-surface) extended the electrode life to almost double than the electrode life of A-surface.

Another interesting observation from electrode life tests was the initial joint strength for these surfaces. Though there was considerable overlap in the data, the joint shear force of the L2-surfaces, during the initial stage of the life, were slightly lower than that of A-surfaces. However, after the first few welds, the joint shear force of the L2-surfaces starts exceeding that of the A-surfaces and remains higher to produce longer electrode life. Since welding conditions, failure criterion, and FS characteristics were kept same for all these experiments,

the difference of electrode life occurred due to change of the only variable i.e. the tribology of the worksheet surface associated with the E/W interface. This effect was further investigated in the following sections.

7.2.3 Rate of Electrode Pitting

The sequence of significant events in electrode life included detection of pitting, peak joint shear strength, and ultimately the failure of electrode tip (Table 7.2). While welding on L6-surfaces, significant physical damage of electrodes occurred; for L2-surfaces and the A-surfaces, it was alloying, pick-up and pitting that were the main indicators of electrode degradation.

Table 7.2: Significant events of electrode life during life tests for each surface condition.

Electrode Condition	L2-surface			A-surface			L6-surface		
	Test-1	Test-2	Test-3	Test-1	Test-2	Test-3	Test-1	Test-2	Test-3
Visible pit initiation on electrode	395	49	81	65	96	180	12	2	4
Pitting visible in Carbon Imprint	440	110	110	110	110	220	53	33	33
Peak Strength	445	225	225	110	110	165	108	35	35
Electrode Fail	775	720	700	420	325	435	198	37	58

The degradation behaviour of the electrode tip surfaces during these life tests were illustrated by carbon imprints taken at various stages of the life (Figure 7.6 – Figure 7.8). Different alloying and pitting behaviour was expected for different surface conditions and were

observed from these carbon imprints. Also, as explained in chapter 5 of this thesis, the pitting of all these electrodes started in ring around the centre which was confirmation of that work.

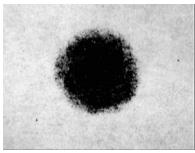
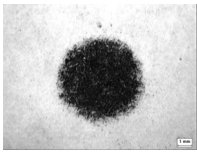
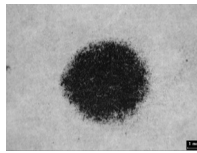
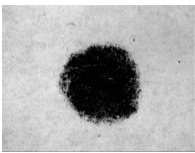
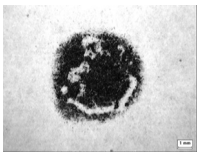
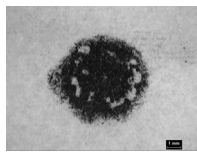


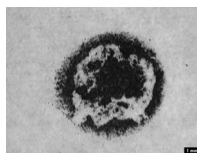

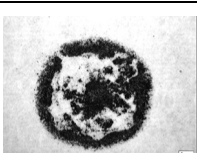
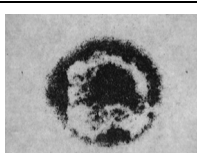
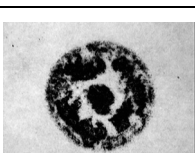



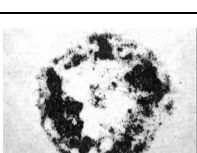
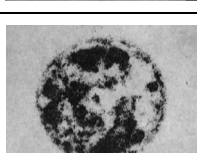
L2-surface					
Test-1		Test-2		Test-3	
Spot #	Carbon Imprint	Spot #	Carbon Imprint	Spot #	Carbon Imprint
0		0		0	
165		110		110	
440		220		220	
550		330		330	
660		495		495	
770		715		695	

Figure 7.6: Carbon imprints of upper (positive) electrodes at different stages of electrode life used for L2-surface.

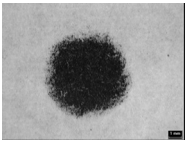
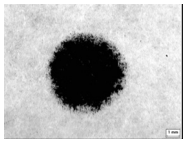
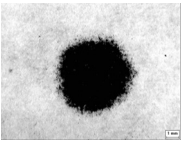
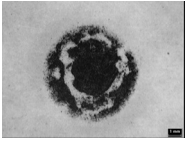
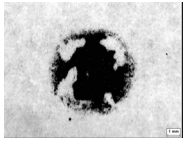
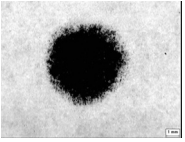
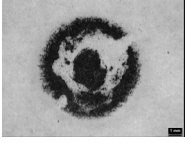







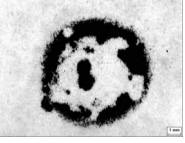



A-surface					
Test-1		Test-2		Test-3	
Spot #	Carbon Imprint	Spot #	Carbon Imprint	Spot #	Carbon Imprint
0		0		0	
120		108		162	
180		162		216	
300		216		270	
360		270		378	
420		324		432	

Figure 7.7: Carbon imprints of upper (positive) electrodes at different stages of electrode life used for A-surface.

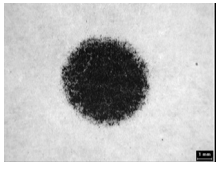
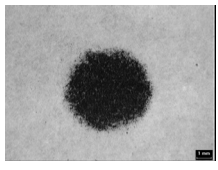
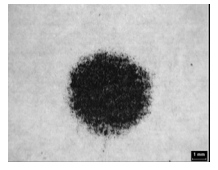
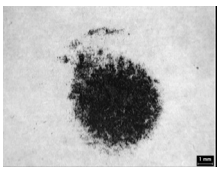
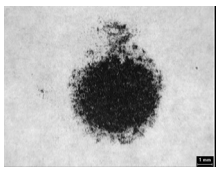
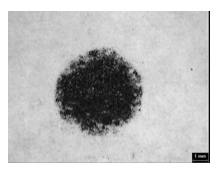
L6-surface					
Test-1		Test-2		Test-3	
Spot #	Carbon Imprint	Spot #	Carbon Imprint	Spot #	Carbon Imprint
0		0		0	
53		33		33	
212	Electrode damaged	37	Electrode damaged	66	Electrode damaged

Figure 7.8: Carbon imprints of upper (positive) electrodes at different stages of electrode life used for L6-surface.

In general, an early start of pitting cause an early failure of electrode, however, based on the present observations, it was discovered that the rate of alloying and pitting should also be considered for predicting electrode lives. In two out of three tests of both the L2-surface and the A-surface, pitting started at around 110 welds. However, for all of the L2-surfaces, the rate of pitting was slower than the A-surface with large central portions of the electrode not pitted and remaining in contact until about 500 welds compared with about 200 welds for the A-surfaces and hence an extended electrode life for L2-surfaces. The larger number of welds needed (Table 7.2) for the L2-surfaces to reach the peak joint strength (Stage II, Figure 2.8) supported this view of the importance of pitting rate.

7.3 Features of Boundary Lubricated RSW

Purpose

As mentioned earlier, there was a very slight difference between the initial joint strength of A-surface and L2-surface, though there was considerable overlap. The average initial joint shear force for each of the three tests of the L2-surfaces was 4.88 ± 0.32 kN whereas for the A-surfaces it was 5.06 ± 0.26 kN and for the L6-surfaces it was even higher at 5.57 ± 0.23 kN. These differences, though not very huge in terms of joint shear force, provided some insight into the tribological mechanisms that were eventually responsible for the increased electrode tip lives with the L2-surfaces. Series of experiments were performed and several mechanical, chemical, and physical aspects of the E/W contacts were analyzed in details. The intent was to determine how the boundary lubricants influenced electrode life.

Materials and Methods

A detailed investigation was conducted to explore the possible reasons for the different performance of the two lubricated surfaces (L2-surface and L6-surface) compared with A-surface. Experiments were performed that involved RSW on the two selected lubricated surfaces (mostly concentrating on the L2-surface that performed the best in the electrode life experiments) and the A-surface. When planning this second set of experiments, it was realized that it was not possible to provide exactly the same electrode (even if they are selected from same batch) or worksheet surfaces (even if they are from same sheet). Small variations in microstructure and roughness of the surfaces were essentially inherent in them and they could significantly influence the tribological interaction of the surfaces and thus the weld strength and ultimately the electrode tip life. However, if the same electrodes were used for small numbers of successive welds on the A-surface and the L2-surface, the variable nature of the electrode tip could be eliminated and the variable nature of the worksheet surfaces could be tested.

Four identical experiments were performed to explore the repeatability of the results. Each experiment consisted of performing RSW on overlapped (shear force measurement) specimen (Figure 3.2) alternatively five each on L2-surfaces and A-surfaces with the same pair of electrodes. All conditions were kept the same and the electrodes were wiped with methanol between each spot weld. In this manner, the influences of the subtle differences between electrode surfaces on RSW were much reduced and only the influences of the surface characteristics of the worksheet at the E/W interface on RSW were highlighted.

These experiments included joint shear force measurements along with measurements of weld nugget diameter as well as the diameter of the indentation of the electrode tip into the worksheet surface. Also, hardness measurements, prior to the welding, were performed, on L2-surface and A-surface to explore the change in hardness of the worksheet surface with the application of lubricant (L2). Procedure for all these measurements were explained earlier in chapter 3 (section 3.5) of this thesis. The various differences between the L2-surface and A-surface were assessed with an elementary statistical analysis (Student's t-test with a 0.05 significance level).

Results and Discussions

Results from these experiments were analyzed in details to understand how the boundary lubricants influenced electrode life during RSW of AA5182. These analyses are presented as follows.

7.3.1 Initial Joint Shear Force

Each of these sets showed higher values of joint shear force for A-surface compared with L2-surface (Figure 7.9). For same surfaces (A-surface or L2-surface), the variability between these sets were related to randomly distributed differences between these surfaces inherent to these kind of experiments [52]. However, within one set, where the surface variability of the electrode tip was removed, the differences in joint shear force of spot welds for the A-surfaces compared with the L2-surfaces were only related to the lubricant action. So, two sets of data were assembled, one containing all of the L2-surface data and the other

containing all of the A-surface data. The average joint shear force for the L2-surface of 5.01 kN was lower than the average shear force for the A-surface of 5.37 kN. Although, this difference was not huge in terms of joint strength, it was statistically different ($p < 0.005$).

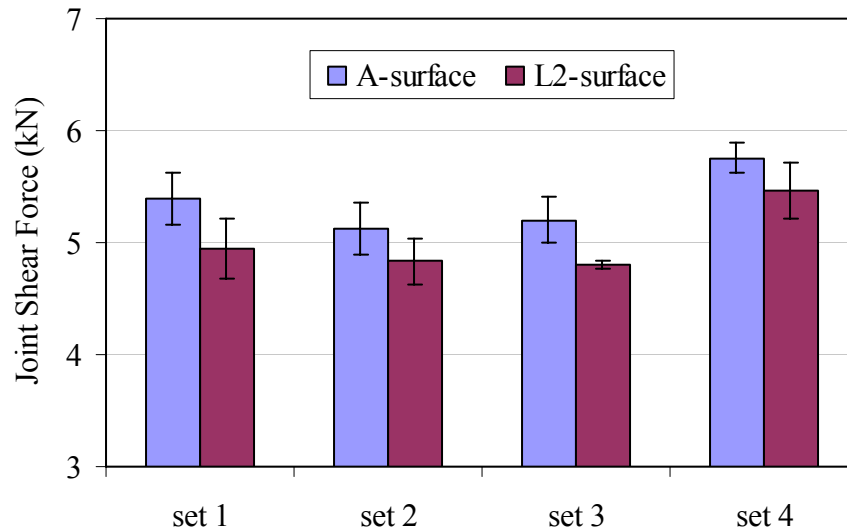


Figure 7.9: Average joint shear force of A-surface and L2-surface; each set welded with the same pair of electrodes.

7.3.2 Nugget Diameter

For good quality weld, joint shear force was considered very likely to be related directly to the nugget diameter [71]. Therefore, it was decided to investigate the nugget diameter in order to validate its relation with the joint strength as well as the weld quality. As expected, the nugget diameter distributions (Figure 7.10) looked very similar to the joint shear strength distributions (Figure 7.9). Using the same assumptions as before, two sets of data were assembled, one was containing all of the L2-surface data and the other containing all of the A-surface data. The average nugget diameter for the L2-surface of 6.57 mm was statistically

significantly different ($p < 0.001$) from the average nugget diameter for the A-surface of 6.78 mm.

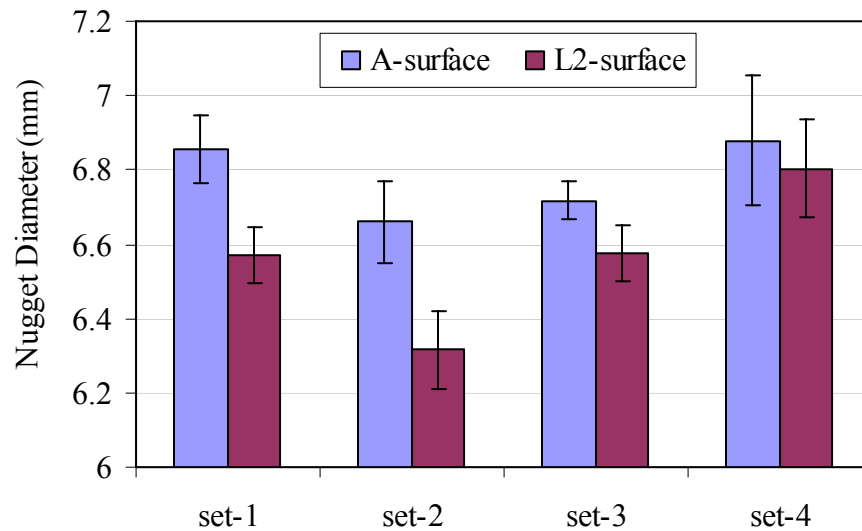


Figure 7.10: Average nugget diameter of A-surface and L2-surface; each set welded with the same pair of electrodes.

7.3.3 Electrode Indentation into the Worksheet

In the process, it was also found to be interesting that the two surfaces showed a difference in terms of indentation of the upper electrode into the worksheet surface (Figure 7.11). This was measured as the contact diameter between electrode and worksheet as explained earlier (Figure 3.10) in chapter 3 of this thesis. The same data assembly was performed as described in the previous two paragraphs. The average indentation diameter for the L2-surface of 8.30 mm was again statistically significantly different from the average indentation diameter for the A-surface of 8.42 mm ($p < 0.001$).

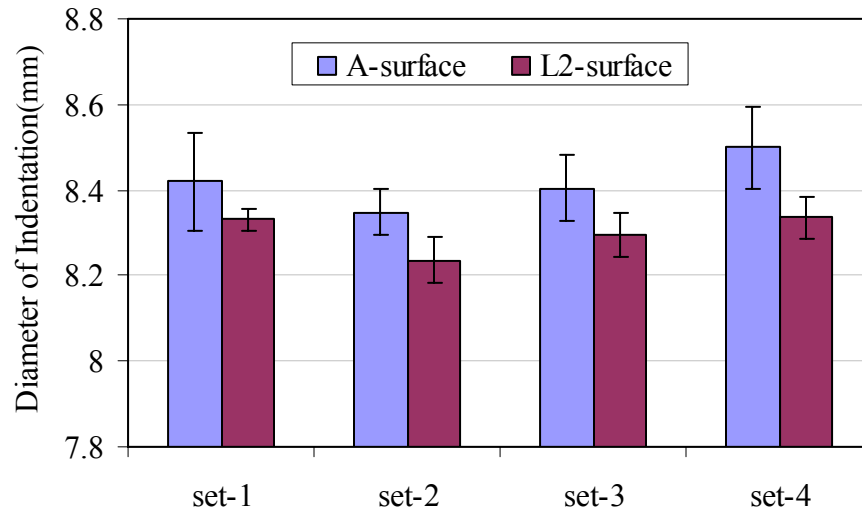


Figure 7.11: Electrode indentation into the worksheet for A-surface and L2-surface; each set welded with the same pair of electrodes.

7.3.4 Heat Generation at E/W Interface

It was established that the lower joint shear force of L2-surface was due to the smaller nugget size compare to A-surface. Since all welding conditions including the FS characteristics were kept constants for all these experiments, one possible explanation for this difference was related to the heat transfer from the FS through the E/W interface to the cooling water that was circulated within the electrode (Figure 1.1). As explained earlier in chapter 6 of this thesis, during the weld current phase of the welding sequence, heat was generated at the FS and melted the surrounding material to form the weld nugget which grew until the end of solidification. The electrodes were water cooled and majority of the heat generated at the interfaces was transferred to the cooling water through the E/W interface [88]. Clearly, the rate of heat transfer from the FS to the cooling water would be directly influenced by the temperature of the E/W interface which was related to the heat generation at this interface. Since boundary lubricants were applied only at the E/W interfaces and not at the faying surface, for the same amount of current and time, the heat generation at the faying interface

would always be same. However, a lower heat generation at E/W interface would allow a faster rate of heat transfer from the FS. This would result in lowering the time of solidification and hence a smaller weld nugget. Thus, the smaller average nugget diameter, reported in the previous section for the L2-surfaces compared with the A-surfaces, indicated that there was less heat generation (lower temperature) at the E/W interface of the L2-surfaces. This smaller nugget diameter was illustrated by typical longitudinal sections of the L2-surface and A-surface welds (Figure 7.12).

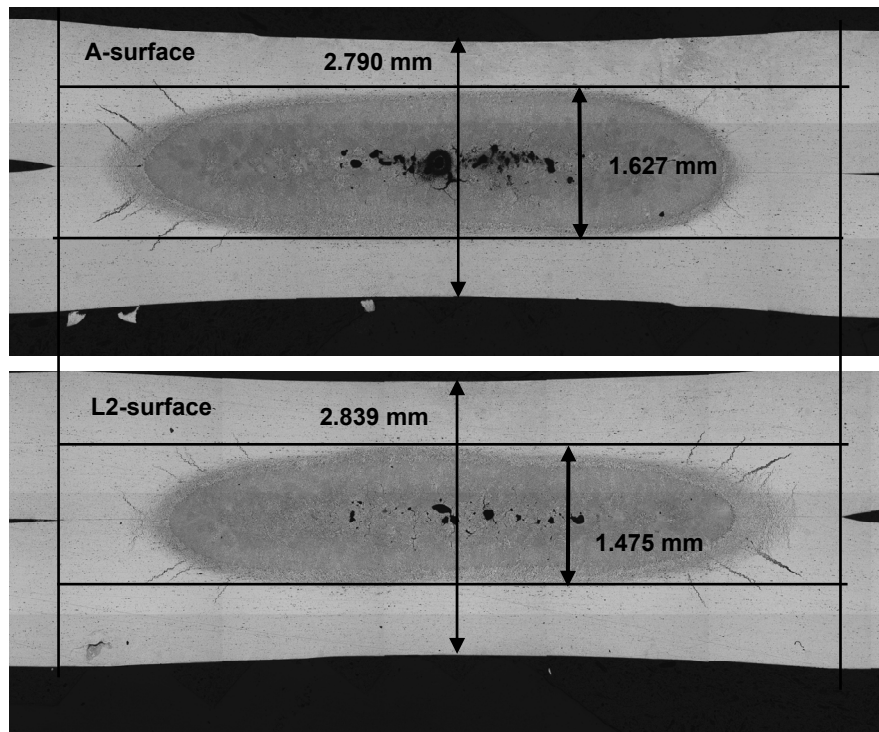


Figure 7.12: Typical nugget cross section of spot weld of A-surface and L2-surface.

There was further support for the concept of less heat generation and lower temperature at the E/W interface for the L2-surface. Vickers hardness testing of the L2-surface and A-surfaces (20 specimen for each) were conducted prior to any welding. It was observed that the hardness of the aluminum worksheet was not changed with the application of lubricant L2 to

its surface; the average hardness values for A-surface and L2-surface prior to any welding were 80.89 ± 3.8 and 80.79 ± 5.1 VHN respectively. However, the results presented in the previous section indicated that, during the RSW, the average diameter of the indentation of electrodes into the sheet surface was smaller for the L2-surface compared with the A-surface (Figure 7.11). Since both these surfaces started with the same hardness level one plausible explanation for different indentation was related to the heat generation at the E/W interface. Since thermal softening of metals and alloys occurs at high temperature [98], less penetration of electrode into worksheet for L2-surfaces suggested less thermal softening hence lower heat generation at this interface compare with A-surface.

7.3.5 Surface Oxide Layer

A lower heat generation at the E/W interface implied lower electrical contact resistance of that interface. A lower electrical contact resistance would occur at the E/W interface if the L2 lubricant acted to alter the oxide geometry of the worksheet surface as observed in chapter 4 of this thesis. This reduction of the electrical contact resistance would result in low heat generation at this interface. The possibility of a reduced and/or uniform oxide layer thickness was suggested by the following observation. While applying the L2 lubricant to the worksheet surface, it was found that the colour of the white cotton balls turned grey or black whereas for the “poor” L6 lubricant they retained the actual colour of the L6-lubricant. This observation suggested that some chemical change occurred at the surface of the aluminum sheet when the lubricant L2 was used and investigations were performed to explore this possibility.

Optical microscopy provided further insight. The same points on regular aluminum worksheet were examined before and after the application of L2 lubricant (Figure 7.13). Same magnification was used for all examination and all those surfaces were wiped with acetone before viewing them. The L2-surface appeared lighter in colour and seemed to have material removed from the sheet surface.

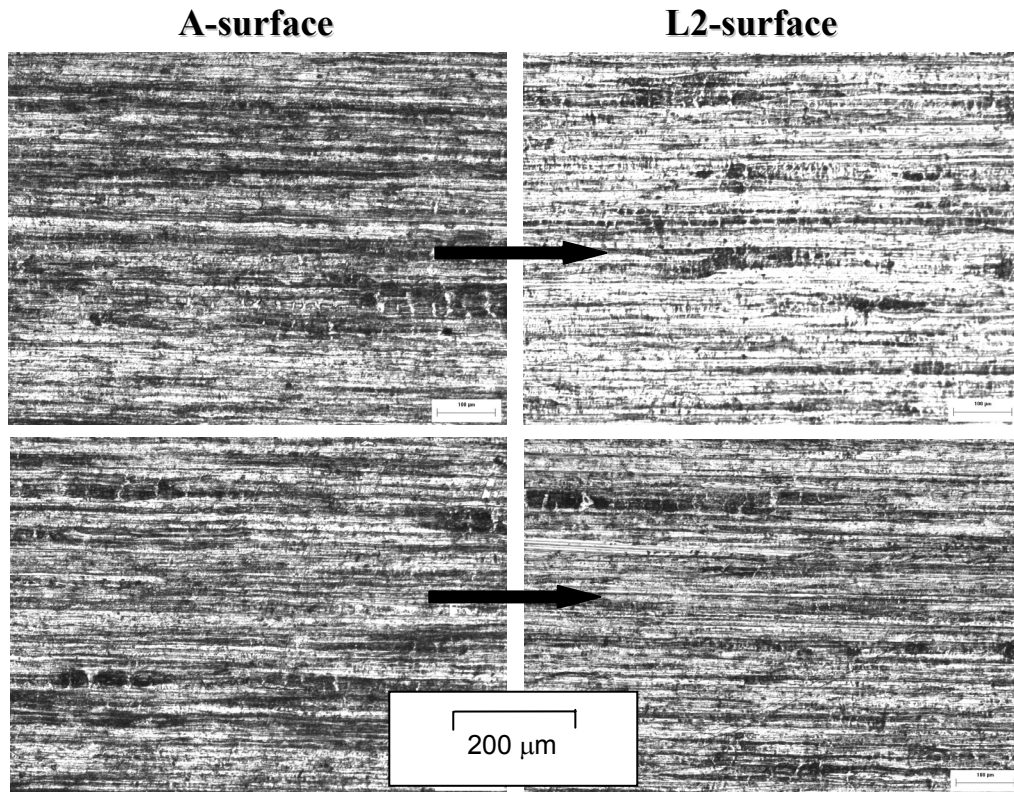


Figure 7.13: Optical microscopy showing the effect of good lubricant (L2) on an unpolished worksheet surface.

This action of the lubricant L2 on the worksheet surface was further analyzed through higher resolution SEM microscopy. Equivalent points on the worksheet surface were focused before and after the application of lubricant L2. Again, all those surfaces were wiped with acetone and images of same magnification were presented for comparison (Figure 7.14). It was observed that the application of the lubricant L2 reduces the size of those non-uniform bright spots presented on the worksheet surface before the application. These spots were Mg-rich and reported earlier (chapter 4) as magnesium oxide (MgO). Thus it was believed that the application of the lubricant made the oxide layer more uniform and smooth.

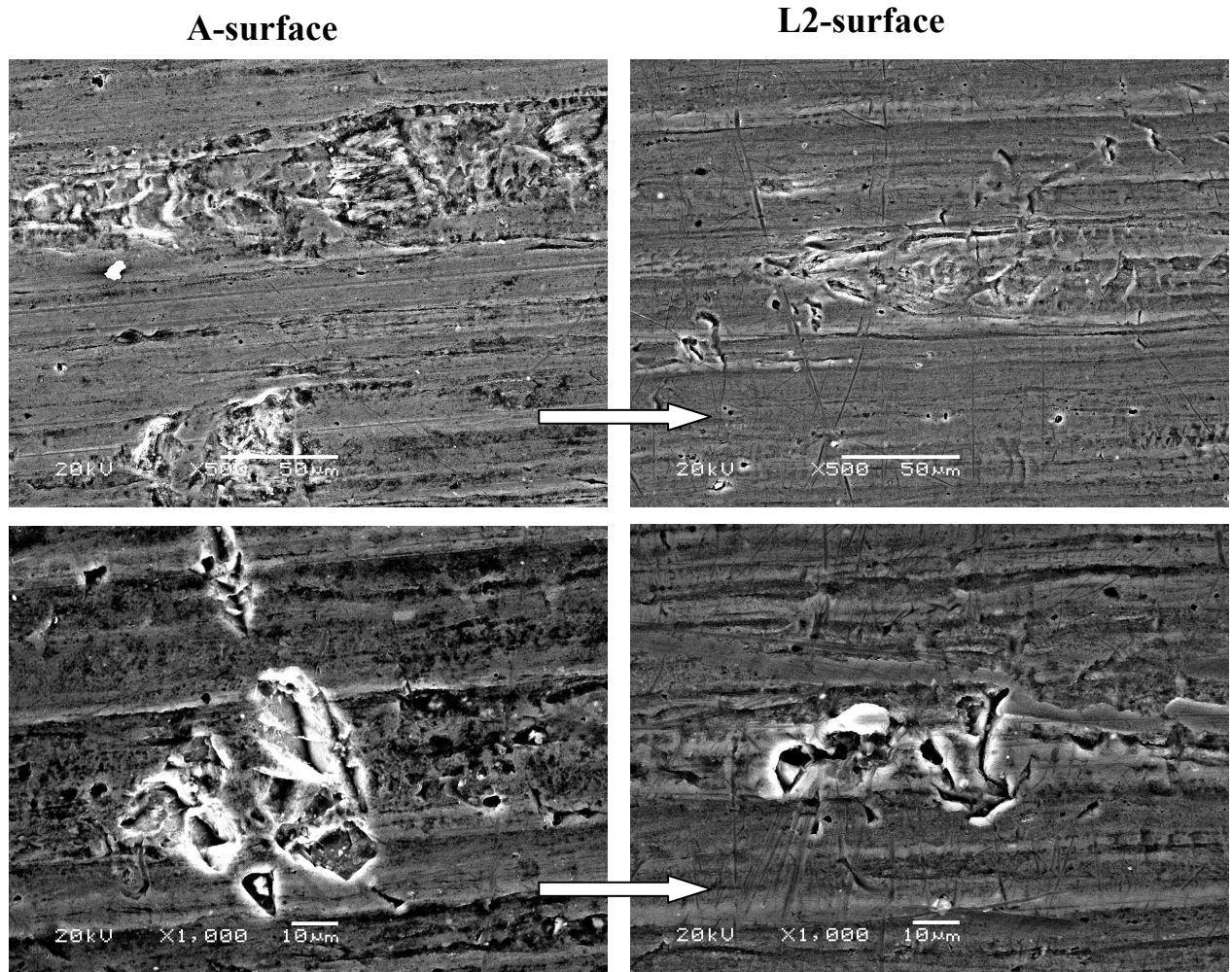


Figure 7.14: SEM micrographs showing the effect of good lubricant (L2) on unpolished worksheet surfaces (equivalent spots and may not be exactly the same position).

Interestingly, when this procedure was repeated for freshly polished surfaces, there was no apparent change in the appearance of the L2-surface (Figure 7.15). A fresh polished surface would have much thinner oxide layer than as-received surface and would have needed considerable time to develop an increased thickness [29, 33, 37]. This finding indicated that the effect of lubricant L2 was more significant when the oxide layer of the worksheet was thick.

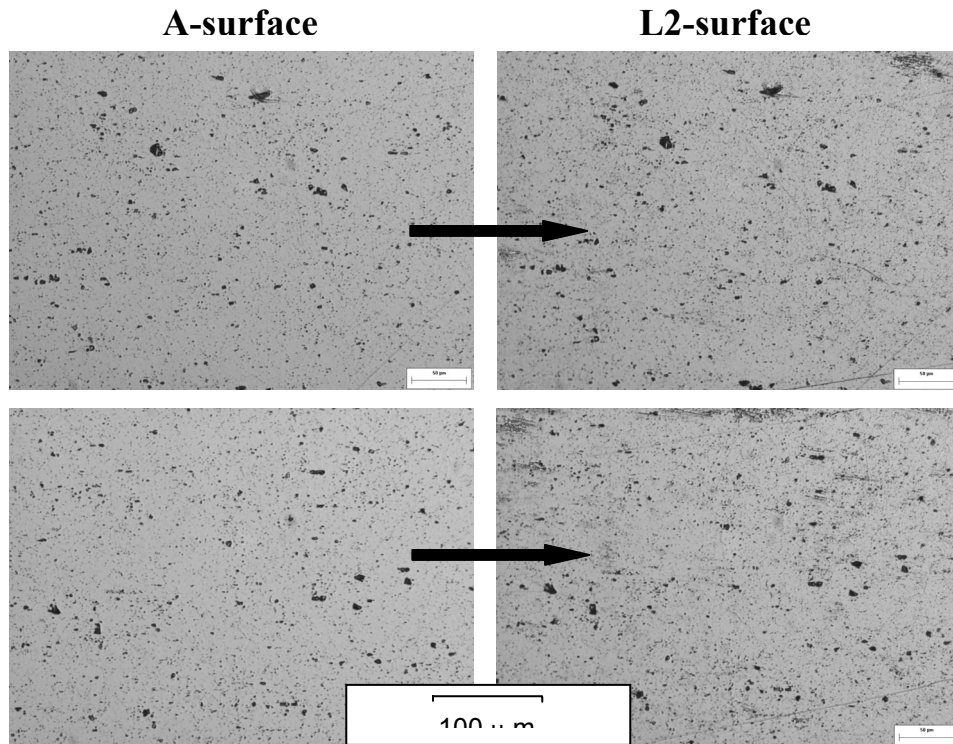


Figure 7.15: Optical microscopy showing the effect of good lubricant (L2) on a polished worksheet surface.

In order to provide further proof that the oxide layer had thinned with the application of lubricant L2, one sample each from the A-surface and the L2-surface were examined by ESCA. This is a technique used for surface analysis of first 10 nm of the sample surface in a high vacuum chamber [49]. The surface is bombarded with specific X-rays which excites first few atomic layers and resulted in emission of photoelectrons from the surface layer. These photoelectrons contain specific energy level that is characteristic of the parent atom. The peak height of the intensity indicates the amount of an element which shifted a little if the element is bounded with other element. Thus ESCA is good to indicate both the element as well as compounds present in the first few atomic layer of the surface.

Specimens were cut in 6 mm x 6 mm size and were cleaned with methanol before being placed into vacuum chamber. Both samples were placed in the same chamber at the same time. The results were plotted for the intensity (count per second or CPS) of radiation of oxygen, presented in the surface oxide (Al_2O_3) layer [104], against sputtering time (Figure 7.16). More intensity (CPS) at the same sputtering time suggests more concentration of that particular element on the surface. Similarly, longer sputtering time to achieve same intensity level suggests a thick surface layer for that particular element. Interestingly, the intensity of oxygen at any sputtering time was lower for L2-surface compare with that of A-surface; thus showing a thinner (or low concentration of) oxide layer on the aluminum sheet surface that was treated with the lubricant L2.

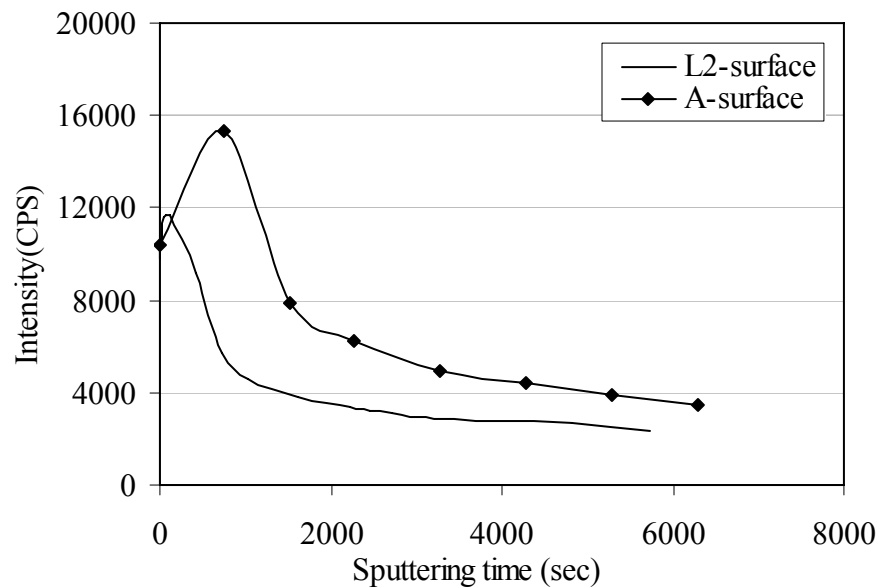


Figure 7.16: Thickness of the oxide layers on A- and L2-surfaces from ESCA; intensity of Oxygen in oxides of the worksheet of AA5182 surface.

It was clearly observed from these analyses that lubricant L2 had very significant effect on the oxide layer of the worksheet surface by reducing its thickness and/or making it uniform. This action of the lubricant L2 on AA5182 was presented schematically in Figure 7.17.

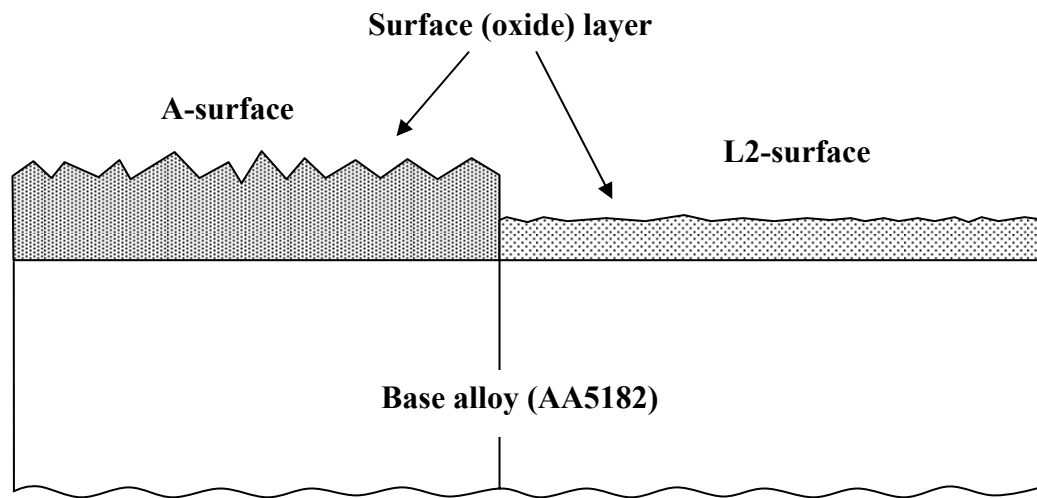


Figure 7.17: Schematic illustration of the influence of the boundary lubricant L2 on the surface (oxide) layer of AA5182.

7.3.6 Alloys on the Electrode Surface

In another attempt, 100 spot welds were performed on each of the L2-surface and A-surface; these spot welds were performed on 10-weld standard coupons (Figure 3.2). The intent was to understand the type and properties of intermetallic phases formed during the spot welds and their influence on the subsequent electrode life. This was done by analyzing the top (positive) electrodes with X-ray diffraction (XRD); detail of this procedure was given in chapter 3 (section 3.2) of this thesis. Since electrodes are made of copper, higher intensities of Cu than Cu-Al phases were expected. At the same time, the occurrence of the intensity peaks for Cu-Al phases were also well matched with the standard XRD pattern for different phases (Figure 7.18). The Cu_9Al_4 (γ_1 phase) was observed at about 44.2° on both electrodes while the

intensity peaks for CuAl_2 (θ phase) were found only at the electrode that had been in contact with the L2-surface. These peaks occurred at 42.7° , 47.4° , and 47.9° which matched the standard XRD-pattern for the first peak at 42.6° , second peak at 47.3° , and third peak at 47.8° for this phase [105]. The match was good enough to believe that CuAl_2 phase was present on the electrode surface used for welding the L2-surface but not on the electrode surface used for welding the A-surface.

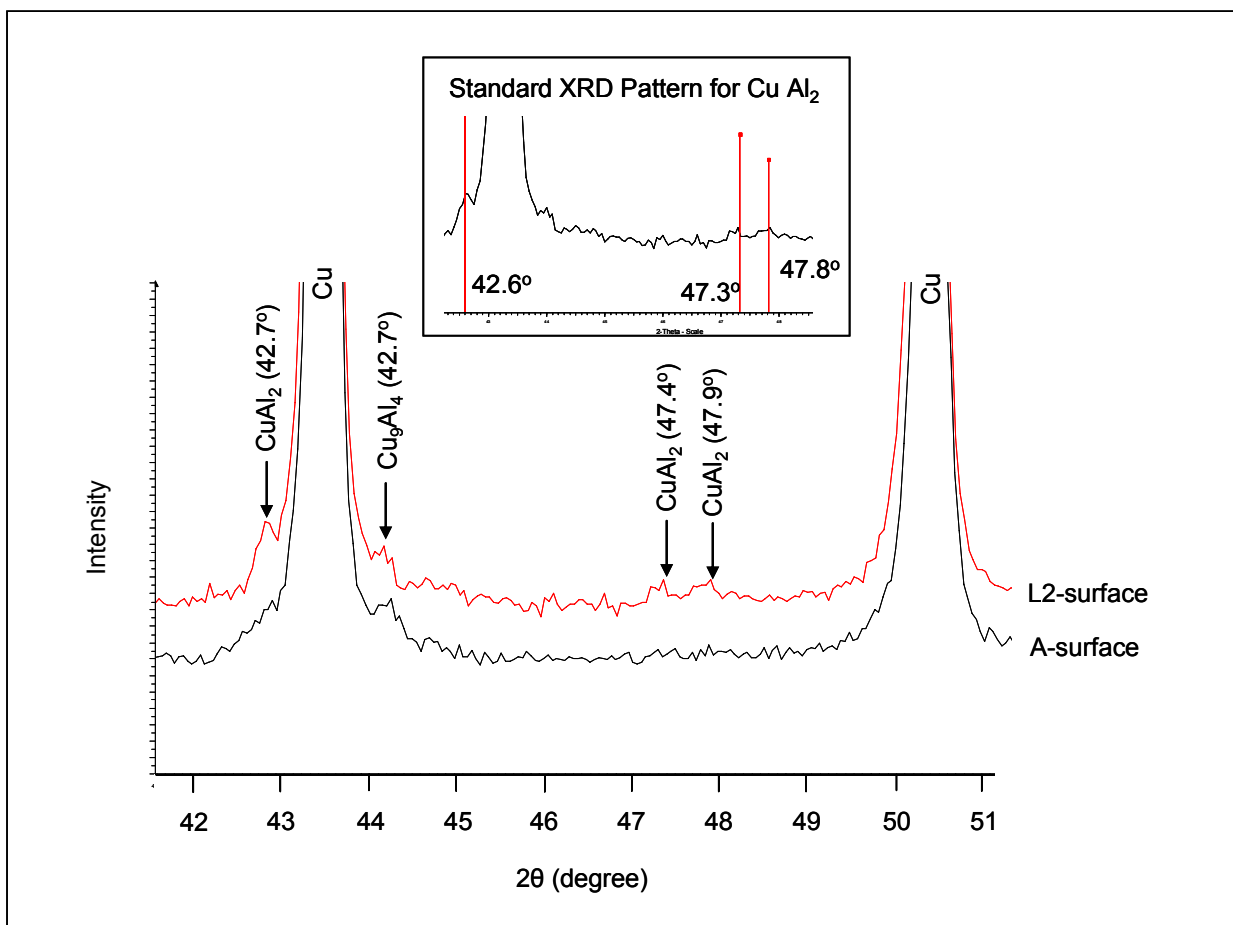


Figure 7.18: Typical XRD intensity spectra showing different Cu-Al intermetallic phases found on the electrode surfaces after 100 spot welds on A-surface and L2-surface; small window is showing the standard XRD pattern for CuAl_2 phase.

Dilthey et al [56] found CuAl_2 on the face of electrode even after first spot weld and Cu_9Al_4 after fifth spot welds when welding AA6016 sheet of thickness 1.31 mm. However, they used different electrode and did not even present any XRD data. For similar material and welding conditions, Lum [59] also confirmed both these intermetallic on electrode tip face. However, he could not see CuAl_2 phase through XRD and could only confirmed the presence of that phase through EDS analysis.

Based on the reaction kinetics of Cu-Al intermetallic phases (Table 7.3), the CuAl_2 formed at a lower temperature (550 - 600 °C) while the Cu_9Al_4 formed at a higher temperature (780 - 873 °C) [106]. Finding Cu_9Al_4 when both L2-surface and A-surface were subject to RSW meant that higher temperatures at the E/W interface were present in both cases. However, finding CuAl_2 only on the electrode tip which was used for RSW of L2-surface meant that some lower temperatures were experienced. This finding was consistent with the idea of lower heat generation at the E/W interface for the L2-surface due to the reduction of oxide layer thickness.

Table 7.3: Intermetallic reaction for different Cu-Al phases [106].

Reaction	Temperature (° C)
$\text{L} \leftrightarrow \text{Al} + \theta$	548.2
$\text{L} + \eta_1 \leftrightarrow \theta$	591
$\text{L} \leftrightarrow (\text{Cu}) + \beta$	1032
$\beta \leftrightarrow (\text{Cu}) + \gamma_1$	567
$\gamma_0 \leftrightarrow \beta + \gamma_1$	780
$\gamma_0 + \epsilon_1 \leftrightarrow \gamma_1$	873

There was also likely to be a further contributing factor. Aluminum-copper alloys were considered to be electrical insulators compared with pure aluminum or copper. However, the

conductivity of CuAl_2 was almost double than that of Cu_9Al_4 [56]. Thus, once CuAl_2 was present it helped reduce the electrical resistance and keep the interface temperatures lower compared with the regions having Cu_9Al_4 . Presumably, this helped reduce the rate of surface pitting and cavity formation during the electrode life tests for the L2-surface.

7.3.7 Electrical Contact Resistance

It was observed in chapter 4 of this thesis that the electrical contact resistance at the E/W interface measured prior to the passage of the high weld current was an indicator of the likely performance of the electrodes in subsequent RSW. Thus, electrical contact resistance across the top E/W interface was measured for all the surface conditions. Centerline average roughness (Ra) of the worksheet associated with the E/W interface and electrical contact resistance at the E/W interface were measured. These experiments were performed using the similar procedure described earlier in chapter 4 of this thesis (section 4.2.1). Ten samples were used for each surface condition (L2-surface, A-surface, and L6-surface) and the results were summarized in Table 7.4. It was discovered that the average electrical contact resistance of L2-surface was lower than that of the A-surface while L6-surface had very high electrical contact resistance. This observation was very consistent with the electrode life tests and pitting rate on these surfaces. Lower electrical contact resistance associated with the L2-surface caused low heat generation and hence slower pitting rate than A-surface. Very high electrical contact resistance of the L6-surface was the main reason of the early failure of electrode. This finding provided additional support for the idea that the oxide layer thickness of the worksheet surface was reduced by the application of the lubricant L2.

Table 7.4: Electrical contact resistance at the E/W interface and centerline average roughness (Ra) of the worksheet.

	L2-surface		A-surface		L6-surface	
	Roughness (Ra) (μm)	Resistance ($\mu\Omega$)	Roughness (Ra) (μm)	Resistance ($\mu\Omega$)	Roughness (Ra) (μm)	Resistance ($\mu\Omega$)
Lowest	0.28	7.8	0.30	10.3	0.34	102
Highest	0.34	9.4	0.52	13.5	0.98	362
Average	0.31	8.6	0.34	11.2	0.56	207
Std Dev	0.02	0.5	0.06	1.0	0.22	81

It can also be observed from Table 7.4 that the application of lubricant L2 improved the roughness of the worksheet. This finding was consistent with the other observations presented earlier in this chapter and in chapter 4. It was observed in chapter 4 that the effect of surface roughness was related to the geometry of the oxide layer at the worksheet surface. Recalling the results presented in chapter 4 of this thesis, it was found that the electrical contact resistance at the E/W interface of ground surface was decreased from $9.1 \mu\Omega$ for a roughness level $0.24 \mu\text{m}$ to $7.2 \mu\Omega$ for a roughness level of $1.08 \mu\text{m}$ while the electrical contact resistance of the A-surface with a roughness value of $0.32 \mu\text{m}$ was higher than that of all ground and abraded worksheets. This was due to the fact that the ground surfaces had fresh (thin) oxide layer and hence lower electrical contact resistances compare with as-received surface. In the present study, while comparing the A-surface with L2-surface, the roughness levels were very close to each other ($0.34 \mu\text{m}$ and $0.31 \mu\text{m}$ respectively, Table 7.4). It was believed that this small variation in roughness was not significant enough to reduce the contact resistance from $11.2 \mu\Omega$ (A-surface) to $8.6 \mu\Omega$ (L2-surface). Thus, a reduction in oxide layer thickness seemed to be the most likely explanation for the reduced electrical contact resistance and hence lower temperature at the E/W interface for the L2-surfaces.

7.4 Concluding Remarks

A practical solution for enhancing the electrode tip life for RSW of aluminum alloys was presented. Different metal working lubricants were placed on the worksheet surface associated with the electrode worksheet interface (i.e. top and bottom E/W interfaces). Extensive electrode life tests along with other experimental and analytical procedure was adopted using aluminum alloy 5182. The findings of this research can be summarized as follows.

Presence of a boundary lubricant at the worksheet surface associated with the E/W interface can increase or decrease the pitting rate of electrode compared with non-lubricated (as-received) worksheet surface. Electrode life tests revealed that a good lubricant for RSW process extended the electrode tip life to almost double than the A-surface. The extended electrode tip life associated with L2-surface was due to the slower pitting rate. The application of the lubricant L2 on the worksheet surface had both chemical and physical effect on the surface layer. Chemically, lubricant L2 reduced the oxide layer thickness and hence the electrical contact resistance. Physically, application of the lubricant L2 improved the surface roughness and hence made the surface layer more uniform. Electrical contact resistances of different surfaces measured prior to any welding were consistent with the electrode life results and pitting rate of electrode.

Chapter 8

8 Conclusions

An understanding of some tribological influences on RSW of an aluminum alloy has been presented along with a practical way to extend electrode life. A common configuration was chosen for the present investigation that had spherical-tipped electrodes being used for RSW of 5182 aluminum alloy. The investigation had a focus on the tribology at both the E/W and FS interfaces. Aspects of the contact mechanics at the interfaces were shown to influence the electrode pitting behaviour and nugget formation. Both experimental studies and FEA were employed.

In the first step, all the main features of the worksheet surface were characterized and their effects on RSW were investigated. In the next step, the contact mechanics at both the E/W and FS interfaces were investigated. The final step was to improve electrode life using a boundary lubricant.

The findings of the present thesis were organized into Chapters 4 - 7 and the conclusions were listed under headings that corresponded to these chapter titles, as shown below.

8.1 Electrode Worksheet Interface (Chapter 4)

The influences of surface roughness and oxide layer geometry on the electrical contact resistance of E/W interface, pitting of the electrode and joint shear force were determined in a series of experimental studies. The detailed conclusions are given in the following list.

1. Attempts to modify the surface roughness of the worksheet caused damage to the surface oxide layer and a decrease in electrical resistance at the E/W interface (thus indicating a decrease in heat generation).
2. Extensive plastic deformation of the worksheet occurred at the E/W interface which indicated that the real and apparent contact area at this interface would be virtually identical.
3. Direct experimental evidence was provided to show that the oxide layer on the surface of AA5182 was non-uniform in composition with magnesium and oxygen rich spot of magnesium oxide (MgO) dispersed over the entire surface.
4. Abrading the worksheet surface decreased the oxide layer concentration as well as reduced the size of magnesium and oxygen rich spot compared with the as-received worksheet surface.
5. Electrical contact resistance at the E/W interface had direct influence on the electrode pitting rate and joint strength. Lower electrical contact resistances at the E/W associated with the abraded surface indicated less heat to be generated and thus less pitting compare with the as-received surface.

8.2 Contact Mechanics at the E/W Interface (Chapter 5)

Contact mechanics of the E/W interface was studied experimentally and with FEA. Factors influencing the pitting of the electrode tip were identified and investigated.

1. Experimental investigation as well as finite element analysis strongly suggested that contact mechanics during the squeezing process influenced the pitting behaviour of electrode and ultimately the life of the electrode. This conclusion was very important because much RSW research had concentrated on the complex welding process itself rather than the “stage setting” contact mechanics.
2. The pitting of the electrode started in a ring around the centre of the electrode tip. The diameter of the initial pitting ring was in the vicinity of 5.0 mm which was same as the contact diameter between electrode and worksheet at the end of squeezing.
3. During squeezing in the RSW sequence, electrode indented the worksheet surface. Microscopy revealed that abrasion of the worksheet surface occurred near the periphery of the contact. This abrasion was observed for both the as-received electrodes with some machining marks and polished electrodes without any apparent machining marks.
4. FEA of the squeezing process predicted that the frictional shear stress at the E/W interface was much higher near the peripheral zone of the contact than in the central zone. Contact pressure was fairly uniform over the entire contact but was predicted to be somewhat higher near the periphery. Significant slip was predicted in the peripheral zone in a ring whose diameter was in the range of 4.0 – 5.0 mm. If this slip occurred, it might cause enough damage to the surface oxide layer to allow good metal-to-metal contact between electrode and worksheet and thus a reduced electrical resistance. This, in turn, would cause current concentration and thus high heat generation due to constriction resistance and eventually ring-pitting of electrode.

8.3 Contact Mechanics at the FS (Chapter 6)

Contact mechanics of the FS interface was studied experimentally and with FEA. Factors influencing the melting and nugget formation were identified and investigated.

1. Once again, the contact mechanics at the FS during squeezing process was found to be very important for the outcome of RSW process. The tribological interactions at the FS during squeezing had significant effect on the start of melting and hence the nugget formation.
2. A complete weld nugget was formed at the end of first current cycle and grew larger during the remaining current time. The heat generation at this interface was higher during the first current cycle than the remaining weld time and this was confirmed by joint shear strength measurements. The rate of nugget growth during the first current cycle was higher than the remaining four current cycles.
3. The melting at the FS did not start at the centre of the contact; rather it started at the periphery at a diameter of between 4.0 and 5.0 mm. This melting around the periphery proceeded rapidly towards centre to form a complete weld nugget. This pattern of melting produced nuggets which resembled a "doughnut" with a thin central plug filling the "hole".
4. FEA of this interface predicted sheet separation and thus sheet bending at the edge of the contact zone. This sheet bending would produce high surface strains that might disrupt the oxide layer on the worksheet surface. Visual observations of the worksheet surfaces showed cracks at the periphery of the contact zone. Sheet bending started towards the centre of the contact zone and moved outwards as the load increased rapidly during the squeeze phase of the welding sequence. However, the maximum sheet bending occurred once the maximum load was achieved and it was at a diameter between 4.0 and 5.0 mm.

5. Considering the contact mechanics of both the E/W and FS surfaces an overall explanation of the influence of contact mechanics on RSW was proposed as follow. Surface oxide layers were disrupted at the periphery of both the E/W and FS contacts during the squeezing phase of the RSW sequence. This disruption was more severe at the E/W contact where slip occurred. Thus, current flow occurred through the peripheral zone of the E/W contact and then down towards the peripheral zone of the FS contact. The current density built in the peripheral zone of the FS contact despite the disrupted oxide layer because it still provided the lowest resistance current path. However, as the current density built, the resistance increased and enough heat was generated to form the nugget and thus the resistance weld with the doughnut-like shape.

8.4 Effect of Boundary Lubricants (Chapter 7)

High electrical contact resistance was required at the FS for good weld nugget while it was not required at the E/W interface for longer electrode life. This aspect of RSW of aluminum alloys was investigated by applying boundary lubricants to the worksheet surface of the E/W interface thus altering the surface of worksheet at the E/W interface without altering any features of the FS. This method was new and has the advantages of being simple and practical for the industry.

1. RSW of worksheet surfaces coated with different lubricants showed different electrode degradation behaviour compare to non-lubricated (as-received) surfaces. Both increased and decreased pitting rates were observed with the use of these lubricants.
2. One good lubricant (L2) had positive effect on electrode pitting behaviour and extended the electrode life to almost double (an average of 730 spot welds) than the

as-received surface (an average of 393 spot welds). This improved electrode life was associated with the slower pitting rate of electrode compare to as-received surface.

3. The application of the lubricant L2 on the worksheet surface alters the surface characteristics both chemically and physically. It was found that the application of lubricant L2 reduced the thickness of the oxide layer and made it more uniform. The reduction of oxide layer thickness, in particular, caused reduced electrical contact resistance at the E/W interface which resulted in a slower pitting rate and hence longer electrode life.
4. The effect of the lubricant was related to the nature of oxide layer. The effect of the good lubricant (L2) was observed only on the as-received surface which had thick oxide layer compare with the polished surfaces that had thin (fresh) oxide layers.
5. For the various lubricants, a higher electrical contact resistance at the E/W interface measured prior to any welding caused a higher pitting rate and thus a lower electrode life.

8.5 Recommendations

Although it would be quite a challenging task, but taking the lead from this study, a FEA model of the squeezing process of RSW process that include either oxide layer or surface roughness or both will be quite interesting. That model will provide a better understanding of the tribo mechanics at these interfaces. Also, since it has been established in this work that the electrical contact resistance at the interfaces were not uniform in the entire contacts, a FEA work that include this actual surface behaviour for the current phase of the RSW process will provide more insight of the nugget formation particularly at the beginning of the weld current.

FEA analysis of the squeezing process that investigates different electrode geometry for significant slip in the entire contact zone of the E/W interface can be performed. The success

in this study will lead towards electrode life improvement as more sliding between electrode and workpiece decrease the electrical contact resistance at this interface and hence slower pitting of electrode.

Another aspect of the present study that can be further investigated is the development of a suitable boundary lubricant for RSW of aluminum alloys. This requires the knowledge of both the materials science and lubricant chemistry.

References

1. N. B. Potluri. Joining of shape memory alloys. *Welding Journal*, 78:39-42, 1999.
2. W. A. Baeslack III, P.S. Liu, P.R. Smith, and J. Gould. Characterization of solid state resistance welds in SiC-reinforced orthorhombic-based Ti-22Al-23Nb (at%) titanium aluminum. *Material Characterization*, 41(1):41-51, 1998.
3. J. Lantz. Principles of resistance welding, part-1. *Welding Design and Fabrication*, 73:26-29, 2000.
4. Welding, Brazing, and Soldering. ASM Handbook Volume 6. *ASM International*, USA, 1993.
5. G. Sitter. Resistance spot brazing on steel sheets with a thick up to 3 mm – recent developments. *Welding and Cutting*, 54(5):242-245, 2000.
6. Giroux, Denis, and James F. D. ‘*Resistance Welding Manual*’, Fourth Edition. Philadelphia, PA. George H. Buchman Co. 1995.
7. Wan Tan. Small-scale resistance spot welding of thin nickel sheets. *PhD thesis*, University of Waterloo, 2004.
8. Welding Handbook. *American Welding Society*, USA, 1991.

9. R. Ikeda, K. Yasuda, K. Hashiguchi. Resistance spot weldability and electrode wear characteristics of aluminum alloy sheet. *Welding in the World*. 41, 492-498, 1998.
10. L. Xu and J. A. Khan. Nugget growth model for aluminum alloys during resistance spot welding. *Welding Journal Research Supplement*, 367s – 372s, 1999.
11. H. Murakawa, F. Kimura, and Y. Ueda. Weldability analysis of spot welding on aluminum using FEM. *Mathematical Modeling of Weld Phenomena 3*, Ed. H. Cerjak, The Institute of Materials, 944-966, 1997.
12. R.W. Messler Jr and Min Jou. Review of control system for resistance spot welding: past and current practice and emerging trends. *Science and Technology of Welding and Joining*, 1(1):1-9, 1996.
13. R. Ikeda, K. Yasuda, K. Hashiguchi, T. Okita, and T. Yahaba. Effect of electrode configuration on electrode life in resistance spot welding of galvanized steel and aluminum alloy for car body sheets. *Proc. Advanced Technologies & Processes (IBEC '95)*: pp.44-51. 1995.
14. M. Rashid. Mathematical modeling and optimization of precipitation hardening of extrudable aluminum alloys. *MSc. KFUPM*, 1997.
15. E. A. Avallone and T. Baumeister III: *Mark's Standard Handbook for Mechanical Engineers*, 9th edition, McGraw Hill Book Company, New York, 1978.
16. I.N. Fridlyander, V.G. Sister, O.E. Grushko, V.V. Berstenev, L.M. Sheveleva, and L.A. Ivanova. Aluminum alloys: promising materials in the automotive industry. *Metal Science and Heat Treatment*. 44(9), 365-370, 2002.

17. M.C. Thornton, C.J. Newton, B.F.P. Keay, P.S. Sheasby, and J.T. Evans. Some surface factor that affect the spot welding of aluminum. *Interfinish 96 World Congress, England*, 259-276, 1996.
18. M. J. Wheeler, Sheasby, and P. G., Kewley, D. Aluminum Structured Vehicle Technology – A Comprehensive Approach to Vehicle Design and manufacturing in Aluminum. *SAE Technical Paper-870146*. 1987.
19. D. M. Moor. Environment & life cycle benefits of automotive aluminum. *Alcan Automotive at Climate Change 2, Canadian technology Development*, Toronto, 2001.
20. B. Irving. Building tomorrow's automobiles. *Welding Journal*: 29-34, 1995
21. N. T. Williams. Suggested topics for future research in resistance welding. *Welding in the World* 22(1/2): pp.28-34. 1984.
22. E. P. Patrick and D. J. Spinella. The effects of surface characteristics on the resistance spot weldability of aluminum sheet. *AWS Sheet Metal Welding Conference*, Detroit Section VII, Troy, Mich., Oct 8-11, (1996), Paper No.B4. 1996.
23. Properties and Selection. ASM Handbook Volume 1-2. ASM International, USA, 1993.
24. C. J. Newton. The Fundamentals of Resistance Spot Welding Aluminum. *Sheet Metal Welding Conference VI*, 1994.
25. D. J. Browne, C. J. Newton, and D. Boomer. Optimization and Validation of A model to predict the Spot Weldability Parameter Lobes for Aluminum Automotive Body Sheet. *Proc. Advanced Technologies & Processes (IBEC '95)*:100-106, 1995.

26. M. Thornton, C. Newton, B. Keay, and T. Evans. Spot welding of aluminum sheet: a statistical approach to measure the influence of different surfaces. *Proc. Advanced Technologies & Processes (IBEC '96)*:58-66, 1995.
27. S.C. Wang and P.S. Wei. Modeling dynamic electrical resistance during resistance spot welding. *Journal of Heat Transfer*, 123(3):576-585, 2001.
28. W.L. Roberts. Resistance variation during spot welding. *Welding Journal*, 30, 1004-1019, 1951.
29. P. S. James, H. W. Chandler, J. T. Evans, D. J. Browne, and C. J. Newton. The effect of mechanical loading on the contact resistance of coated aluminum. *Materials Science and Engineering A-230*. pp. 194-201. 1997.
30. P. H. Thornton, A. R. Krause, and R. G. Davies. Contact resistance of aluminum. *Welding Journal Research Supplement*, 331s-341s, 1997.
31. E. Crinon and J.T. Evans. The effect of surface roughness, oxide film thickness and interfacial sliding on the electrical contact resistance of aluminum. *Materials Science and Engineering A-242*, 121-128, 1998.
32. P. H. Thornton, A. R. Krause, and R. G. Davies. Contact Resistance in Spot Welding. *Welding Journal Research Supplement*: pp. 402s-412s. 1996.
33. E. P. Patrick, J. R. Auhl, and T. S. Sun. Understanding the process mechanism is key to reliable resistance spot welding aluminum autobody components. *SAE technical paper*. 1984.
34. K.C. Wu. Resistance spot welding of high contact-resistance surfaces for weldbonding. *Welding Journal Research Supplement*: 436s-443s, 1975.

35. R.L. Cohen and K.W. West. Aluminum spot weld strength determined from electrical measurements. *Welding Journal*, 37-41, 1985.
36. Q. Song, W. Zhang, and N. Bay. An experimental study determines the electrical contact resistance in resistance welding. *Welding Journal Research Supplement*: 73s-76s, 2005.
37. J. C. Kucza, J. R. Butrulle, and E. Hank. Aluminum as-rolled sheet for application-effect of surface oxide on resistance spot welding and adhesive bonding behavior. *SAE-Technical Paper*, 1997.
38. K. Kotani, K. Ikeuchi, and F. Matsuda. Behaviour of interfacial phases in diffusion bonding of commercial aluminum alloys by transmission electron microscopy. *Trends in Welding Research, Proceedings of the 4th International Conference*: 791-796, 1995.
39. Y. Imamura and S. Sasabe. Resistance spot weld quality in Al-Mg alloy sheet. *Welding International*: 9(9), 686-696, 1995.
40. Ceramics and Glasses. Engineering Materials Handbook, Volume 4. *ASM International*. USA, 1991.
41. H. Zhang and J. Senkara, Resistance Welding – Fundamentals and Applications, Taylor and Francis, Florida, 2006
42. D. J. Spinella, J. R. Brockenbrough, and J. M. Fridy, Strategies to reduce cost of automotive resistance spot welding. *Sheet Metal Welding Conference-XII*, 2006
43. R. Holm. Electric Contacts. Theory and Application, 4th Edition. Springer-Verlag, New York, 1967.

44. T.S. Sun. Electrode Deterioration Mechanisms in Resistance Spot Welding of Aluminum. *Alcoa Internal Report No. 53-82-3*, March 1982.
45. J.A. Edwards. Improving weld consistence of aluminum body sheet. *Welding Review-The International Journal of Welding and Fabrication*, 24-27, 1986.
46. J.H. Hennings and W.H. Singen. New process for improving spot weldability of sheet aluminum. *Aluminum*, 57(9), 612-614, 1981.
47. U.D. Mullyay. Effect of contact resistance in resistance welding of aluminum. *Welding Journal*, 41-44, 1984.
48. H. Hennings and J. Maier. Improvement of spot welding of aluminum sheet by surface treatment. *Second International Conference on Aluminum Weldments*, I.8, A1-A16. 1982.
49. R.M. Rivett. Spot welding electrode life tests on aluminum sheet-Effect of parent metal composition and surface treatment. *Welding Institute Research Board Report*. 132/1980.
50. H. A. Mohamed and J. Washburn. Mechanics of solid state pressure welding. *Welding Journal Research Supplement*, 302s-310s, 1975.
51. J. E. Gould. Mechanics of bonding of solid-state welding processes. *11th Annual North American Welding Conference: Advances in Welding Technology*, 259-279, 1995.
52. F.J. Studer. Contact Resistance in Spot Welding. *The Welding Journal*, vol-18, 374s-380s, 1939.
53. S.E. Arrington Jr. Twisting electrodes improve tip life and weld quality on resistance spot weld aluminum sheet. *SAE Transaction*, 104(5), 653-656, 1995.

54. J. I. McCool. Comparison of Models for the contact of rough surfaces. *Wear*, 107, 37-60, 1986.
55. K. Sugimura and A. Nagae. Lubricant for some plated contacts. *Proceeding of 36th Annual Holm Conference on Electrical Contacts, Illinois Institute of Technology Chicago*, 417-424, 1990.
56. U. Diltthey, and S. Hicken. Metallographic Investigation into Wear Processes on Electrodes during the Resistance Spot Welding of Aluminum. *Welding and Cutting I*, 34-40, 1998.
57. I. Lum, S. Fukumoto, E. Biro, D.R. Boomer, and Y. Zhou. Electrode Pitting in Resistance Spot Welding of Aluminum Alloy 5182. *Metallurgical and Materials Transaction A (35A)*, 217-225, 2004.
58. S. Fukumoto, I. Lum, E. Biro, D.R. Boomer, and Y. Zhou. Effect of Electrode Degradation on Electrode Life in Resistance Spot Welding of Aluminum Alloy 5182. *Welding Journal Research Supplement*, 307s-312s, 2003.
59. I. Lum. Electrode deterioration in the medium frequency DC resistance spot welding of 5182 aluminum alloy. *MASc thesis*, University of Waterloo, 2002.
60. H. Zhang, Y. J. Huang, and S. Jack Hu. Nugget growth in resistance spot welding of aluminum alloys. *Sheet metal Welding Conference VII*, 1996.
61. X. Sun and P. Dong. Analysis of aluminum resistance spot welding process using coupled finite element procedure, *Welding Journal Research Supplement*, 215s-221s 2000.
62. R. Heimbuch, A. Houchens, and J. Thomas. Contact resistance of 2036-T4 aluminum and its effect on resistance spot welding. *American Society for Metals*, 179-206, 1982.

63. G.L. Leone and B. Altshuller. Improvement on the resistance spot weldability of aluminum body sheet. *SAE-technical paper 0148-7191/84*. 1984.
64. U. D. Mullay and M.G. Kurve. Arc cleaning for increased electrode life-process parameters. *Indian Welding Journal*, 128-131, 1983.
65. F.F. Ashton and D. Rager. An arc cleaning approach for resistance welding aluminum. *Welding Journal*, 750-757, 1976.
66. D.J. Spinella and E.P. Patrick. Advancement in aluminum resistance spot welding to improve deformation and reduce energy. *Sheet Metal Welding Conference X*, 2002.
67. Y. Cho, W. Li, and S. J. Hu. Design of experiment analysis and weld lobe estimation for aluminum resistance spot welding. *Welding Journal Research Supplement*, 45s-51s, 2006.
68. M.R. Finlay. Resistance Spot Welding of Metallic Coated Steels and PVD Coated Electrodes. *Australian Welding Research, Welding Technology Institute of Australia*, CRC No. 18, 1996.
69. M. Kimichi and J.E. Gould. The evaluation of resistance spot welding electrode material for welding galvanized steel. *Sheet metal Welding Conference VIII*. 1998.
70. T. Satio, T. Nishi, and Y. Takahashi. Electrode Tip Life in Resistance Spot Welding of Zinc Alloy Coated Sheet Steels. *Nippon Steel Technical Report No 37*, April 1988.
71. J. Matsumoto and H. Mochizuki. Spot welding of aluminum alloy - electrode life for various electrodes. *Welding International*, 8(6), 438-444, 1994.

72. Y. Tanaka and M. Noguchi. An alumina dispersion strengthened copper composite electrode for spot welding. *Welding International*. No. 11, 1074-1078, 1987.
73. E. Ostgaard. Spot welding of aluminum as delivered. *The Danish Welding Institute*, Doc III-614-79, 1979.
74. M.A. Glagola and C.A. Roest. Nickel plated electrodes for spot welding aluminum. *SAE-Technical paper-760167*, 1976.
75. M.R. Finlay. PVD coating of resistance spot welding electrodes. *Australasian Welding Journal*. , Volume 42, 1997. pp. 39-42.
76. R.J. Bowers, C.D. Sorensen, and T.W. Eager. Electrode geometry in resistance spot welding. *Welding Journal Research Supplement*, 45s-51s, 1990.
77. F.R. Hoch. Joining of aluminum alloy 6009/6010. *SAE-Technical paper-780396*, 1978.
78. R. Holliday, J.D. Parker, and N.T. Williams. Relative contribution of electrode tip growth mechanisms in spot welding zinc coated steels. *Welding in World* 37. 186-193, 1996.
79. United State Military Specification. Welding, Resistance: Spot and Seam. MIL-W-6858D, 1978.
80. B. B. Keay. Welding of aluminum for automotive body assembly. *Sheet Metal Welding Conference V*. 1992.
81. K.A. Osman, M. Hao, C.J. Newton, D.R. Boomer, M.J. Thornton, A.M. Higginson, P.G. Sheasby, and H.R. Kelly. Monitoring of spot weld quality in aluminum structures: A comprehensive approach. *6th European Congress on Lightweight and Small cars The Answer to Future Needs*, Volume-II, 1997.

82. M. Hao, K.A. Osman, D.R. Boomer, and C.J. Newton. Development in Characterization of Resistance spot welding of aluminum. *Welding Journal Research Supplement*, 1s-8s, 1996.
83. B.H. Chang, Y. Zhou, I. Lum, and D. Du. Finite element analysis of effect of electrode pitting in resistance spot welding of aluminum alloy. *Science and technology of Welding and Joining*, 10(1), 61-66, 2005.
84. H. Murakawa, J. Zhang, K. Fujii, J. Wang, and M. Ryudo. FEM simulation of spot welding process (report IV). *Transaction of JWRI*, 2000, vol. 29, no. 1, pp. 73-80
85. Z. Feng, S. S. Babu, M. L. Santella, B. W. Riemer, and J. E. Gould. An incrementally coupled electrical-thermal-mechanical model for resistance spot welding. *5th International Conference on Trends in Welding Research*, paper 1-5.71, 1998.
86. J.A. Khan, L. Xu, Y Chao, and K Broach. Numerical simulation of resistance spot welding process. *Numerical Heat Transfer, Part-A*, 37, 425-446, 2000.
87. P. Dong, M. Victor, and M. Kimchi. Finite element analysis of electrode wear mechanism: face extrusion and pitting effects. *Science and technology of Welding and Joining*, 3(2), 59-64, 1998.
88. H. A. Nied. The finite element modeling of the resistance spot welding process. *Welding research Supplement*, 123s-132s. 1984.
89. J. Kaiser, G.J. Dunn, and T.W. Eager. The effect of electrical resistance on nugget formation during spot welding. *Welding research Supplement*, 167s-174s. 1982.
90. D.J. Browne, H.W. Chandler, J.T. Evans, P.S. James, J. Wen, and C.J. Newton. Computer simulation of resistance spot welding in aluminum part-II, *Welding research Supplement*, 417s-422s. 1995.

91. D.J. Browne, H.W. Chandler, J.T. Evans. Computer simulation of resistance spot welding in aluminum part-I, *Welding Journal Research Supplement*, 339s-344s. 1995.
92. M. Rashid, J.B. Medley, and N. Y. Zhou. Effect of Surface Characteristics on Contact Resistance and Resistance Spot Welding Behaviour of 5182 Aluminum Alloy Sheet. *Proceeding of the CSME Forum 2006*.
93. ABAQUS User's Manual-Interactive Version 6.5. Habbitt, Karlsson & Sorensen, Inc. 2004.
94. Properties and Selection: Nonferrous Alloys and Special-Purpose Materials, Metals Handbook, 10th edition, vol. 2, ASM International. USA. 1990.
95. Friction, Lubrication, and Wear Technology, Metals Handbook, 10th edition, vol. 18, ASM International. USA. 1990.
96. L. Tam, J. Hua, and S. Ma, The Physics FactbookTM, An educational Fair Use website (<http://hypertextbook.com/facts/2005/aluminum.shtml>), 2005.
97. J. A. William, Engineering Tribology, Oxford University Press, UK, 1994.
98. R. Tewari, G. K. Dey, P. K. Fotedar, T. R. G. Kutty, and N. Prabhu, Deformation Behavior of Zr₃Al-Nb Alloys I: Room-Temperature and High Temperature Deformation Study. *Metallurgical and Materials Transaction A*. Volume 35A. 2004.
99. C. L. Tsai, W. L. Dai, D. W. Dickinson, and J. C. Papritan, Analysis and Development of a Real-time Contact Metallography in Resistance Spot Welding, *Welding Research Supplement*, , 339s-351s, 1991.
100. C. Lea and J. Ball, The Oxidation of Rolled and Heat Treated Al-Mg Alloy, *Application of Surface Science* 17, 344-362, 1984.

101. Standard Practice for Microetching Metals and Alloys. Annual Book of ASTM Standards. Volume 03.01, ASTM International, 2005.
102. M. Rashid, S. Fukumoto, J.B. Medley, and Y. Zhou. Effect of Lubrication on Electrode Life in Resistance Spot Welding of Aluminum Alloys, *Sheet Metal Welding Conference XI*, 2004.
103. M. Rashid, S. Fukumoto, J.B. Medley, J. Villafuerte, and N. Y. Zhou. Influence of Lubricants on Electrode Life in Resistance Spot Welding of Aluminum Alloys, *Welding Journal Research Supplement*, vol. 86 (3), 62s-70s, 2007.
104. J.F. Moulder, W.F. Stickel, P.E. Sobel, and K.D. Bomben. Handbook of X-ray Photoelectron Spectroscopy. Perkin-Elmer Corporation, Eden Prairie, 1992.
105. Havinga, (XRD Standard Card # 25-0012), 1973. Phillips Research Lab, Eindhoven, the Netherlands.
106. J. L. Murray, Binary Alloy Phase Diagram, Second Edition, Volume 1, ASM International. 1990.
107. Standard Test Methods for Tension Testing of Materials: E8M-04, ASTM International, USA, 2004.
108. P. G. Slade, Electrical Contacts: Principles and Applications, CRC Press, 1999.
109. Medar MFDC Invert Technical Reference Guide # B98200, Revision 3, 1999.
110. http://encyclopedia.laborlawtalk.com/Peltier_effect#Peltier_effect
111. K. L. Johnson, Contact Mechanics, Cambridge University Press, Cambridge, 1985.

Appendix A

Table A-1: Summary of all the major experiments conducted for the present work.

Experiment	Variable	Specimen type/size	Number of sets/measurements	Measurement or Observation	Where in thesis (section)
Roughness	Worksheet surface – as-received – rough – smooth	50 mm x 40 mm	15 measurements on each surface	Centre line average roughness (Ra)	4.2.1
Electrical Contact Resistance	Worksheet surface – as-received – rough – smooth	50 mm x 40 mm	5 measurements on each surface	Electrical contact resistance at the E/W interface	4.2.2
Roughness	Electrode tip	50 mm x 40 mm	50 measurements	Centre line average roughness (Ra)	4.2.1
Roughness	Worksheet surface – as-received – abraded	50 mm x 40 mm	20 measurements on each surface	Centre line average roughness (Ra)	4.2.3
RSW	Worksheet surface – as-received – abraded	– 10-weld standard coupon (Fig 3.2) – Overlapped shear force specimen (Fig 3.3)	100 spot weld on each surface	– RSW – Joint shear force – Carbon Imprint	4.2.3

RSW	Electrode pitting during early stage of electrode life	10-weld standard coupon (Fig 3.2)	3-sets (100 spot welds on each)	<ul style="list-style-type: none"> – RSW – Carbon Imprint – Pitting location 	5.2.1
Contact Diameter	Current time	Overlapped shear force specimen (Fig 3.3)	30 specimens	<ul style="list-style-type: none"> – RSW – Contact Diameter at the E/W interface – Joint shear force 	5.2.2 6.2.1
Electrode Roughness	Electrode tip surface <ul style="list-style-type: none"> – regular – polished 	Electrode (Fig 3.4)	5 –regular 5-polished	<ul style="list-style-type: none"> – Centre line average roughness (Ra) – Radius of electrode 	5.2.3
Squeezing	Electrode tip surface <ul style="list-style-type: none"> – Regular – polished 	<ul style="list-style-type: none"> – Electrode (Fig 3.4) – Overlapped shear force specimen (Fig 3.3) 	5 –regular 5-polished	Effect of squeezing	5.2.3
RSW	<ul style="list-style-type: none"> – Current-time – Weld-current 	Overlapped shear force specimen (Fig 3.3)	3-sets + for each surface	<ul style="list-style-type: none"> – Nugget cross-section – Nugget growth – Nugget shape 	6.2.1
RSW	<ul style="list-style-type: none"> – Current-time – Weld-current 	Overlapped shear force specimen (Fig 3.3)	20 + for each surface	<ul style="list-style-type: none"> – Start of melting at FS – Melting growth at FS 	6.2.2

Contact Diameter	Squeezing	Overlapped shear force specimen (Fig 3.3)	5 specimen	Contact diameter of the FS	6.3.2
Sheet Separation	Squeezing	Overlapped shear force specimen (Fig 3.3)	10 specimen	<ul style="list-style-type: none"> – Squeezing – Sheet separation – Surface cracking 	6.3.3
Bending	Sheet separation	30 mm x 120 mm	3 specimen	Effect of bending on sheet surface	6.3.4
Screening (RSW)	Worksheet surface condition at the E/W interface <ul style="list-style-type: none"> – Lubricated – As-received 	10-weld standard coupon	7-set (100 spot welds on each surface)	<ul style="list-style-type: none"> – Electrode tip – Carbon Imprint 	7.2.1
Electrode Life Test	As-received worksheet surface	<ul style="list-style-type: none"> – 10-weld standard coupon (Fig 3.2) – Overlapped shear force specimen (Fig 3.3) 	3-sets (complete electrode life tests)	<ul style="list-style-type: none"> – RSW – Electrode life – Joint shear force – Carbon Imprint 	7.2.2
Electrode Life Test	L2-surface	<ul style="list-style-type: none"> – 10-weld standard coupon (Fig 3.2) – Overlapped shear force specimen (Fig 3.3) 	3-sets	<ul style="list-style-type: none"> – RSW – Electrode life – Joint shear force – Carbon Imprint 	7.2.2
Electrode Life Test	L6-surface	<ul style="list-style-type: none"> – 10-weld standard coupon (Fig 3.2) – Overlapped shear force specimen 	3-sets	<ul style="list-style-type: none"> – RSW – Electrode life – Joint shear force – Carbon Imprint 	7.2.2

		(Fig 3.3)			
RSW	Worksheet surface – as-received – L2-surface	Overlapped shear force specimen (Fig 3.3)	4-sets on each surface conditions	– RSW – Joint shear force – Contact diameter at the E/W interface – Nugget diameter	7.3.1 7.3.2 7.3.3
Hardness	Worksheet surface – as-received – L2-surface	30 mm x 120 mm	20-specimen (each surface)	Vickers Hardness	7.3.4
Roughness	Worksheet surface – as-received – L2-surface – L6-surface	40 mm x 50 mm	10-specimen of each surface (3 readings on each specimen)	Centre line average roughness (Ra)	7.3.7
Electrical Contact Resistance	Worksheet surface – as-received – L2-surface – L6-surface	40 mm x 50 mm	10-specimen of each surface	Electrical contact resistance at the E/W interface	7.3.7
<u>Major Analytical tools/methods</u>					
Finite Element Analysis (FEA), Scanning Electron Microscopy (SEM), Electron Spectroscopy for Chemical Analysis (ESCA), Electron Dispersive Spectroscopy (EDS), X-ray Diffraction (XRD), Optical Microscopy, Stereo Microscopy, Metallography					

Appendix B

Constriction Resistance

No real surface is true (ideally) flat and comprises of many asperities. When two such metallic surfaces brought into contact with each other, asperities of one surface penetrate into other surface and established localized contacts. However, due to the presence of oxide film or other contaminating film at the metallic surfaces, there would be only few spots where a true metal-to-metal contact would be established and in general it is much smaller than 1% of the nominal or apparent contact area [108]. During the current flow through such interfaces, the passage of current is constricted to such small metal-to-metal contact (Figure B.1). The concentration of current in such small metal-to-metal contact zone caused electrical constriction resistance. Holm [43] related this constriction resistance to the basic properties of the contacting metals such as hardness and electrical resistivity. He quantified the constriction resistance (R_c) for a perfectly circular metal-to-metal contact zone of diameter d_o by the following formula.

$$R_c = \frac{\rho_1 + \rho_2}{2d_o} \quad \text{equation B-1}$$

where ρ_1 and ρ_2 are the resistivity of the two contacting bodies.

If the two materials are same then $\rho_1 = \rho_2 = \rho$ and the above equation can be simplified as

$$R_c = \frac{\rho}{2d_o} \quad \text{equation B-2}$$

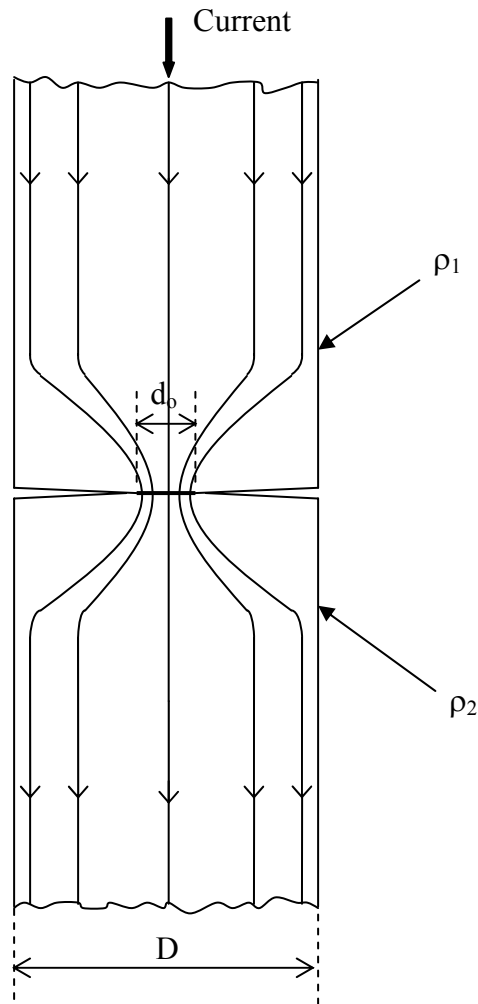


Figure B-1: Constricted current flow through a small spot of diameter d_o .

As mentioned earlier, in case of RSW of aluminum alloys where the oxide film is relatively thick and non-conductive, the current flow was only possible through these small metal-to-metal contact and the contact resistances at the interfaces was only due to the constriction resistance [29-33, 44]. Practically, it is very difficult to estimate the size and number of these small spots at the two interfaces. Even a rough estimate required several assumptions and therefore an exact solution for RSW of aluminum alloys were not yet established. Several work [29, 31] tried to estimate the constriction resistance of the FS interface for RSW of aluminum alloys. For example, Crinon et al [31] tried to estimate the upper and lower limit of the constriction resistance of the FS of 5xxx aluminum alloy. They found that some of the

measured values were order of magnitude different then the estimated contact resistance. James et al [29] also tried to estimate the constriction resistance at the two interfaces using aluminum alloy 5754. They found irregular behaviour of resistance at the interfaces and speculated some other mechanism than the constricted metal-to-metal conduction.

Some Calculations

The electrical contact resistances of the E/W interface presented in chapter 4 can now be used to estimate the size and number of contacting metal-to-metal contact at this interface. Since the proposed slip at the E/W interface was expected to produce large number of small metal-to-metal contact zone near the periphery. This following calculation assumes that there were n such perfectly circular contacting spots of diameter d_o . Since, with present techniques, it is not possible to observe such contacting spots at the interface, so only a crude estimate is presented as follows.

Equation B-1 above provide the constriction resistance of one spot, if there are n such spots, the total constriction resistance would be $(1/n)$ times the value for one spot. For n such spots, the equation 1 can be re arrange as follows

$$n = \frac{\rho_s}{2 d_o R_c} \quad \text{equation B-3}$$

where ρ_s is the sum of ρ_1 and ρ_2 (or $\rho_s = \rho_1 + \rho_2$). Using the value of resistivity of copper ($1.7 \times 10^{-8} \Omega\text{m}$) and aluminum ($2.8 \times 10^{-8} \Omega\text{m}$), equation 3 can be used to obtain the number of contacting spots (n) by assuming there size (d_o). Tables B-1, B-2 and B-3 provide these calculations. These tables also compare the total contact area of all the contacting spots (A_t) with the nominal contact area of the periphery (A_p) between the diameter of 5 mm and 4 mm as shown below.

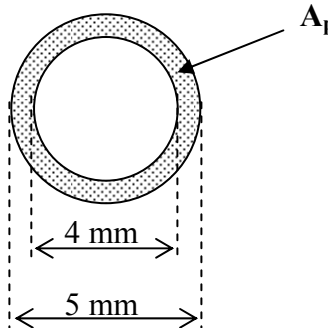
$$A_p = \frac{\pi}{4}(5^2 - 4^2)$$


Figure B-2: Peripheral contact area at the electrode-worksheet interface.

Table B-1: Estimate of the size (d_o) and number (n) of the metal-to-metal contact for A-surface (Resistance = 11.6 $\mu\Omega$).

Surface	d_o	n	A_o	A_t	A_t/A_p
	(μm)	(number)	(μm^2)	(mm^2)	(%)
as-is	1	1940	0.786	0.00152	0.0216
	2	970	3.142	0.00305	0.0431
	3	647	7.070	0.00457	0.0647
	4	485	12.568	0.00609	0.0862
	5	388	19.638	0.00762	0.1078
	10	194	78.550	0.01524	0.2155
	50	39	1963.750	0.07618	1.0776
	100	19	7855.000	0.15236	2.1552

Table B-2: Estimate of the size (d_o) and number (n) of the metal-to-metal contact for A-surface (Resistance = 9.1 $\mu\Omega$).

Surface	d_o	n	A_o	A_t	A_t/A_p
	(μm)	(number)	(μm^2)	(mm^2)	(%)
smooth	1	2473	0.786	0.00194	0.0275
	2	1236	3.142	0.00388	0.0549
	3	824	7.070	0.00583	0.0824
	4	618	12.568	0.00777	0.1099
	5	495	19.638	0.00971	0.1374
	10	247	78.550	0.01942	0.2747
	50	49	1963.750	0.09711	1.3736
	100	25	7855.000	0.19422	2.7473

Table B-3: Estimate of the size (d_o) and number (n) of the metal-to-metal contact for A-surface (Resistance = $7.2 \mu\Omega$).

Surface	d_o	n	A_o	A_t	A_t/A_p
	(μm)	(number)	(μm^2)	(mm^2)	(%)
rough	1	3125	0.786	0.00245	0.0347
	2	1563	3.142	0.00491	0.0694
	3	1042	7.070	0.00736	0.1042
	4	781	12.568	0.00982	0.1389
	5	625	19.638	0.01227	0.1736
	10	313	78.550	0.02455	0.3472
	50	63	1963.750	0.12273	1.7361
	100	31	7855.000	0.24547	3.4722

It can be observed that for the same spot size, the number of contacting spots was less for as-received surface than the ground (smooth and rough) surfaces and hence the effect of oxide layer thickness was validated. The FEA showed that the amount of slip was about $1 \mu\text{m}$ near the periphery. Also, it was generally considered that the actual metal-to-metal contact area would be much smaller than 1% of the real contact area [108]. Therefore, most of the metallic contacts would have a diameter of about $1 \mu\text{m}$ or less. However, since the sliding was observed between the contact diameter of 5 mm and 4 mm (contact area A_p), it was quite possible that some of the contacts would align or overlap each other to form bigger contacts than $1 \mu\text{m}$., based on this assumption, it can be estimated from these tables that the size of the contacting spots could be as greater as $5 \mu\text{m}$. This result was a little comparable with the results of Crinon et al [31] who estimated the contact diameter of one spot as $4 \mu\text{m}$ with a total of 130 such contacting spots after induced sliding. However, all these results are on the basis of several assumptions and the actual size and number of contacting spots could be different in addition to different current conduction mechanism.

Appendix C

Table C-1: Table showing the relative mesh density used for convergence.

Mesh	Number of Elements	Relative Mesh Density
Normal	1080	1
Fine	1950	1.8
Very Fine	4536	4.2
Ultra Fine	5364	5.0

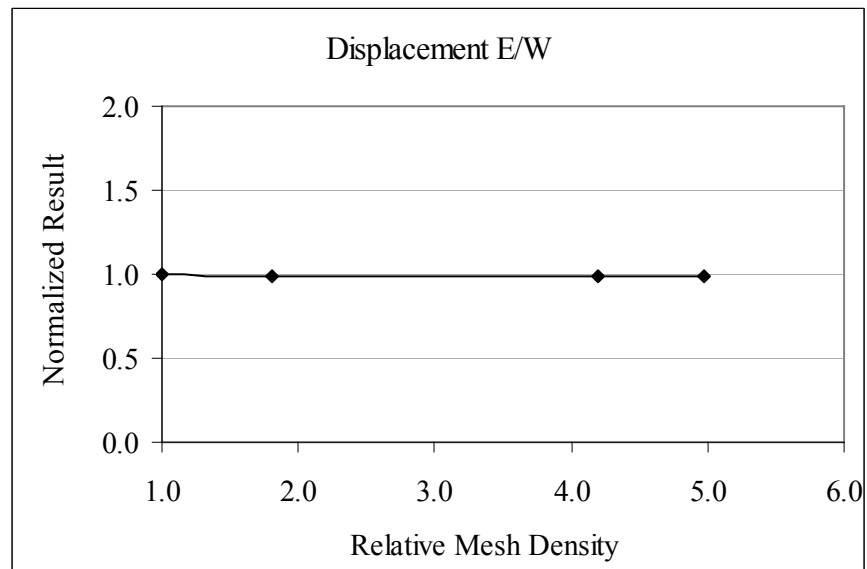


Figure C-1: Mesh density convergence for displacement at the E/W interface

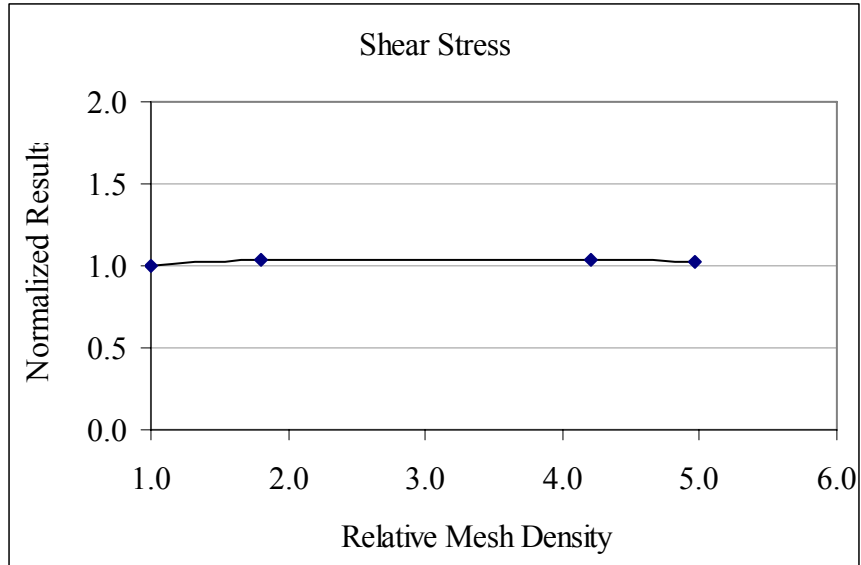


Figure C-2: Mesh density convergence for shear stress along the E/W interface.

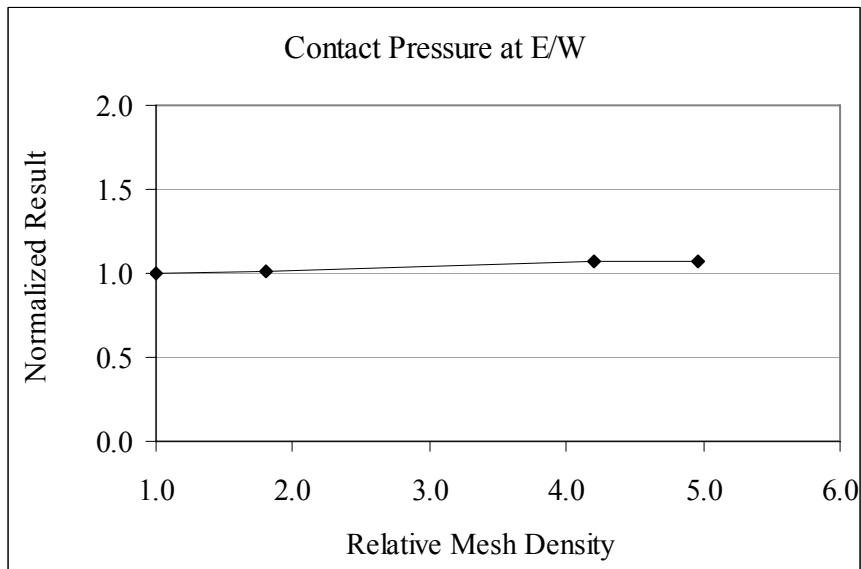


Figure C-3: Mesh density convergence for contact pressure at the E/W interface.

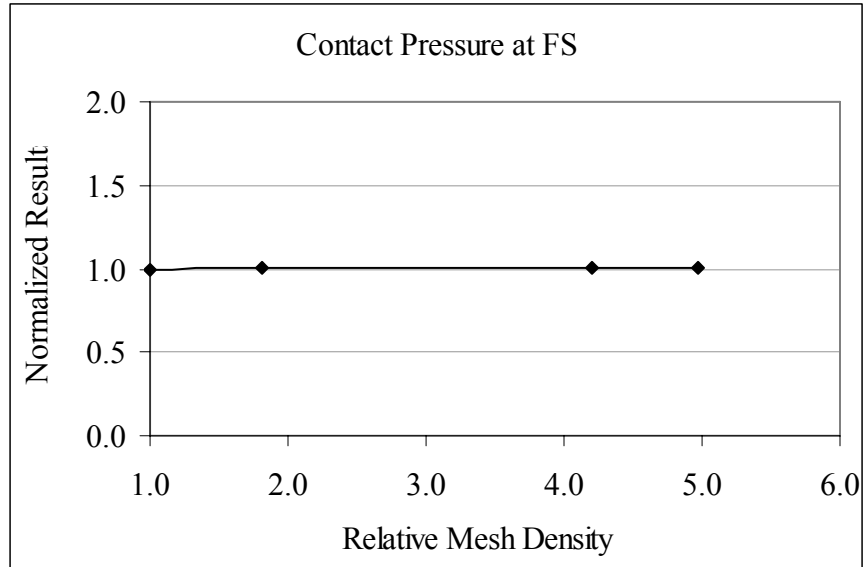


Figure C-4: Mesh density convergence for contact pressure at the FS.